Geomorphology 450 (2024) 109066

Contents lists available at ScienceDirect

Geomorphology

journal homepage: www.journals.elsevier.com/geomorphology

Evolution of the Júcar-Cabriel fluvial system on the Mediterranean watershed of the Iberian Peninsula (Valencia, eastern Spain)

Pablo G. Silva [a,*], Fernando Tapias [b], Javier Élez [b], Elvira Roquero [c], Francisco Gutiérrez [d], Miren del Val [e], Francisco José Perez-Torrado [f], Jorge Luis Giner-Robles [g], Davinia Moreno [e]

[a] Depto. Geología, Universidad de Salamanca, Escuela Politécnica Superior de Ávila, Ávila, Spain
[b] Depto. Geología, Universidad de Salamanca, Facultad de Ciencias, Salamanca, Spain
[c] Dpto. Edafología, E.T.S.I. Agrónomos, Universidad Politécnica de Madrid, Madrid, Spain
[d] Dpto. de Ciencias de la Tierra, Universidad de Zaragoza, Zaragoza, Spain
[e] Programa de Geología y Geocronología, Centro Nacional de Investigación sobre la Evolución Humana (CENIEH), Burgos, Spain
[f] Dpto. Física – GEOVOL Universidad Las Palmas de Gran Canaria, Gran Canaria, Spain
[g] Dpto. Geología y Geoquímica, Universidad Autónoma de Madrid, Tres Cantos, Madrid, Spain

ARTICLE INFO

Keywords:
Fluvial evolution
Terrace system
Quaternary
Geochronology
Volcanic activity
Salt tectonics Júcar Valley
East Spain

ABSTRACT

This study presents the characterization and chronology of the Quaternary terrace sequence developed in the confluence zone of the Júcar and Cabriel river valleys. The study area covers a radius of 10 km from the confluence of the two valleys near the locality of Cofrentes (Valencia). It is located in the northern zone of the Ayora-Cofrentes Graben in the northeastern sector of the External Prebetic Zone adjacent to southern Iberian Chain. This N-S graben is an inherited tectonic feature with an axial salt wall subject to different periods of fluvial dissection and refilling since at least the end of the Messinian Salinity Crisis (MSC). Regional isostatic uplift and local uplift and subsidence processes related to salt flow and dissolution during the Quaternary period, favored by fluvial entrenchment and terrace development. The terrace system and the previous pre-incision erosional and depositional surfaces are analyzed from a geomorphological point of view. The terrace system only develops within the soft Mio-Pliocene sedimentary fill of the graben, whilst upstream and downstream this zone the studied valleys develop important gorges (canyons) carved in the Cretaceous tablelands (Caroch Massif) and Mio-Pliocene deposits (Llanura Manchega). The geochronological control is established from 20 numerical ages obtained by different dating methods, such us Electron Spin Resonance (ESR), Optically Stimulated Luminescence (OSL) in detrital sequences and Th/U series in calcareous tufa deposits. Additionally, four K/Ar dates available for volcanic materials disrupting the upper and oldest terrace have been considered. A total of 14 terrace levels were identified between +130–135 m (T1) and +3–4 m (T14) of relative height above the river thalwegs. The T1 has an approximate age of c. 1.6–2.0 M.a. as indicate the age of the volcanic materials from the Agras Volcano intruded in the terrace, marking the onset of Quaternary fluvial dissection in the zone. The obtained geochronological data indicate that the Lower-Middle Pleistocene boundary is slightly above T6 (+60–65 m), which has an ESR age of 577 ± 43 ka. This terrace also documents the onset of the most important period of rise of the salt within the graben interfering drainage development. The geochronological data indicate the occurrence of a second eruptive event during the second half of the Middle Pleistocene related to the terraces T7 (+50 m) and T8 (+35–40 m), updating the volcanic activity in the zone. The beginning of the Upper Pleistocene is recorded by the top sequences of the T9 terrace (+25–30 m) where numerous OSL and Th/U data have been obtained with ages between ca. 105 and 81 ka (MIS 5). However, these young terraces (T8 to T13) are thickened (8–10 m) recording Middle Pleistocene sediments in their basal sequences with ages between ca. 193 and 137 ka (MIS 6). The study provides important data on valley evolution under the interference of volcanic activity, salt –related deformation (diapirism, solution subsidence) and fluvial incision fostered by the rise of the axial diapir (salt wall) protruding the graben since at least the Brunhes-Matuyama boundary. The analyzed fluvial evolution documents interesting cases of river capture, drainage antecedence and tectonic adaptation of the drainage

* Corresponding author.
E-mail addresses: pgsilva@usal.es (P.G. Silva), ftapias@usal.es (F. Tapias), j.elez@usal.es (J. Élez), elvira.roquero@upm.es (E. Roquero), fgutier@unizar.es (F. Gutiérrez), miren.delval@cenieh.es (M. del Val), franciscojose.perez@ulpgc.es (F.J. Perez-Torrado), jorge.giner@uam.es (J.L. Giner-Robles), davinia.moreno@cenieh.es (D. Moreno).

https://doi.org/10.1016/j.geomorph.2024.109066
Received 7 September 2023; Received in revised form 9 January 2024; Accepted 10 January 2024
Available online 22 January 2024

throughout the Quaternary Period. The paper also poses interesting geochronological data on the long-term Quaternary evolution of Mediterranean valleys in the Iberian Peninsula, poorly explored to the date.

1. Introduction

The Quaternary evolution of fluvial valleys in the Atlantic watersheds of the Iberian Peninsula is relatively well constrained thanks to the publication of numerous terrace dates during the last two decades. The published geochronological data comprise Optically Stimulated Luminescence (OSL), Electro Spin Resonance (ESR), and cosmogenic nuclides age determinations (e.g., Cunha et al., 2005, 2019; Benito-Calvo et al., 2008; Silva et al., 2017; Moreno et al., 2019; Karampaglidis et al., 2020). These numerical ages are also complemented with valuable information derived from Quaternary vertebrate fossil sites, as well as Acheulean and Mousterian sites (e.g., Silva et al., 2017; Santonja et al., 2016; Moreno et al., 2019; Méndez-Quintas et al., 2020). In contrast, knowledge on the evolution of most fluvial valleys in the Mediterranean watershed is rather limited, with most geochronological data related to the Ebro River and its northern and southern tributaries providing pictures of valley evolution for almost the whole Quaternary in NE Spain (e.g., Soria-Jáuregui et al., 2016; Whitfield et al., 2013; Sancho et al., 2020; Parés et al., 2021; Regard et al., 2021; Benito-Calvo et al., 2022). However, there is still a significant lack of geochronological data for the main Mediterranean fluvial systems located south of the Ebro River catchment, such as the Alfambra-Turia fluvial system (Gutiérrez et al., 2020) and the Júcar-Cabriel system, within the Iberian Chain (Fig. 1). Data from fluvial systems within the Betic Cordillera in SE Spain (Segura, Almazora, Guadalhorce, etc.) are still scarce and normally restricted to the last 50–60 ka (e.g., Santisteban and Schulte, 2007).

Data from the Atlantic rivers indicate that Quaternary valley development (i.e., fluvial entrenchment) started at ca. 1.8–2.0 Ma, around the Olduvai Subchron during the Gelasian as reported for the Tagus and Duero basins in Central Spain (Silva et al., 2017). However, in the Portuguese waterfront the headward-propagating fluvial incision in the Duero and Tagus basins started earlier, at around 3.3–2.4 Ma, as determined by different dating methods applied to several pre-incision surfaces (e.g., Cunha et al., 2019; Karampaglidis et al., 2020; Silva and Roquero, 2022). Nonetheless, fluvial entrenchment in the different river basins was a time-transgressive process, starting earlier in the south, such as in the Guadalquivir and Tagus drainage basins, with fluvial terraces at maximum relative height of +220 m and mean computed Gelasian ages of ca. 2.4 ± 0.26 Ma (Silva and Roquero, 2022). The onset of fluvial incision and terrace development occurred later in the northern sector, from the base of the Calabrian and after the Olduvai Subchron, with the formation of the highest terraces of the Duero and

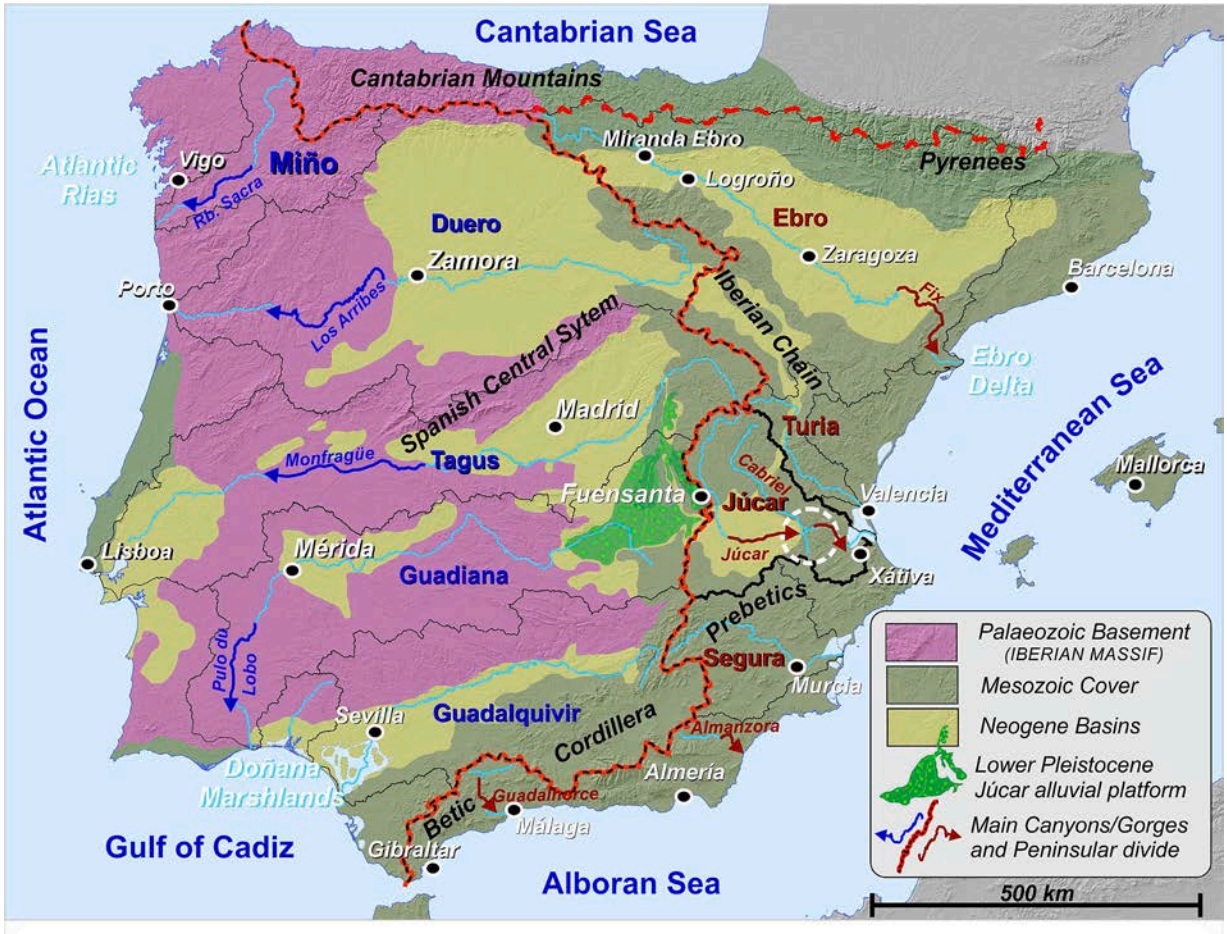

Fig. 1. Location of the Júcar-Cabriel Fluvial system and the study area (circle with dashed line) in relation to the Atlantic and Mediterranean drainage basins within the Iberian Peninsula. The Lower Pleistocene alluvial platform of the Júcar river is highlighted in green. Note the asymmetry between the Mediterranean and Atlantic catchments highlighted by the peninsular divide. (For interpretation of the references to colour in this figure legend, the reader is referred to the web version of this article.)

Miño (+150–145 m) at around 1.5–1.4 Ma (Silva et al., 2017; Méndez-Quintas et al., 2020). From this initial period, a total of 21 terrace levels were formed in the Tajo and 14 in the Duero, with the terraces at +75–70 m recording the normal Jaramillo Subchron (1.0–1.1 Ma), and the levels at +60 m the Brunhes-Matuyama reversal (0.78 Ma) (Moreno et al., 2012, 2019; Pérez-González et al., 2013; Baena et al., 2014; Silva et al., 2017). Subsequently, fluvial incision accelerated, especially after the Mid-Pleistocene Transition (MPT), generating deeply entrenched valleys flanked by escarpments (≥60 m high), locally with hanging tributary valleys and perched terraces (Silva, 2003; De Vicente et al., 2007). In the case of the Tagus drainage basin, with thick salt-bearing evaporite sequences in the central sector of the Madrid Cenozoic Basin, most of the terrace deposits display thickenings with growth stratal geometries and soft-sediment deformations attributable to syn-sedimentary dissolution-induced subsidence and paleoseismic activity, respectively (Silva, 2003; Silva et al., 2013). Here, the deposits of different terrace levels can be superimposed and bounded by angular unconformities, showing fill-inset relationships (Silva, 2003). These subsidence processes dominated terrace development from levels lying at +30–25 m, with a good geochronological control and relevant Palaeolithic and paleontological records spanning from the Marine Isotopic Stage MIS13 (ca. 500 ka) to the present (e.g. Silva et al., 2013; Baena et al., 2014; Santonja et al., 2016; Benito-Calvo et al., 2017; Panera et al., 2019; Méndez-Quintas et al., 2020). In these Atlantic valleys canyon formation is only significant in sectors underlain by resistant lithologies, located between the Portuguese zone with the Cenozoic sedimentary basins currently dissected and drained by the main fluvial systems. This is the case of *"La Ribera Sacra-Sil Canyons"* in the Miño Valley (Viveen et al., 2012), *"Los Arribes Canyon"* in the Duero River (Rodríguez-Rodríguez et al., 2022), the *"Monfragüe Gorge"* in the Tagus Valley (Goy et al., 2020), or the *"Pulo do Lobo Gorge"* in the Guadiana Valley (Ortega-Becerril et al., 2018). In all these cases, the valley is deeply entrenched into metamorphic and igneous rocks of the Palaeozoic Iberian Massif, coinciding with substantial knickpoints along the river longitudinal profiles (Fig. 1).

Data from the Mediterranean watershed is mainly available for the Ebro River, with the oldest terraces around Logroño lying at +200 m and with an age of 2.8 ± 0.7 Ma estimated by ^{10}Be cosmogenic dating (Regard et al., 2021). The most complete terrace sequence of the Ebro River was dated by Benito-Calvo et al. (2022) applying ESR, OSL and TCN protocols. These authors identified 22 terrace levels between +203 m and +4–5 m along the upper and medium reaches of the Ebro River, always within the domain of the dissected Ebro Cenozoic Basin (Fig. 1). In this zone, the highest dated fluvial terrace is the Early Pleistocene level at +166 m (T3) for which ages range between 1.18 ± 0.05 (ESR) and 1.26 ± 0.16 Ma (TCN). These authors indicate that assuming erosion rates commonly considered for the Ebro catchment, the maximum burial cosmogenic age would result in an older age of 1.6–2.8 Ma. ESR dates for lower terrace levels between +90 and +80 m place their formation around 1.1 and 0.9 Ma (Parés et al., 2021; Benito-Calvo et al., 2022).

Works integrating geochronological data from the Pyrenean tributaries of the Ebro River (e.g., Sancho et al., 2020; Regard et al., 2021) differentiate five main groups of terraces with average ages of 2.8 ± 0.7 Ma (T1 + 200 m), 1.15 ± 0.15 Ma (T2 + 180–150 m), 850 ± 70 ka (T3 + 140–100 m), 650 ± 130 ka (T4 + 100–70 m) and 400 ± 120 ka (T5 + 50–60 m). In contrast, Benito-Calvo et al. (2022) indicate in the upper reaches of the Ebro the +60–65 m terrace is close to the Brunhes-Matuyama boundary (ca. 780–717 ka), suggesting more rapid incision in the Pyrenean tributaries. The rest of the Middle to Late Pleistocene terrace sequence of the Ebro River and tributaries (synthetized by Lewis et al., 2009, 2017; Soria-Jáuregui et al., 2016; and Benito-Calvo et al., 2022) present always older ages than those of the Atlantic watersheds for similar relative heights.

For similar relative heights the Lower Pleistocene terraces (>+90 m) in the Ebro Basin are relatively younger than those in the valleys of the Atlantic catchment as derived from the works by Silva et al. (2017) and Benito-Calvo et al. (2022). However, data from these authors also indicate that this situation is reversed from the MPT (ca. 1.1–0.8 Ma), since Middle to Upper Pleistocene terraces down to +70–65 m in the Ebro Basin are gradually older than those Atlantic watersheds. This variable trend suggests renewed uplift in the Atlantic margin during the Late Quaternary, whilst uplift was progressively attenuated in the Mediterranean watershed from the Middle Pleistocene. In this sense, the Ebro River basin is the oldest and most mature fluvial catchment in the Iberian Peninsula (Struth et al., 2019), connected with the Mediterranean Sea before the MSC, as early as the late Tortonian >5.9 Ma ago (García-Castellanos et al., 2009; García-Castellanos and Larrasoaña, 2015). Several authors have considered isostatic rebound related to erosional unloading as the main driving mechanism for fluvial incision and topographic development in the Ebro Basin (García-Castellanos and Larrasoaña, 2015; Lewis et al., 2017; Benito-Calvo et al., 2022). These authors also indicate that uplift *persisted during the development the early Quaternary terraces increasing* eastwards towards the lower catchment of the basin, where the Ebro River cuts across the Catalan Coastal Ranges along 50 km to flow into the Mediterranean Sea. There, the Ebro River displays a case of gorging (Mequinenza-Flix Canyon) like those of the Atlantic rivers (Fig. 1) but apparently excavated before the Pliocene. On the contrary, cases of gorging for the Atlantic rivers seems to occur from the middle Pliocene onwards (<3.5 Ma) as indicated by Cunha et al. (2019) and Karampaglidis et al. (2020). This seems be also the case south of the Ebro River catchment, where several younger and smaller basins present important gorges before their coastal outlets (i.e., Júcar-Cabriel, Almanzora and Guadalhorce Fig. 1). Palaeogeographical numerical models for the Guadalhorce Basin indicate that fluvial incision and gorging were certainly triggered by the MSC (Elez et al., 2016, 2020). Nevertheless, geochronological data on fluvial terraces for the Mediterranean watersheds south to the Ebro is practically absent. Only there are fragmentary chronological data for small rivers located in the Eastern Betic Cordillera (Almanzora and Aguas-Feos rivers in Almería) or some isolated dates for the rest (e.g., Stokes and Mather, 2003; Santisteban and Schulte, 2007; Schulte et al., 2008a). The chronological data for these fluvial systems are mainly radiocarbon dates covering the last ca. 50 ka (Silva et al., 2021), which is an insufficient time span to analyse long-term fluvial evolution in southeast Spain. The studied Júcar Basin has the particularity that during the Lower Pleistocene it formed part of both the Atlantic and Mediterranean catchments. This stage is featured by a large alluvial plain developed in the former water divide between the Guadiana and the Júcar basins, and currently perched above the Jucar River between +100–110 m (apex) and +60 m (distal zone) (Fig. 1). During the final stages of the Lower Pleistocene, the eastern portion of the alluvial plain (a large alluvial fan with multiple distributary channels) was captured by the Júcar, whilst the rest of the channel system was integrated in the upper catchment of the Guadiana River draining towards the Atlantic (Pérez-González, 1994). At present this relict alluvial platform constitutes the water divide between the Guadiana and the Júcar basins (Fig. 1).

This study documents the terrace sequence of the middle reach of the Júcar River in its confluence zone with the Cabriel River, within the northern sector of the N-S Ayora-Cofrentes Neogene Graben (Figs. 1 and 2). Here, both rivers flow eastwards, from the Plio-Quaternary plains of the Llanura Manchega towards the Mediterranean coast. Within the Ayora-Cofrentes graben, which is intruded along its axis by an elongated salt diapir (i.e., salt wall) of Triassic evaporites, these drainages locally show N-S oriented reaches. Both rivers flow along deeply entrenched canyons (~200–300 m deep) upstream of the graben, and downstream the Júcar River has excavated a remarkable canyon 400–500 m deep dissecting the El Caroch tablelands, underlain by folded Mesozoic carbonate formations truncated by a planation surface (Fig. 2). Well-preserved terrace sequences only occur on the easily erodible and locally soluble bedrock of the graben, including Neogene continental sediments and Triassic evaporitic formations of the salt wall. Here, the

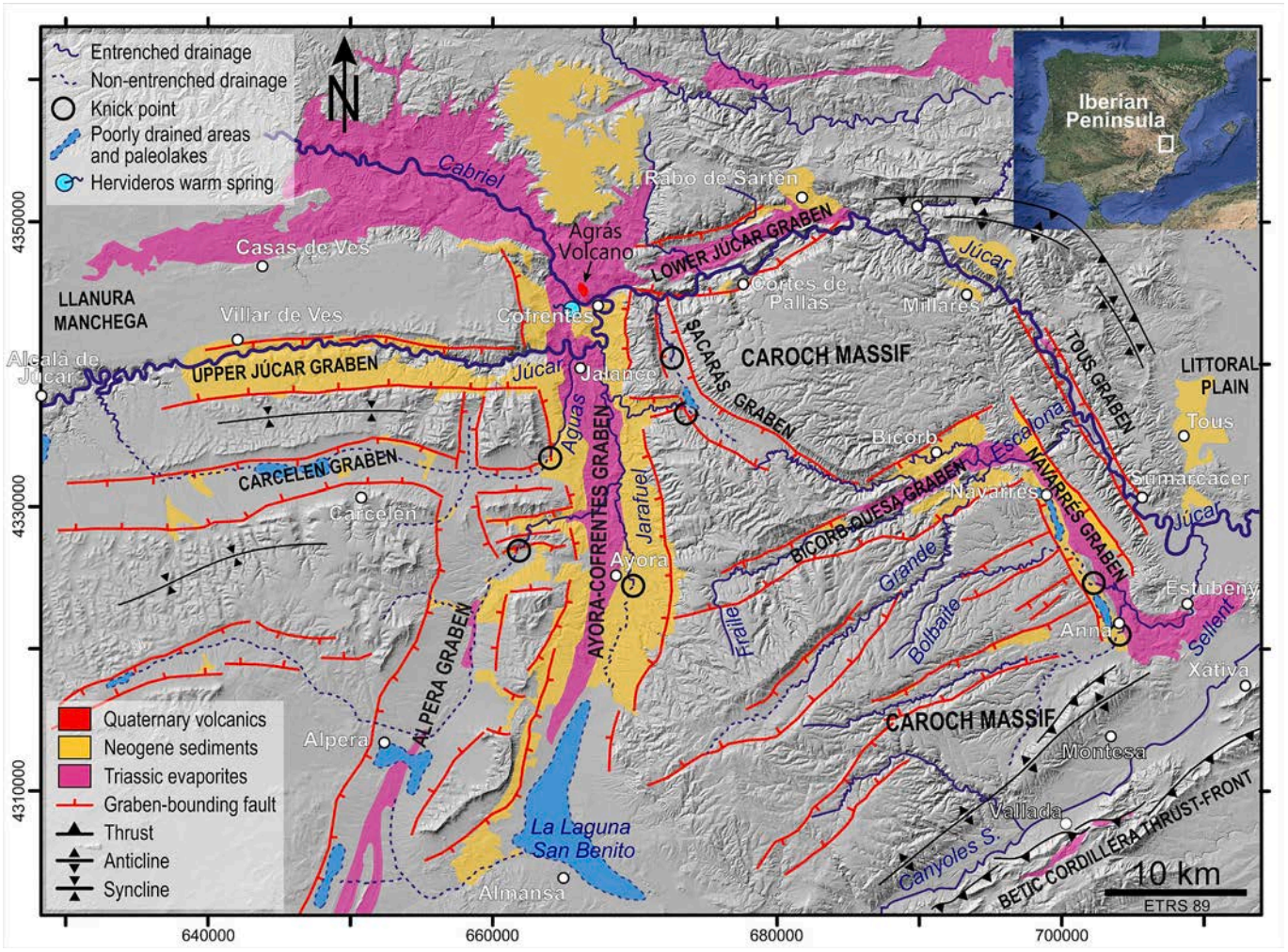

Fig. 2. Morpho-structural sketch on shaded relief model of the Caroch Massif region depicting the distribution of post-orogenic grabens, Neogene graben-fill sediments, outcrops of Triassic evaporites (Keuper facies), the main drainage network (entrenched and non-entrenched), knickpoints and poorly- or internally-drained areas.
(Modified from Gutiérrez et al., 2019).

evolution of the fluvial system and its incision patterns are influenced by external factors such as climate, diapirism, evaporite-dissolution subsidence, volcanism, and neotectonics. The studied terrace sequence displays a staircase of 14 levels situated at relative heights between +135 m and +4–5 m. This work includes 12 novel numerical ages from selected terraces determined by ESR, OSL and U/Th. This chronological data is complemented by previously published K/Ar dates of volcanic materials that disturb the uppermost terrace (Sáenz-Ridruejo and López-Mariñas, 1975; Silva et al., 2015). Understanding incision mechanisms and patterns have important implications for unravelling the interplay between landscape evolution, climate change, and the abovementioned external controls. The integrated analysis of pre-incision geomorphic surfaces and terrace levels provides an interesting case study illustrating fluvial superposition and antecedence in the Mediterranean catchments of the Iberian Peninsula. Since fluvial incision has been shown to be a good approximation for crustal uplift in numerous areas (e.g., Burbank and Anderson, 2001), a link has been proposed between accelerated river incision (and erosion) and the change to the more intense climate cycles (100 ka) after the MPT (Bridgland and Westaway, 2008; Westaway et al., 2009). These links consider river incision as a fluvial response to the isostatic rebound induced by erosional unloading of rivers, as illustrated by the Mediterranean river basins in the Eastern Betic Cordillera (Elez et al., 2020). These feedbacks will be explored in relation with the probable impact of the MSC base-level drop and the early development of the Upper and Lower Júcar Canyons, the last around 20 km away for the present Mediterranean coast. The results are used to discuss the differences in the evolution of the Atlantic and Mediterranean fluvial valleys of the Iberian Peninsula.

2. Geological and geomorphological framework

The investigated area is located in eastern Spain (Caroch Massif physiographic region), at the transition zone between two Alpine orogens; the intraplate Iberian Chain to the north and the external zone of the Betic Cordillera to the south (External Prebetics). It also lies east of the Llanura Manchega plains, mainly underlain by Plio-Quaternary continental carbonates (Santisteban et al., 1990; Gutiérrez et al., 2019; Fig. 2). This region is designated as the “fractured Betic foreland” (Santisteban et al., 1990), and has been traditionally defined as the Valencian Domain or the External Prebetics (Vera, 1983). According to Roca et al. (2013, 2021), the Caroch Massif is the outermost unit of the eastern Betic Cordillera, corresponding to a thrust sheet made up of a 1.2–1.5 km thick Jurassic-Late Cretaceous carbonate-rich succession detached along Triassic evaporites of the Keuper facies. These formations record two main deformation phases (Vera and Martín-Algarra, 2004; Gutiérrez et al., 2019): (1) compression during the orogenic stage, related to the N-S to NNW-SSE convergence and collision between the Iberian and African plates; and (2) post-orogenic extension resulting in

the development of a polygonal system of Neogene grabens. A number of these grabens display along their axis exposed salt walls (passive diapirism), some of them with clear evidence of Quaternary activity (e.g., Martínez del Olmo et al., 2015; Gutiérrez et al., 2019 and references therein).

The thick Mesozoic succession overlying the Triassic evaporites mainly consists of carbonates locally affected by low-amplitude buckle folds with prevailing NW-SE trend. The general tabular structure and topography of the Mesozoic limestone outcrop is disrupted by grabens up to 40 km long with various orientations (N-S, E-W, NW-SE) and orthogonal arrangement in the analyzed area (Martínez del Olmo et al., 2015; Gutiérrez et al., 2019; Fig. 2). Some of these grabens include a significant Neogene continental fill intruded by elongated diapirs (salt walls) with prominent geomorphic expression along their axes, which split the basins into two half-grabens, as is the case of the Ayora-Cofrentes, Bicorb-Quesa, Navarrés basins (Fig. 2; Roca et al., 2013; Gutiérrez et al., 2019). At the edges of the salt wall exposures, the upturned Mesozoic and Miocene sediments (i.e., flaps) typically display steep dips away from the diapiric extrusions and may be even overturned (Santisteban et al., 1990). Other graben-basins remain undissected, lack exposures of diapiric Triassic materials and do not show a significant Neogene fill (Fig. 2). The basin-bounding normal faults may reach throws higher than 1000 m and the Mesozoic succession rests unconformably on a faulted Palaeozoic basement as revealed by geophysical surveys (e.g., Rubinat et al., 2010; Roca et al., 2013, 2021). Deep-seated normal faulting rooted in the Palaeozoic basement participates in the formation of the N-S Ayora-Cofrentes Graben and the development of the associated salt wall. Basement faults were already active during the Mesozoic sedimentation is indicated by substantial thickness changes of some units across the graben (Roca et al., 2021). These structures have also guided the Quaternary volcanism disrupting the upper terrace sequences around the Júcar-Cabriel junction area near the locality of Cofrentes (Sáenz-Ridruejo and López-Mariñas, 1975; Silva et al., 2015).

The diapiric evaporites correspond to the Upper Triassic Keuper facies, with an original thickness of around 600–700 m in the area (Suárez Alba, 2007). It comprises five lithostratigraphic units (K1 to K5), described in outcrops and in oil-exploration wells (Carcelén-1; Fig. 2) (Ortí, 2004; Suárez Alba, 2007). They can be grouped into two evaporitic sections (K1 and K4-K5) with an interbedded clastic interval (K2−K3) consisting of sandstones and shales. At Carcelén-1 borehole, located on the western margin of the Ayora-Cofrentes Graben, halite has an aggregate thickness of 325 m within an Upper Triassic succession 650 m thick. Close to the surface, halite raised by diapiric activity has been removed by subsurface dissolution, involving the near-surface condensation of the stratigraphic succession and subsidence in the overlying sediments (Gutiérrez et al., 2019).

The Keuper evaporites functioned as a major detachment, decoupling the deformation between the basement and the overburden, affected by thin-skinned extensional tectonics accommodated by the development of grabens. These basins are filled by Mio-Pliocene terrestrial sediments dominated by detrital facies capped by lacustrine limestones (Santisteban et al., 1990; Silva et al., 2015; Fig. 2). These uppermost limestones merge to the west with the Plio-Quaternary limestones of the LLanura Manchega plains, which contain numerous Ruscinian and Villafranchian mammal fossil sites (e.g., Alcalá et al., 1985; Alberdi et al., 1997). Late Tortonian estuarine deposits with littoral foraminifera are restricted to the NE sector testifying the early occurrence of ria environments around the Lower Jucar Canyon (Lendínez and Tena, 1980; Silva et al., 2015 The sparse outcrops of these littoral sediments are presently about 560 (Los Millares) and 600 m (Castil-Blanques) above the present sea-level between 80 and 130 km away from the present coastline. Similar elevation values present the Late Tortonian littoral sediments in the Guadalhorce Basin (Elez et al., 2016). Applying eustatic and isostatic corrections to the present elevation of the littoral Tortonian sediments imply a regional uplift of ~450–500 m across the Mediterranean waterfront for the last ca. 5.5 Ma (Elez et al., 2016, 2020). Following these authors accelerated uplift triggered by the MSC allowed enhanced fluvial dissection in the Mediterranean waterfront during Plio-Quaternary times. Eventually, some endorheic basins were captured by the external drainage network, leading to the dissection of the sedimentary fill of the basins by new drainages and the excavation of deeply entrenched limestone canyons upstream and downstream of the study area.

The headward-propagating incision wave has not reached yet some basins, which remain undissected and essentially preserve a late Neogene landscape, as occurs in the Carcelén, Alpera, and Las Rochas grabens west of the Ayora-Cofrentes Graben. A similar situation is found in the southern sector of the latter graben, which remains as an internally drained area with a desiccated paleolake known as La Laguna (Gutiérrez et al., 2019) (Fig. 2). The regional morpho-structural framework indicates that fluvial incision has propagated southwards and westwards from the Júcar River, mainly through headward migration of knickpoints in longitudinal drainages entrenched within the grabens (Gutiérrez et al., 2019). Incision in these drainages has propagated about 80–100 km upstream from the ancient outlet of the Júcar River in the Mediterranean. This long-term incision wave has determined a time-transgressive change in the morpho-sedimentary behaviour of the grabens during the Quaternary. It changed over the last 1.5–2.0 Ma from relatively stable relict landscapes to landscapes rejuvenated by aggressive fluvial entrenchment and canyon formation. Through this process, differential unloading related to fluvial erosion locally favored salt flow in the salt walls within the grabens, generating local deformations in Quaternary terraces. Similar processes have been described and dated in the nearby Navarrés Graben (Gutiérrez et al., 2019; Fig. 2).

The Mesozoic limestone tablelands on both sides of the Ayora-Cofrentes Graben display an extensive planation surface (S_0) cut across folding structures. This erosional surface predates both extensional tectonics (grabens) and river incision. In the study area, the top of the sedimentary fill of the grabens, consisting of Plio-Quaternary lacustrine limestones, define a younger aggradational surface S_1 inset into the planation surface S_0. This latter surface seems to be deformed by a domal flexure, showing regional slopes to the north, east, south and west, where it is overlapped and buried by the Pliocene limestones (S_1) of the Llanura Manchega plains that feature central Spain (Fig. 2). This is the so-called Pliocene "Páramo surface", which largely pre-dates river incision in central Spain (e.g., Pérez-González, 1994; Silva et al., 2017). The radial decline of the surface S_0 occurs around the junction area of the Júcar and Cabrial valleys, in the northern sector of the Ayora-Cofrentes Graben, near the locality of Cofrentes (Fig. 2). This is also the location where volcanic activity has occurred in the Quaternary (Sáenz-Ridruejo and López-Mariñas, 1975; Ancochea and Huertas, 2002; Carner, 2001; Silva et al., 2015). In the Neotectonic Map of Spain this is considered a case of doming and associated deep-seated faulting facilitating the rise of magma from the asthenospheric mantle (Baena et al., 1991).

3. Methods

Geological-geomorphological mapping was carried out through the interpretation of aerial photographs, orthoimages and shaded relief models derived from digital elevation models with 5 m and 1 m horizontal resolution. Detailed field surveys were carried out in the region to check and refine the preliminary maps produced with remotely sensed data. Selected outcrops were cleaned by hand and basic stratigraphic and sedimentological features were analyzed before the selection of the best points for geochronological sampling. Where existing, soil textural properties were described and relevant soil horizons sampled for conventional laboratory analyses. Key outcrops and sampling points were located using GPS devices and digital maps uploaded in digital tablets with GPS sensor (horizontal accuracy ~3 m). A total of 14 samples were

dated by Optically Stimulated Luminescence (OSL), plus three samples from old terraces above +50 m by Electron Spin Resonance (ESR), and two complementary samples from calcareous tufa deposits of the lower terraces (+15 m and +20–25 m) by means of U-series. All samples were processed in the Geochronological Laboratories of the *"Centro Nacional de Investigación sobre la Evolución Humana"* (CENIEH Lab.; Burgos, Spain). Only one OSL sample was processed in the CITIUS OSL Lab of the University of Sevilla, following similar protocols to those of the CENIEH (Table 1). In the following subsections we describe the basic protocols of the different dating methods used to establish the geochronological scheme of the terrace sequence. More detailed explanations on the dating protocols of the CENIEH are given in Duval et al. (2017) and Moreno et al. (2021).

3.1. Optically Stimulated Luminescence (OSL) and Electro-Spin Resonance (ESR)

Samples for OSL and ESR dating were collected from fluvial deposits following the standard procedure, by hammering a light-tight PVC tube into the selected sections. In situ gamma dose rate measurements were performed using a CANBERRA portable gamma spectrometer with an InSpector 1000 analyzer, and additional bulk sediment samples were collected from the same sampling point for laboratory dose rate analysis and moisture-content estimates. Samples for OSL and ESR dating were prepared following standard procedures under red light conditions to avoid signal depletion.

Luminescence measurements were carried out by a Risø TL/OSL DA20 reader equipped with bialkali EMI 9235QB15 photomultiplier tubes, a 90Sr/90Y beta source (dose rate of ~0.10 Gy/s) and a blue light of 470 nm for stimulation. The Single Aliquot Regenerative-dose (SAR) protocol (Murray and Wintle, 2000) was performed on 24 multi-grain (MG) aliquots for OSL dose evaluation (see SAR protocol in SI Table S2). A preheat temperature of 220/240 °C was selected after a Preheat-Plateau test. Dose recovery tests with the selected temperature were performed. Infrared (IR) depletion assessments were conducted and no detectable IRSL signal was observed. Acceptance criteria for Equivalent Dose (D_e) determination of OSL measurements included IR depletion ratio (<10 %), recycling ratio (<10 %), recuperation (<10 %), sensitivity change (<10 %), and natural normalized signal (Lx/Tx) above saturation of the dose response curve (DRC: $D_e < 2 * D0$) (Murray and Wintle, 2000). Rejected D_e values were discriminated using Analyst 4.57 (Duller, 2015). An interpolation of the natural sensitivity-corrected signal (Lx/Tx) onto the dose response curve (DRC) fitted using a sum of two exponential functions. Final D_e values were estimated following the Central Age Model (CAM) (Duller, 2008; Galbraith and Roberts, 2012) for samples with low overdispersion (OD) values (<20 %) and the Minimum Age Model (MAM, Galbraith and Roberts, 2012) was applied on samples with high OD values. The latter ages should be considered as minimum age estimates for the time of sediment accumulation. OSL results for the 13 dated samples are displayed in Table 1. D_e distribution (displayed as weighted histograms and radial plots), decay curves and dose response curves are presented in Fig. S1 (Supplementary material).

To estimate the ESR Equivalent Dose (D_e), the Multiple Aliquots Additive (MAA) dose and the Multiple Center (MC) approaches (Duval et al., 2015; Tissoux et al., 2007; Toyoda et al., 2000) were applied to all samples. Each sample was divided into 10 multiple-grains aliquots. Eight of these aliquots were irradiated with a calibrated Gammacell-1000 ^{137}Cs gamma source from 150 to 15,000 Gy following a sub-exponential dose step distribution. For each sample, one aliquot was preserved (natural) and one aliquot was optically bleached for ~1500 h using a SOL2 (Dr. Hönle) solar light simulator, to evaluate the ESR intensity of the non-bleachable residual signal associated to the Aluminum center of quartz (Voinchet et al., 2003). Dose rate values were obtained from a combination of in situ and laboratory analyses. ESR measurements were taken at low temperature (90 K), using a nitrogen gas flow system connected to an EMXmicro 6/1 Bruker X-band ESR spectrometer. The angular dependence of the ESR signal on sample heterogeneity was taken into account by measuring all aliquots three times after successive ~120° rotations in the cavity. Furthermore, the data reproducibility was verified by running ESR measurements over different days. The Equivalent Dose (D_e) values were calculated with the software Microcal Origin 8.5 using the Levenberg-Marquardt algorithm, by chisquare minimization. For the Al center, a single saturating exponential + linear function (SSE + LIN) (Duval et al., 2009) was fitted through the experimental points. For the Ti centers, the Ti-2 function (Woda and Wagner, 2007) was used. With the SSE + LIN function, data were weighted by the inverse of the squared ESR intensity ($1/I^2$), whereas with the function Ti-2, data were weighted by the inverse of the squared error ($1/s^2$). Results are showed in Table 2. Dose Response Curves are summarized in Figs. S2, S3 and S4 in Supplementary Information.

Dose rate and OSL and ESR age calculations were performed with DRAC v1.2 (Dose Rate and Age Calculator, Durcan et al., 2015), using U, Th and K concentrations of the raw sediment determined by gamma spectrometry and/or ICP-MS/OES analyses, and gamma dose rate derived from in situ gamma measurements, and the following parameters: dose rate conversion factors from Guérin et al. (2011), alpha and beta grain size attenuation factors from Brennan et al. (1991) and Guérin et al. (2012), respectively, water content attenuation from Aitken and Xie (1990), and etching attenuation factors from Brennan (2003) and Grün (1994). Cosmic dose rate was calculated following the works of Prescott and Hutton (1994) considering depth, altitude, longitude and latitude. Long-term water content was based on the present-day content measured for each sample and with an associated absolute error of ±10

Table 1
Summary of the OSL results on quartz grains (90–125), including the number of aliquots that passed acceptance criteria (n), Overdispersion (OD), applied age model, corresponding Equivalent Dose (De) value, Total dose rate, and calculated age. CAM = Central Age Model; MAM = Minimum Age Model. Extended dosimetry data is included in SI Table S1. For location of samples see Figs. 4 and 6.

Lab. Code (Terrace)	# discs (n)	OD (%)	Age model	D_e (Gy)	Total dose rate (Gy/ka)	Age (ka)
C-JU-OSL1 (T9 Alluvial)	22	15	CAM	87.4 ± 2.9	1.3 ± 0.1	67.7 ± 4.2
C-JU-OSL2 (T9 Alluvial)	22	15	CAM	79.5 ± 2.6	1.5 ± 1.5	54.7 ± 3.2
C-JU-OSL3 (T9 Top)	21	13	CAM	106.3 ± 3.2	1.0 ± 0.1	106.0 ± 7.1
C-JU-OSL4 (T10 Top)	19	10	CAM	203.6 ± 5.5	1.1 ± 0.1	193.4 ± 12.0
C-JU-OSL5 (T11 Base)	20	10	CAM	162.0 ± 3.9	1.4 ± 0.1	117.5 ± 6.8
C-JU-OSL6 (T11)	19	19	CAM	235.8 ± 11.6	1.4 ± 0.1	167.9 ± 11.6
C-JU-OSL7 (T11 Top)	22	12	CAM	101.3 ± 2.9	0.9 ± 0.1	117.0 ± 8.3
C-JU-OSL8 (T8 Base)	22	11	CAM	318.5 ± 9.1	1.8 ± 0.1	177.9 ± 9.7
C-JU-OSL9 (T6 Alluvial)	20	45	MAM	132.6 ± 8	1.8 ± 0.1	75.9 ± 5.7
C-JU-OSL10 (T7 Alluvial)	22	16	CAM	369.2 ± 17.4	2.8 ± 0.1	133.9 ± 8.2
C-CA-OSL1 (T12)	21	18	CAM	173.2 ± 8.3	2.2 ± 0.1	80.3 ± 5.2
C-JU-OSL11 (T13)	20	12	CAM	70.7 ± 2	1.0 ± 0.1	72.0 ± 4.9
C-JU-OSL12 (T12)	22	19	CAM	105.4 ± 4.5	0.8 ± 0.1	137.0 ± 10.9
CITIUS-OSL20 (T11 Top)	–	–	MAN	90.4 ± 0.6	1.1 ± 0.1	82.0 ± 5.2

Table 2
ESR (Electro-spin Resonance) results obtained on quartz grains for the Júcar and Cabriel rivers. (Bl: bleaching; Dint: internal dose rate; Dα: alpha dose rate; Dβ: beta dose rate; Dγ: gamma dose rate; Dcos: cosmic dose rate; D: total dose rate; DE: equivalent dose).

Laboratory determinations	*Júcar river*		*Cabriel river*
	T11 (+25–30 m)	T6 (+60–65 m)	T7 (+50–55 m)
	C-JU-ESR1	C-JU-ESR2	C-CA-ESR1
D_{int} (μGy/a)	50 ± 30	50 ± 30	50 ± 30
D_{α} (μGy/a)	23 ± 6	28 ± 6	36 ± 8
D_{β} (μGy/a)	571 ± 12	874 ± 21	911 ± 20
D_{γ} (μGy/a)	287 ± 53	477 ± 66	612 ± 72
D_{cos} (μGy/a)	95 ± 10	67 ± 7	194 ± 19
Bl (%)	50.3 ± 0.3	57.8 ± 0.4	46.8 ± 1.1
D (μGy/a)	1026 ± 63	1496 ± 76	1803 ± 83
D_E (Gy) Al	459 ± 28	844 ± 26	738 ± 42
D_E (Gy) Ti-Li D option	437 ± 27	882 ± 67	664 ± 53
D_E (Gy) Ti-H C option	185 ± 18	–	394 ± 47
Age (ka) Al	447 ± 39	**564 ± 33**	**409 ± 33**
Age (ka) Ti-Li D option	426 ± 37	**550 ± 54**	**368 ± 34**
Age (ka) Ti-H C option	**180 ± 21**	–	218 ± 34

Reported as maximum values.

%. Extended dosimetry information is included in SI Table S1 and S3. Age estimates are given at 1σ error margin.

3.2. Uranium – Thorium series (U/U)

Two samples of calcareous tufa deposits were collected for U-series dating to complement and cross-check ages obtained by OSL. Sampling in the laboratory was conducted using a micro-drill with a tungsten carbide tipç. The isotopic measurements were carried out with a Multicollector Inductively Coupled Plasma Mass Spectrometer (MC ICP-MS Thermo NEPTUNE equipment). Multiple measurements were carried out to obtain the isotopic ratios $^{234}U/^{238}U$, $^{235}U/^{238}U$, $^{236}U/^{238}U$, $^{229}Th/^{232}Th$, $^{130}Th/^{232}Th$ by the standard bracketing method with errors below 5 %. The concentrations of ^{238}U and ^{232}Th were determined by the isotopic dilution mass spectrometry (IDMS) method. Age estimates have been derived using the general equation of radioactive decay (Cheng et al., 2013) and corrected following the approach proposed by Ivanovich and Harmon (1992) (Table 3). Since the tufa samples cannot be considered perfectly closed systems, the obtained corrected ages should be considered as rough or minimum age estimates for the sampled carbonate deposits. Consequently, the incision or deformation rates derived from them are reported as maximum values.

4. Morpho-structure of the studied area: the Ayora-Cofrentes Graben

The N-S-trending Ayora-Cofrentes Graben constitutes a 46 km-long depression of tectonic origin, developed between the localities of Cofrentes (North) and Almansa (South). The depression can be divided into two sectors with contrasting landscape related to different river entrenchment and fluvial evolution (Fig. 2): (1) A northern sector around the localities of Cofrentes and Jalance, in which the graben is deeply entrenched by the Júcar River and its tributaries (e.g., Cabriel, Jarafuel, Cautabán). Here, a prominent salt wall intrudes a thick (~300 m) Mio-Pliocene fill dominated by alluvial facies capped in the western sector by Plio-Quaternary lacustrine limestones (Lendínez and Tena, 1980). (2) A southern sector south of Jalance and Ayora, where the graben floor is poorly dissected by the drainage network and mantled by Quaternary alluvial deposits interrupted along the axis by inliers of Triassic evaporites and deformed Neogene detrital deposits (Gutiérrez et al., 2019). In the southernmost sector around Almansa, the graben floor remains as an internally drained area with mantled pediments that grade into a large lacustrine area desiccated during historical times and locally known as Laguna de San Benito (Lendínez and Tena, 1980). This type of undissected landscape also occurs in the graben depressions located on the western margin of the Ayora-Cofrentes Graben south of Jalance (Fig. 2). The boundary between undissceted and entrenched areas is marked by headcuts (i.e., knickpoints) in the longitudinal streams of the graben depressions (Fig. 3).

North of Jalance the grabens are dissected by canyons deeply incised into the Mesozoic bedrock, as is the case of the Cabriel and Upper and Lower Júcar canyons (Fig. 2). The studied zone is confined to the northern sector of the Ayora-Cofrentes Graben, where fluvial terrace development was facilitated by the presence of easily erodible bedrock, including Triassic evaporites and shales and Miocene detrital sediments. In this northern sector only the graben-basins of Sacarás and Cortes de Pallás are poorly dissected (Fig. 2). These constitute deep and flat-floored graben depressions in Cretaceous limestones, which floor is mantled by strongly cemented early Quaternary alluvial deposits and perched about 150–200 m above the Lower Júcar Canyon (Lendínez and Tena, 1980; Silva et al., 2015). These perched basins might represent pristine stages of fluvial dissection during the earliest Quaternary or maybe inherited and exhumated from previous stages during the late Neogene (e.g., Ruscinian: Micromammal Biozone MN16; Silva et al., 2015). In any case, they can be interpreted as "straved graben basins" with limited sedimentation generated in the early stages of drainage development in the zone.

Within the graben, the N-S oriented diapir splits the basin into two growth half grabens with a Mio-Pliocene fill ~450–600 m thick dominated by alluvial facies (Gutiérrez et al., 2019; Roca et al., 2021). The Júcar River crosses transversally the salt wall through a tortuous E-W oriented gorge near Jalance (Jalance Gorge; Fig. 4). The 14 terrace levels mapped and analyzed in this work occur in this sector, associated with the diapir. On the western flank of the salt wall, both the Triassic evaporitic formations and the Neogene detrital succession are capped by lacustrine Pliocene limestones, forming elongated mesas (S_1) around 300 m above the Júcar River (e.g., Mesa Star; Figs. 4 and 5). In this intersection zone between the N-S trending Ayora-Cofrentes Graben and the E-W oriented Upper Júcar Grabens, these Pliocene limestones and their correlative marginal detrital facies overlap the main basin-bounding fault of the Ayora-Cofrentes Graben (Rincon de Cecilia Fault; Figs. 4 and 5) to the west and penetrates the into the Upper Júcar entrenched graben (i.e., limestones post-date the youngest activity of the fault) (Lendínez and Tena, 1980; Santisteban et al., 1990). Within the Ayora-Cofrentes Graben the aggradational surface defined by the top of the lacustrine limestones (S_1) is preserved as perched mesas on both sides of the Júcar Canyon (Fig. 4). To the SW of Cofrentes, the Pliocene

Table 3
Th/U Measurements and age estimates obtained from the analyzed tufa samples within the Júcar Valley. Bracketed values indicate the 2σ uncertainty. Decay constants used in the calculations: λ238 = 1.55125 × 10^{-10}; λ234 = 2.82206 × 10^{-6}; λ230 = 9.1705 × 10^{-6}.

Lab. Code (Terrace)	[μgg^{-1}]	Th [μgg^{-1}]	$^{230}Th/^{232}Th \times 10^{-6}$ [at/at]	$\delta^{234}U$ [meas]	$\delta^{234}U_{init}$ [calc]	$^{230}Th/^{238}U$ [act/act]	^{230}Th [yr]	^{230}Th corr Age [kyr]
C-JU-SU-1	0.359	0.044	140 (1)	709	918	1.056	96,222	**91,715 ± 4.85**
T9 + 25–30 m	(0.003)	(0.003)		(3)	(18)	(0.003)	(4811)	
C-JU-SU-2	0.552	0.098	113 (1)	752	1019	1.214	114,640	**107,494 ± 0.64**
T12 + 12–15 m	(0.003)	(0.004)		(2)	(30)	(0.003)	(685)	

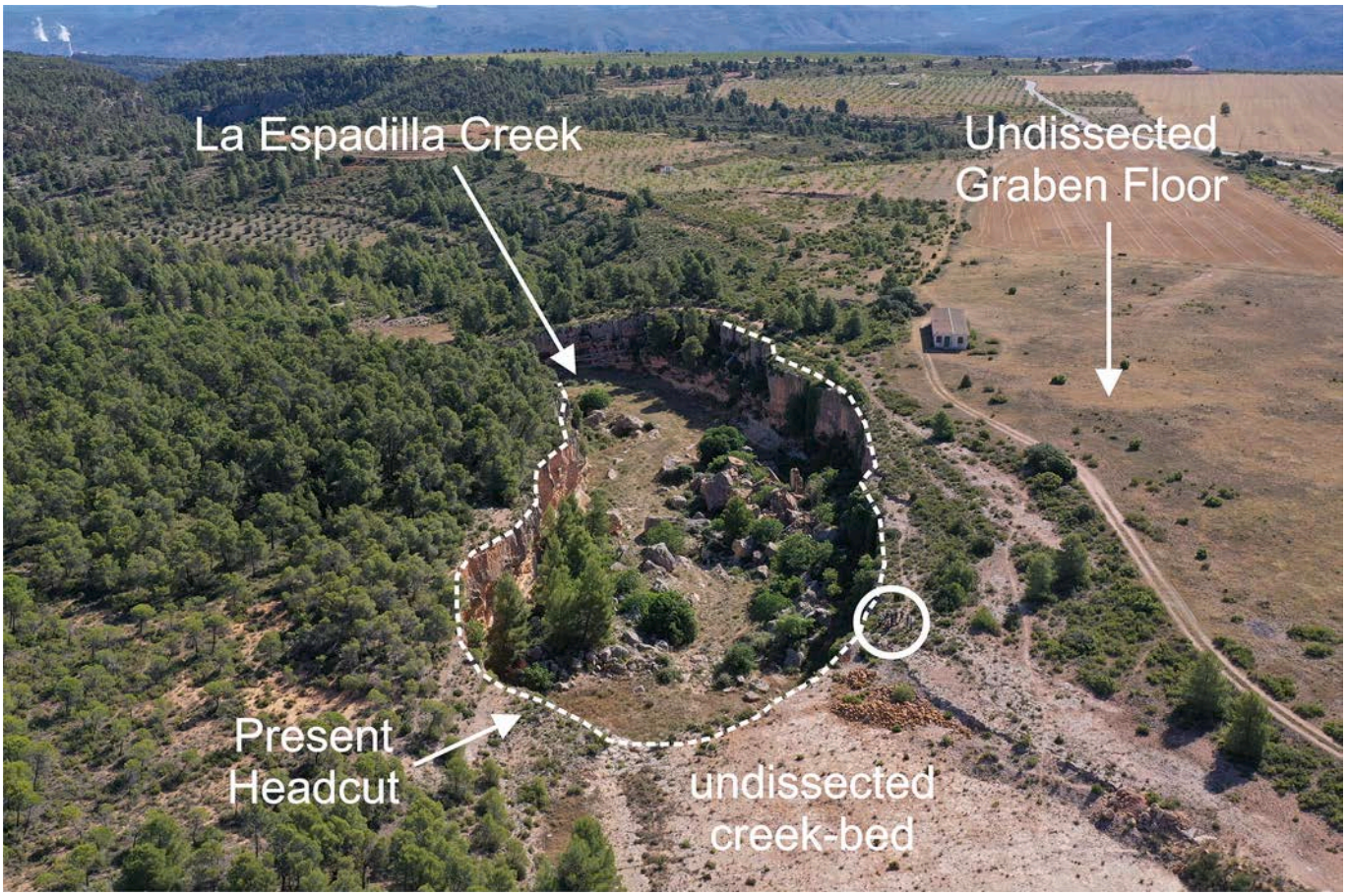

Fig. 3. Aerial view of the 15 m high headcut of the Espadilla Creek generated by the headward propagation of Quaternary fluvial incision upstream of Jarafuel. The observed Knickpoint connects the undissected floor of the Carcelén Graben-(upstream) and the entrenched section of the Espadilla Creek (downstream). The undermined resistant bed controlling this headcut corresponds to the Pliocene limestones. Circle indicates a group of students on the left side of the image standing on the edge of the cliff.

limestone is backtilted and offset by an east-dipping intrabasinal fault swarm spatially associated with the Keuper Facies (Carner, 2001; Gutiérrez et al., 2019). These normal faults display a cumulative throw of 64 m (RSF; Fig. 5) and probably have a gravitational origin related to salt-dissolution subsidence and/or differential salt flow, which may have been fostered by fluvial incision (i.e., base-level drop, erosional unloading; Gutiérrez et al., 2008, 2012, 2019; Carbonel et al., 2013). If this is the case, the onset of surface faulting could be situated at to the MN17 Biozone (Villafranchan period), dated around 2.5 to 2.0 Ma in the area (Alcalá et al., 1985; Alberdi et al., 1997).Plio-Quaternary volcanic activity has also occurred in the northern sector of the Ayora-Cofrentes Graben, around the junction of the Júcar and Cabriel valleys, recorded by the Agrás Volcano and the Pico del Fraile Vent (Silva et al., 2015) (Fig. 2). The volcanic products are early Pleistocene alkaline basanites derived from the asthenospheric mantle (Martí et al., 1992; Carner, 2001; Ancochea and Huertas, 2002), which include a large amount of lithics derived from Triassic, Neogene and Quaternary formations as a consequence of intense phreatomagmatic explosive activity (Silva et al., 2015; Silva et al., 2023a,b). K/Ar dating of volcanic materials of the Agrás Volcano provided a mean age of ca. 2.6–1.8 Ma (Sáenz-Ridruejo and López-Mariñas, 1975; Ancochea and Huertas, 2002). Volcanic materials disrupt the higher fluvial terrace of the Júcar-Cabriel system, lying at +130 m above the present river channel, and therefore post-date the onset of valley development in the area. On the other hand, volcanic materials of the Pico del Fraile Vent are in a lower topographic position related to the +60 and +40 m fluvial terraces also displaying features of important phreatomagmatic activity (Silva et al., 2023a). The available data indicate that repeated volcanic activity occurred within the valley, disrupting the fluvial system and involving significant magma-water interactions. At present, a residual reminder of this past volcanic activity is the occurrence of two permanent CO_2-rich bubbling springs of warm water (Los Hervideros and Hervideros Chicos), with $^3He/^4He$ ratios (0.95Ra) indicating a mantle-sourced helium fraction of 12 % (Pérez et al., 1996). Hydrogeological models indicate that aquifers of meteoric waters are intersected by a deeply rooted basement fault along which CO_2 and mantellic Helium is injected (Pérez et al., 1996).

5. Results: the Júcar-Cabriel terrace system

The Jucar and Cabriel valleys display stepped terrace sequences with essentially the same number of levels and similar relative heights. The 14 terrace levels mapped are better developed and preserved in the Júcar Valley, which also hosts the best outcrops (Fig. 6). Nevertheless, the Cabriel Valley presents interesting elements to understand the Quaternary valley evolution in the area: (1) includes the oldest inset fluviatile deposits in the zone at +200–230 m (La Muela del Valle Tufa Platform; Fig. 6) recording the initiation of valley formation in the zone; (2) the uppermost terrace T1 is strongly disrupted by Early Pleistocene volcanic activity, dated by means K/Ar at ca. 1.6–1.2 Ma; (3) Younger volcanic deposits indicate explosive phreatomagmatic activity during the Middle Pleistocene. The Muela del Valle Tufa Platform occurs on the southern margin of the Cabriel Valley, right at the NW upstream edge of the study area near the outcrops of Casas del Rio (see Fig. 4), covering an area of 4 km^2. This deposit consists of a 20 m thick calcareous tufa with

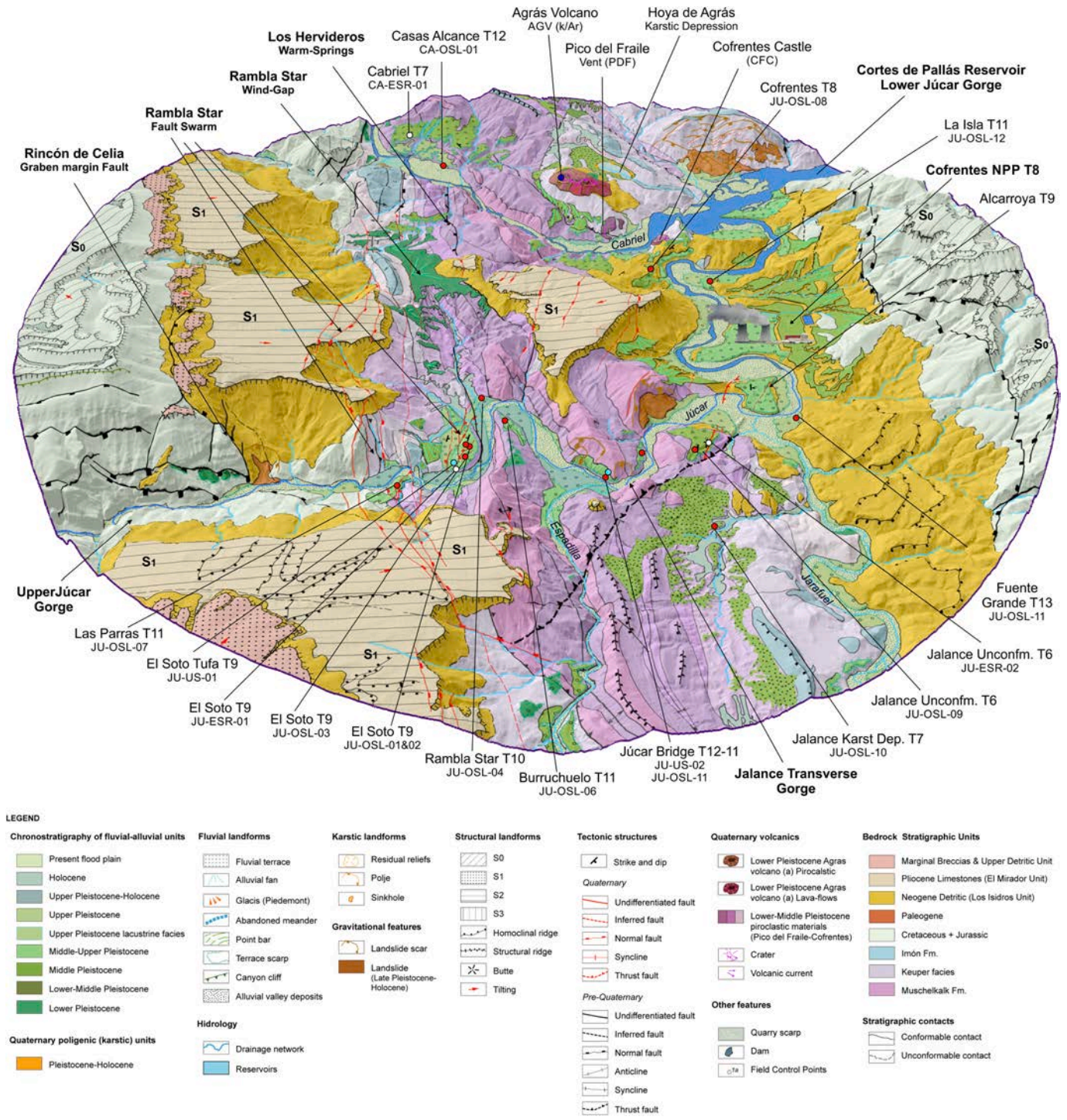

Fig. 4. 3D morphostructural map (radius 5 km) of the study area displaying the most important features of the northern sector of the Ayora-Cofrentes Graben described in the text: salt wall of Triassic evaporites; planation surface on Mesozoic carbonate formations (S_0); Plio-Quaternary (Villafranchian) depositional surface at the top of the graben fill (S_1); main graben-bounding faults (e.g., Rincón de Cecilia RCF); Rambla Start fault swarm (RSF); outcrops of Quaternary volcanics (Q_V); Hervideros warm springs (HWS).

interbedded marly beds and some sand and gravel layers. The tufa deposit includes phytoclasts, phytoherms and gastropod fauna attributed to the Plio-Pleistocene in the old geological maps of the zone (Lendínez and Tena, 1980). Currently, these old Plio-Pleistocene labels can be ascribed to the Gelasian stage (1.8–2.5 Ma) based on the K/Ar age of volcanic materials disrupting T1. This extensive tufa platform is inset about 90–70 m into the aggradational surface (S_1) on Villafranchian limestones at the top of the Cenozoic sedimentary fill of the grabens (Figs. 2 and 4). This tufa deposit is locally disrupted by local normal and reverse faults attributed to gravitational deformation related to the underlying salt-bearing evaporites within the E-W oriented Cabriel Basin (e.g., dissolution-induced subsidence, salt flow, lateral spreading) (Fig. 2). Similar high-elevation tufa terraces occur in other grabens within the Carcoh Massif (e.g., Navarrés Graben), which in the absence of chronological data have also been assigned to a generic Plio-Pleistocene age (Gutiérrez et al., 2019). In several sectors of the

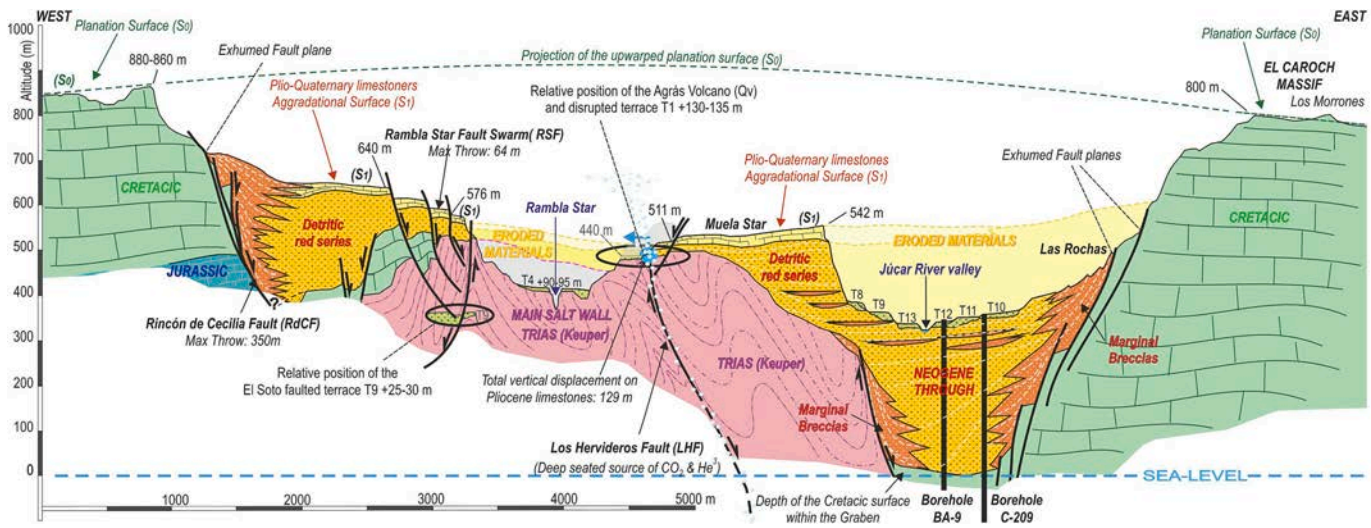

Fig. 5. Schematic geological cross-section of the northern sector of the Ayora-Cofrentes Graben across the Rincón de Cecilia Fault, Muela Star, and Las Rochas, based on mapping and field data. Depth data has been obtained from deep boreholes and seismic refraction lines performed for the construction of the Cofrentes Power Plant in the 1970s.

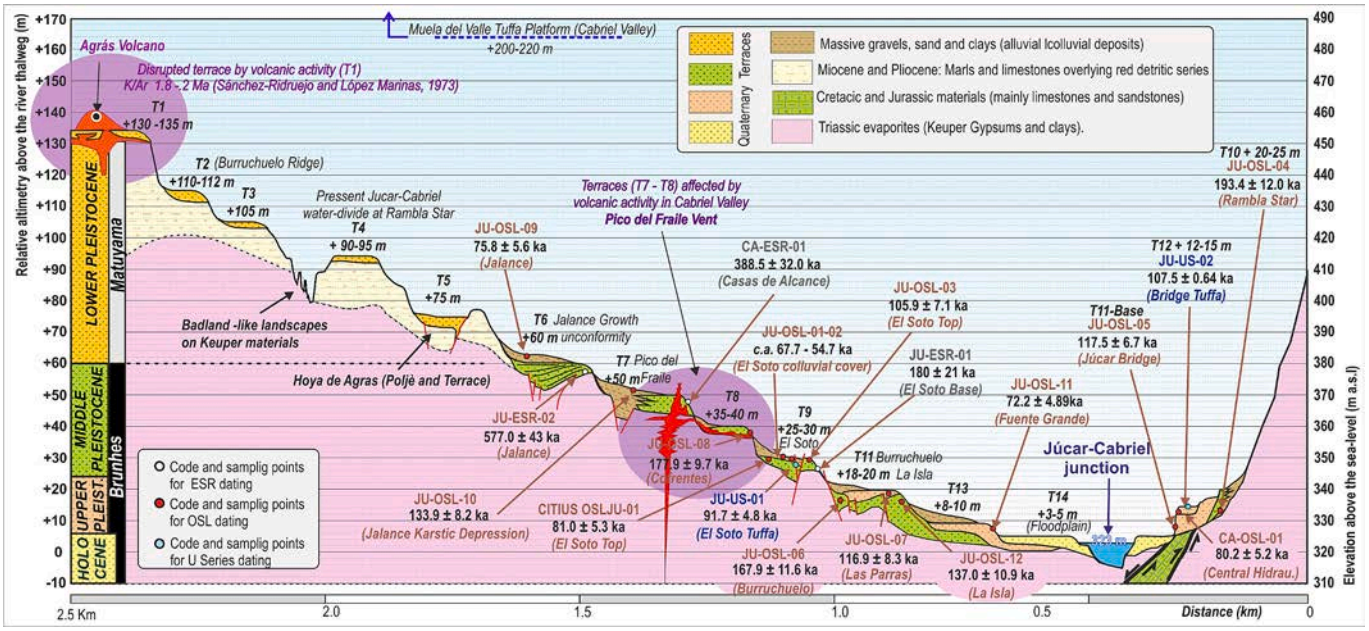

Fig. 6. General sequence of fluvial terraces OF the Júcar and Cabriel river valleys in the studied zone (Jalance – Cofrentes sector). The schematic cross-section displays the relative position of the sampling points for geochronological analyses indicating the different dating methods (ESR, OSL and Th/U) and representative sections. Purple circles indicate the terraces affected by volcanic activity in the northern sector of the Ayora-Cofrentes Graben. (For interpretation of the references to colour in this figure legend, the reader is referred to the web version of this article.)

Cabriel, Lower and Upper Júcar Canyon these tufa deposits are locally related to mainly erosional benches within the canyons defining successive erosional surfaces (S_2 to S_4). These geomorphic surfaces are shouldering the canyons and witness the history of fluvial incision in the zone before the development of the studied terrace system. The significance of these geomorphic surfaces will be analyzed in the discussion section.

The set of the studied terraces also include tufaceous facies but are dominated by sands and gravels (channel facies) capped by laminated silts and clays (floodplain facies). Tufaceous facies are common in the Cabriel Valley, but also in the reach of the Júcar Valley upstream of the locality of Jalance, sometimes forming caprocks up to 5–8 m thick on top of the clastic sequences (e.g., El Soto and Júcar bridge terraces; Fig. 6). There, tufa deposits locally replace the floodplain facies, recording palustrine areas within the valleys. These are especially common in the terraces between +30 and +12 m (T8 to T12), where the obtained ages fall preferentially within the Marine Isotopic Stages MIS 6 and 5 (Fig. 6). These chronologies for tufa deposits are common in other fluvial valleys carved in carbonate terrains in Spain, as is the case of El Caroch Massif, the Iberian Chain or Central Spain (Torres et al., 2005; Sancho et al., 2015; Gutiérrez et al., 2019).

5.1. Upper terrace sequence

This set of upper terraces corresponds to isolated remnants dominantly composed of cemented gravels and sands 2–4 m thick. These

strath terraces have been carved in Cenozoic sediments and more commonly in the Triassic evaporites and mudstones of the salt wall. This is the case of the sequence of strath terraces between +110 and +75–70 m (T2 to T5) preserved in the N-S-oriented Burruchuelo Ridge within the Júcar Valley (Fig. 4). However, the uppermost fluvial terrace (T1) occurs also in the Cabriel Valley, close to its confluence with the Júcar Valley near Cofrentes, at a relative height of +135–130 m. This upper terrace is disrupted and overlain by a small strombolian edifice, the Agrás Volcano, 500 m in diameter and 52 m high (Sáenz-Ridruejo and López-Mariñas, 1975; Silva et al., 2015). This small volcano is well preserved and constitutes a relevant landmark in the study area (Fig. 4).

The outcrops of T1 terrace display large broken blocks of cemented gravels up to 25 m^3 intruded and embedded by the basal pyroclastic materials of the Agrás Volcano (Fig. 7). As preliminary reported by Silva et al. (2023a), these basal pyroclastic materials show abundant cauliflower-shaped bombs, lapilli and chilled-rim pyroclasts supporting the presence of water during magma rise (hydrovolcanism; e.g., Németh and Kósik, 2020). These conspicuous water-magma interaction features agree with the phreatomagmatic explosive activity responsible for the disruption of the upper terrace, indicating that the volcano growth on the pristine floodplain of the Cabriel Valley (T1). In the base of the volcano the pyroclastic deposits also include large meter-sized blocks of Neogene marls, Triassic shales and brecciated dolomites from the underlying bedrock affected by the explosive activity. Towards the top of the volcano the pyroclastic deposits are interbedded with basalt layers up to 8 m thick, which become progressively more abundant, indicating that lava flows prevailed over the explosive activity. These thick basaltic beds are intruded by subvertical N-S- to NNW-SSE-trending basaltic dikes, aligned with the regional fault system of the Ayora-Cofrentes Graben. One of these basaltic dikes was sampled for K/Ar dating by Sáenz-Ridruejo and López-Mariñas (1975). These authors obtained twelve different samples from a single vertical dike intruded into the upper and youngest materials of the Agrás Volcano. Half of the samples were sent to a laboratory at the University the Coimbra (Portugal) and the other half to the US Geochron Company Krueger Enterprises Inc. of Massachusetts. After removing the presumably oldest and youngest erroneous dates, the resulting average K/Ar ages for the analyzed dike were 2.4 ± 04 Ma (99.9 % confidence level) according to the US Lab, and 1.3 ± 02 Ma (94.9 % confidence level) for the Coimbra Lab. Sáenz-Ridruejo and López-Mariñas (1975) adopted a preferred mean age of 1.66 Ma for the analyzed dike.

However, they contended that an average age of ca. 2.0–1.8 Ma for the volcanic activity affecting the terrace matched better to the geomorphology of the area. This average age was later adopted by different studies in the zone (Ancochea and Huertas, 2002; Carner, 2001) and post-date the terrace (Silva et al., 2015). This dating suggests a Lower Pleistocene, probably pre-Olduvay (Gelasian) age for T1, which is consistent with its elevation above the thalweg as indicated by models of fluvial terrace development for central Spain (Silva et al., 2017). Furthermore, preliminary paleomagnetic determinations using a

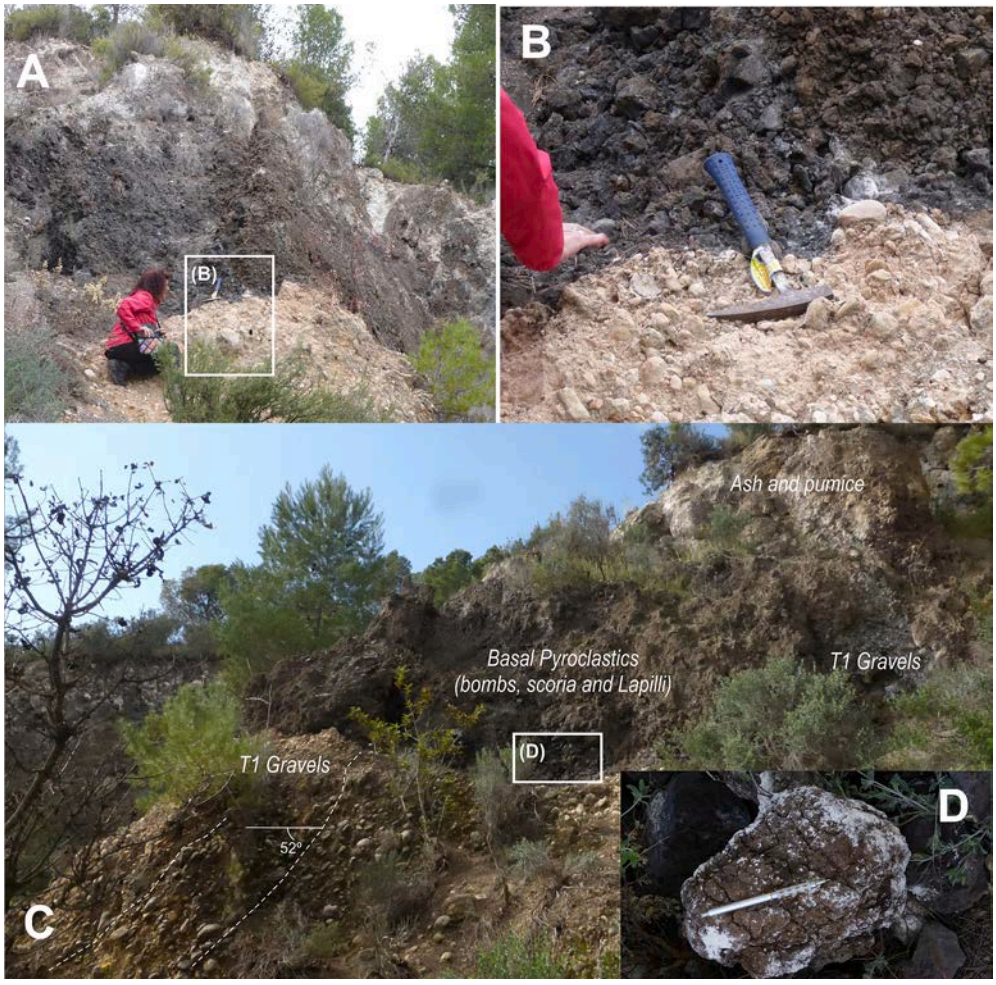

Fig. 7. Fluvial terrace T1+ (130–135) disrupted by the activity of the Agrás Volcano. (a) General view of the distorted terrace deposit in the northern slope of the volcano. (b) Close-up view of the contact between the pyroclastic material (up) and the terrace deposits (down). (c) General view of the outcrop at the base of the Agrás Volcano showing the disrupted terrace gravels, pyroclastic flow depo sits and upper levels of ash and pumice. (d) Detail of a cauliflower-shaped bomb in the basal pyroclastic levels.

portable fluxgate magnetometer consistently recorded reverse polarity (Matuyama) for both the dykes and the upper intruded basaltic beds of the Agrás Volcano (Silva et al., 2023a). The obtained data clearly indicate that the small strombolian monogenetic volcano developed in the ancient floor of the Cabriel Valley. Phreatomagmatic features within the basal materials of the Agrás Volcano support this interpretation. There, large broken blocks of cemented gravels from terrace T1 are embedded by pyroclastic materials, suggesting that volcanic activity took place after the deposit of T1, when the alluvium was already somewhat lithified and terrace T2 was not formed yet.

No geochronological data are available for the rest of the upper terraces, but the ESR age obtained from the oldest of the intermediate terrace T6, lying at +60 m (577.02 ± 43 ka) (Table 2) indicate that the upper terrace sequence mainly belongs to the Calabrian stage of the Lower Pleistocene. Terrace deposits from T2 (+112–110 m) to T5 (+75–70 m) do not display any special distinctive feature, representing a sequence of staircased strath terraces (Fig. 6). However, T4 (+90–95 m) constitutes a landmark in the geomorphology of the area. This terrace occurs in the present-day water divide of the Júcar and Cabriel valleys, west of Cofrentes within a U-shaped wind gap between both valleys (Figs. 4 and 5). The terrace deposits occur in the headwaters of the Rambla Star (tributary of the Júcar) perched above both valleys (Fig. 4). Its deposits merge with laterally-derived alluvial and colluvial deposits delineating an ancient N-S drainage path connecting the Júcar and Cabriel valleys (present wind gap). The 3D map of Fig. 4 illustrates the aggressive erosion of the headwaters of Rambla Star to the south and that of the Hervideros Creek to the north, generating badland-like landscapes in the underlying Triassic evaporates. Other features associated with the T4 wind gap is that it is located in the western zone of the Ayora-Cofrentes Graben, inset into the Plio-Pleistocene limestones and flanked by conspicuous N-S trending normal faults (i.e., Rambla Star Fault Swarm). One of these faults on the eastern side of the wind gap controls the Los Hervideros CO_2-rich warm springs (Fig. 5), which also displays He^3/He^4 ratios indicating deeply rooted faults and deep mantellic gas probably related with the Quaternary volcanic activity (Pinagua, 1998; Pérez et al., 1996; Silva et al., 2015). The significance of the T4 wind gap in the fluvial evolution of the area will be discussed in following sections.

The lowest terrace of the Early Pleistocene sequence is T5 (+75–70 m) forms a wide bench around the Agrás Volcano on the northern margin of the Cabriel Valley (Figs. 4 and 6). This alluvial surface is interrupted by an elongated and internally drained polje-like karstic depression, for which the major axis follows the N-S structural grain of the Ayora-Cofrentes salt wall. This is the so-called Hoya of Agrás, which presents a shaft-like ponor on its southern end draining to the Cabriel Valley. Similar N-S depressions related to evaporate dissolution and subsidence occur along the Ayora-Cofrentes Graben (Jalance, Ayora), but opened and connected with the regional drainage network (Jarafuel River), and always linked to the younger fluvial terraces below +40 m. The Hoya Agrás depression developed on terrace T5 is the only one that preserves its internal drainage. The available dates for the Ebro Basin indicate that terraces at +85–90 m hold chronologies around the Jaramillo subchron (ca. 1.0 Ma; i.e., Sancho et al., 2020; Benito-Calvo et al., 2022). Consequently, terraces as T5 (+75–70 m) in this zone should have a Lower Pleistocene Calabrian age. Data obtained in this study indicate that the interaction between the evaporitic bedrock and fluvial sedimentation intensified from this fluvial terrace onwards. As preliminary noticed by Silva et al. (2015), these interactions are recorded by thickenings and deformations in the deposits of the middle terrace sequence.

5.2. Middle terrace sequence

The middle terrace sequence includes levels T6 to T8 (+60–65 to +35–40 m). These terraces are clearly affected by deformation processes related to the salt-bearing evaporitic bedrock, plus relevant interactions with renewed volcanic activity at the toe of the Agrás Volcano, related to the so-called Pico de El Fraile vent (Figs. 4 and 6). These three staircased terraces display local thickenings (up to 10 m) and multiple synsedimentary deformations. T6 (+60–65 m) is the oldest dated terrace in this study. This fluvial level has been dated by ESR in the Júcar Valley (Jalance section; Table 2). Terrace T7 (+50 m) has been dated in the Cabriel Valley (Casas de Alcance section) a few kilometers upstream of the Júcar-Cabriel junction in Cofrentes (Table 2). Finally, terrace T8 (+35–40 m) was dated by means of OSL in the Júcar Valley near the Cofrentes village (Fig. 4; Table 2). This last terrace displays local disturbances probably related to volcanic activity in the Cabriel Valley. However, as we will see latter, the deformations and disruptions displayed by this set of Middle Pleistocene terraces can be mainly related to the interaction of karstic subsidence and uplift (i.e., halokinesis, salt tectonics, etc.) linked to the reactivation and acceleration of activity in salt bodies.

The ESR ages obtained for the two samples taken in terraces T6 (+60–65 m) m and T7 (+50 m) are given in Table 2. In both cases Al and Ti-Li center determinations at 1σ indicate ages of 566 ± 33 ka and 590 ± 54 ka for T6 and of 409 ± 30 ka and 368 ± 34 ka for T7, respectively (Fig. 4). On the contrary, Ti-H center determinations for these terraces provide null or very young numerical ages that have been discarded (Table 2). Based on the Multiple Centre approach, the older age estimates provided by the Al or Ti-Li centers may be interpreted as evidence for an incomplete bleaching of the ESR signal prior to alluvial deposition (Duval et al., 2015). Consequently, the older ESR age estimates should be considered as maximum possible ages. However, considering the 1σ age uncertainties for the Al and Ti center estimates, average age values of 577.0 ± 43 ka and 388.5 ± 32 ka may be estimated for the formation of T6 and T7 terraces, respectively (Fig. 6). These age estimations situate both terraces within the Middle Pleistocene (Chibanian Stage) and can be roughly related to the warm marine isotopic stages MIS 15 (T6) and MIS 11 (T7). In fact, considering the older ESR age estimates for these terraces they can be related with two of the three first prominent glacial terminations VII and V recorded in the isotopic marine records (e.g., Lisiecki and Raymo, 2005; Bardají and Lario, 2022). In this case, the formation of the two oldest Middle Pleistocene terraces seems to be related to important climatic forcing.

Terrace T6 (+60–65 m) is widely represented in the Júcar Valley, especially around Jalance, where it reaches up to 10 m in thickness and displays a notable growth unconformity as observed in the road cuts in the vicinity of Jalanace (Fig. 8). This synsedimentary thickening is probably related to evaporite dissolution-induced subsidence, favored by fluvial entrenchment and the interaction of groundwater with progressively deeper sediments. These synsedimentary deformations are mainly found on the eastern flank of the Triassic salt wall within the Júcar Valley. The margin of the cumulative wedge-out displays NNE-SSW-trending faults with meter-scale throws and downward displacement towards the depocenter of the subsidence basins. Some faults with apparent reverse displacement may correspond to rotated normal faults (pseudoreverse faults) (Fig. 4). The growth unconformity displays basal dips of about 45–50° WNW (with local rotations up to 72°), whereas the topmost terrace sediments are subhorizontal (Fig. 8). Locally, meter-scale downward distorted gravel bodies and gravel-pockets detached from the terrace deposit are embedded by the evaporitic materials at the base of the growth unconformity. A distinctive feature of this terrace is the interbedding of fluvial facies (with rounded clasts of Cretaceous limestones) with short-transport alluvial facies consisting of angular clasts of the Triassic dolostones and shales coming from the edges of the salt wall. These laterally derived alluvial deposits at the top of this terrace yielded a younger OSL age of 75.8 ± 5.6 ka (Table 2). This age indicates that salt growth in this axial zone of the Ayora-Cofrentes Graben continued during the whole Middle Pleistocene, finishing at the end of the Last Interglacial (MIS 5) during the first part of the Upper Pleistocene. As we will see in the discussion section salt wall activity within the graben played a relevant role in the fluvial evolution of the

Fig. 8. Growth unconformity (cumulative wedge out) in the +60–65 m (T6) terrace at the Jalance road-cut section. Note synsedimentary reverse faults truncated by the upper packages of the fluvial succession. Sample locations for geochronological analyses are shown. To the left, inset showing a closer view of the meter-scale "reverse faults". These could be also forward rotated normal l faults (pseudo-reverse faults).

zone.

Despite the apparent absence of fossil fauna and lithic industry in the terraces of the study area, the +60–65 m terrace of the Júcar River contains faunal assemblages with *Mammuthus meridionalis* and *Hippopotamus major* (Mazo et al., 1990) 45 km upstream of the studied zone at the locality of Fuensanta (Fig. 1). This fossil fauna situates this terrace in the final phases of the lower Pleistocene (Calabrian stage) after the Jaramillo paleomagnetic subchron (~1 Ma), which in the Atlantic drainage basins are normally related to terraces at +75–80 m (Silva et al., 2017). However, the relative elevation of the Júcar terraces in the Llanura Manchega (upstream the Upper Júcar Canyon) cannot be directly correlated with those recorded in the studied zone, because of the different degree of entrenchment of the Júcar River at both areas downstream and upstream of the upper Júcar Canyon (i.e., terraces with longitudinal profiles converging upstream) (Silva et al., 2015). Upstream the canyon this terrace level belongs to the large alluvial surface of the upper Júcar catchment (+100–60 m; Fig. 1) formed by large braided channels flowing both towards de Atlantic (Guadiana Basin) and the Mediterranean (Júcar Basin) (Pérez-González, 1994). The Calabrian fauna found in these alluvial deposits place the reversal of the primary distributary channels towards the Mediterranean Júcar Basin within the Lower Pleistocene (Mazo et al., 1990). However, the ages obtained in the studied zone indicate that for similar relative heights (e.g., +60–70 m), terraces in this Mediterranean watershed of the Iberian Peninsula are younger than those of the Atlantic one in Central Spain, as also occurs in the Ebro Basin (i.e., Lewis et al., 2017; Benito-Calvo et al., 2022).

Terrace T7 (+50 m) is widely developed in the Cabriel Valley, showing thickenings of up to 14 m related to evaporite-dissolution subsidence (Casas de Alcance; Figs. 3 and 6). In these cases, the proportion of alluvial and colluvial deposits sourced from the valley margin in the thickened sequences is significant. These consist of fine-grained sediments with interbedded gravel lenses and 2.5 YR reddish soil horizons. In the outcrops of the Cabriel Valley these soils are represented by banded soils featured by the development of centimetre-thick red clay bands (clay lamellae) intercalations in the sandy parent materials. These clay lamellae record alternating humid and arid periods during interglacial-glacial transitions as reported for southern Spain (Zazo et al., 2008). Following these authors, alternating humid and arid periods initially promote clay illuviation, followed by the reddening of lamellae during the subsequent more arid stages. Consequently, these features are indicative of changing humidity/aridity ratios, rather than oscillating thermal regimes.

Similar sedimentological features are observed in this level in the Cabriel Valley around Cofrentes. This is the case of terrace T7 in the northern slope of this valley at the toe of the Agrás Volcano, which is intruded by the phreatomagmatic breccias of El Pico de El Fraile vent (PDF; Carner, 2001; Silva et al., 2015). The PDF materials are very fragmented pyroclastic materials of basaltic composition including angular fragments of older volcanic rocks and xenoliths of quartzite and dolostones embedded in a devitrified matrix observable in the field and thin section (Carner, 2001; Silva et al., 2023a). Field paleomagnetic measurements with a portable fluxgate device in the more massive PDF materials indicate a consistent normal polarity (Brunhes) consistent with the Middle Pleistocene ESR age obtained for T7 (388.5 ± 32 ka; Table 2) a few kilometers upstream in the upper deposits of this terrace, beneath the clay lamellae soils (Casas de Alcance; Fig. 4). This age places the deposit of this terrace around the MIS 11–10 transition, which corresponds to the first stages of the Mindel-Riss interglacial in Europe (Bardají and Lario, 2022).

As in the case of the volcanic materials intruded in terrace T1, these materials display similar features of water-magma interaction related to explosive activity. These volcanic materials also interacted downslope with the gravels and sands of the +35–40 m terrace (T8) dated by OSL on the opposite valley margin, near Cofrentes at 177.9 ± 9.7 ka (Table 1). As preliminary reported by Silva et al. (2023a), these materials include massive pyroclastic and peperite facies, with abundant clastic components in a palagonite-like matrix, as well as pseudo pillow breccias and pseudo pillow-lavas (Fig. 9). These features indicate relevant phreatomagmatic activity during or soon after the deposit of T7 intruded by the PDF necks and dikes (Silva et al., 2015, 2023a), but also some kind of resurgent late subaqueous volcanic activity with the formation of peperites and pillow-breccias (e.g., Németh and Kósik, 2020) within the river channel concurrent to the deposit of T8. The OSL age of this younger terrace affected by volcanic activity place these late resurgent hydromagmatic events during the late stages of Middle Pleistocene (MIS 6).

The remnants of the PDF affecting T7 and T8 outline a crescent-shaped rim opened to the SSW, facing to the volcanic outcrop of the Cofrentes Castle (CFC) on the opposite side of the valley (Fig. 5). The PDF rim preserves the mentioned pyroclastic and hydromagmatic

Fig. 9. Volcanic materials associated with the fluvial terrace T8 (+35–40 m) around the El Pico de El Fraile outcrops. **(A)** View to the south of the pyroclastic materials overlying deposits of terrace T8 (Cofrentes village in the background). **(B)** View of the pseudo pillow-breccia and peperites with a palagonite-like matrix (yellow materials). **(C)** Close-up view of peperites showing the mixture between basaltic and lithics embedded in a palagonite-like matrix (yellow materials). (**D**) Pseudo pillow lava surrounded by brecciated peperites including terrace clasts and boulders of the Triassic substratum. (**E**) Close-up view of the contact between the pseudo-pillow breccias and the Triassic bedrock. (For interpretation of the references to colour in this figure legend, the reader is referred to the web version of this article.)

materials in several residual outcrops of neck-like morphology. Preliminary petrological analyses suggest that the CFC materials can be interpreted as a volcanic agglomerate and breccia of basanite-tefrite composition, formed by a mixture of pyroclastic materials plus terrace boulders and gravels with flow structures coming from the PDF vent (Silva et al., 2023a). Therefore, the presented results indicate two different eruptive events affecting valley evolution at different times during the Pleistocene. Previously, the PDF and CFC outcrops were considered as coetaneous subsurface subsidiary conduits (or diatremes) linked to the Agrás Volcano formed in the Lower Pleistocene, presently featured as protruding residual reliefs by differential erosion (e.g., Sanz Ridruejo and López Marinas, 1977; Lendínez and Tena, 1980; Ancochea

and Huertas, 2002).

This Middle Pleistocene terrace (T8) is also present in the Júcar Valley, outcropping at the Burruchuelo Ridge and in the area around the locality of Cofrentes. In both zones the terrace is mainly composed by sands and silts with reddish-brown soils (2.5 YR) and displays thickening (>8 m) and local soft sediment deformations. In the Cofrentes outcrop soft-sediment deformations occur associated with the contact of fine sand units overlain by horizontally laminated silt and sand (floodplain facies) overprinted at the top of the sequence by a reddish-brown soil (Fig. 10). The basal level of the floodplain unit is sagged (synsedimentary synform), brecciated, strongly affected by bioturbation, and contains sand lenses. Below the main deformation zone, the underlying sand units have experienced liquefaction, with convolute lamination and numerous water-escape meso- and micro-structures, such as sand dykes, minor sand injections and sand flames, as well as sand clasts with original lamination embedded in a homogenized sand matrix in which the original lamination has been obliterated (Fig. 10B). The lower sand package was sampled for OSL dating (Fig. 10A) resulting in an age of 177.9 ± 9.7 ka for T8 (Fig. 4; Table 1). The soft-sediment deformations can be explained in the context of the explosive activity affecting this terrace level in the Cabriel Valley just 1 km to the north (Fig. 5). However, in absence of additional data, this can be considered as an untested hypothesis to be confirmed by further studies. In this sense, an important data is that fluvial deposits of similar middle Pleistocene age are strongly deformed in the basal sequences of the thickened Upper Pleistocene terraces (T9–T11) at the sites of El Soto, El Burruchuelo and Las Parras (Fig. 5).

5.3. Lower terrace sequence

These terraces are represented by inset surfaces underlain by onlapping thickened deposits (up to 10 m thick) displaying synsedimentary deformations. Terrace T14 (+3–5 m) corresponds to the current floodplain with riverine vegetation that favors the precipitation of calcareous tufa. Calcareous tufa deposits are common in this set of younger terraces, especially in those corresponding to the last interglacial period (T9 to T11; Fig. 6; Table 1). The terrace sequence is submerged downstream of the Júcar-Cabriel confluence by the Cortes de Pallás Reservoir, which dam was built in the lower Júcar Canyon in the 1980s (Fig. 4). The best developed terrace levels are T9 and T11, mainly preserved on the inner banks of the meanders of Las Parras, El Soto, Burruchuelo and La Isla within the Júcar Valley (Fig. 6). In these zones fluvial deposits display nice examples of lateral accretion architectural elements (i.e., point-bar sequences) consisting of packages of sands and gravels topped by fine sands and laminated silty clay floodplain facies. Locally, floodplain facies are replaced by tufa deposits accumulated in swampy areas. These tufa deposits show the typical fluviatile facies, with abundant oncoids, encrusted phytoclasts and micritic tufa, as well as subordinate autochthonous deposits such as small phytoherms and stromatolitic lamination (e.g., Pedley, 1990). The upper sandy packages of terraces T9 and T10 yielded consistent OSL ages of ca. 117 and 80 ka (including error margins (Table 1; Fig. 6). Two dated tufa deposits yielded Th/U age estimates of 107.49 ± 0.64 and 91.71 ± 4.85 ka (Table 3). The similar age estimations obtained for terraces T11 and T12 indicate that the terrace sequence at relative heights between +25 and +12 m (T9 to T12) were deposited during the different isotopic substages of the last major interglacial stage (MIS 5).

These Late Pleistocene deposits overlie the sand and gravel

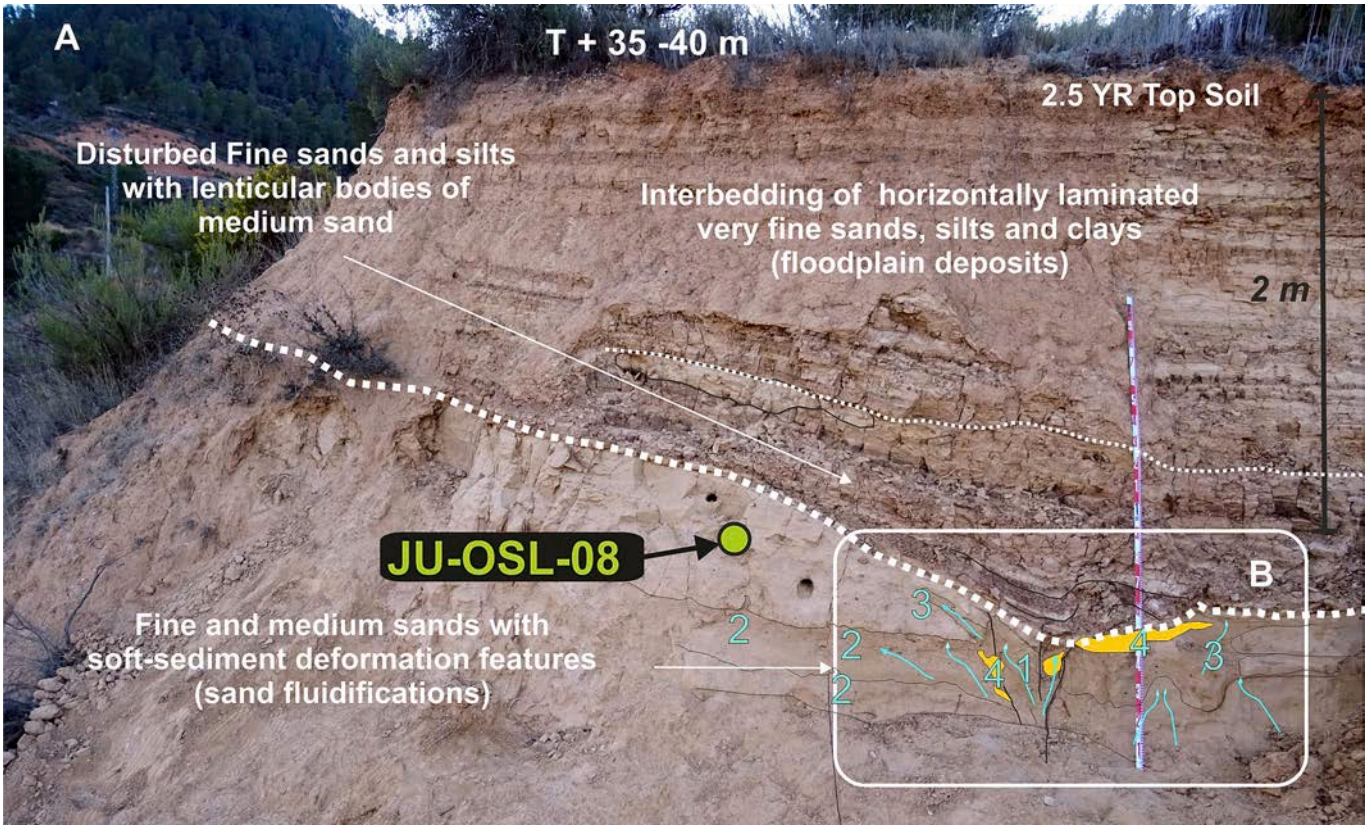

Fig. 10. Stratigraphy of the upper zone (upper 3 m) of the +35 m fluvial terrace near Cofrentes (T8; Júcar Valley). The two sedimentary sequences (Lower-Upper; I-II) described in the text are illustrated. The boxed zone B shows the zone where most of the fluidification structures occurs in the lower sedimentary sequence including: (1) sand injections; (2) sand flames; (3) minor vertical and lateral sand injections; (4) sand clasts; and the overall convolute lamination. The place selected for OSL sampling and dating is also indicated.

sequences that form the lower packages of the terraces, with Middle Pleistocene ages between ca. 193 and 137 ka (Fig. 6). As mentioned above, these middle Pleistocene deposits are thickened and locally show substantial synsedimentary deformation including normal faults and sagging structures related to subsidence induced by dissolution of the underlying salt-bearing Triassic evaporites. These deformations are especially important around El Soto, Las Parras and El Burruchuelo meanders, where the N-S-trending Rambla Star fault swarm traverses the Júcar Valley (Fig. 4). In these zones surface-rupturing normal faults create well-developed fault scarps and associated colluvial wedges like deposits (Fig. 11; El Soto), or more complex deformations with rotated or oversteepened normal faults such as pseudoreverse faults, verticalized gravel bodies and liquefaction structures (Fig. 12; Las Parras, El Burruchuelo). All these deformations clearly related to the evaporitic nature of the bedrock (e.g., dissolution-induced subsidence and in a minor extent salt tectonics). They are mainly concentrated within the Júcar Valley carved into Triassic evaporites upstream of the Jalance Gorge. Here, there are also active landslides in the Triassic evaporites that locally disrupt terrace deposits on the left side of the valley (Fig. 4).

El Soto terrace (T9) displays a good example of surface faulting associated with a main 630-m-long normal fault scarp with N-S trend (N10E) that crosses the entire terrace preserved in the inner side of a large meander of the Júcar River (Fig. 4). The main fault scarp, facing to the west, has a height of about 5.8 m, which can be considered as the minimum cumulative vertical displacement of this specific fault (Fig. 11A). The Quaternary cover in the downthrown block is offset by a series of E-dipping antithetic faults that have produced low-relief ridges and elongated depressions parallel to the main fault (Figs. 4 and 11). The troughs controlled the position of small fault-parallel drainages and ponds at the foot of faults scarps with deposition of calcareous tufa. Th/U analyses of this tufa deposits (Table 3) indicate a MIS 5 age (Table 3; C-JU-SU-01: 91,715 ± 4.85). Considering the OSL ages obtained for the upper units of this terrace (T9) (Table 1), a MIS 5 maximum age can be attributed to the morphogenetic surface faulting. In fact, the OSL age of the interstratified sand layers affected by faulting (CITIUS-OSL-JU-01: 82.0 ± 5.2 ka; Fig. 11B). These ages are consistent with that of Th/U ages obtained for the tufa deposits (Table 3), indicating the maximum age for the main phase of deformation of El Soto terrace during the end of the isotopic stage MIS 5 (Last interglacial). The OSL ages determined for the upper part of this terrace (Table 1) also indicate that the end of fluvial sedimentation in T9 occurred by the end of the Last Interglacial. However, the observed deformations can be younger. Only the ESR age obtained for the base of the deposit underlying this terrace provides a Middle Pleistocene age of 180.0 ± 21 ka, suggesting the stacking of thickened terrace deposits that in the old quarry reach >10 m.

The analysis of the antithetic faults in the downthrown block of the main fault indicates meter-scale throws decreasing towards the main fault scarp from 1.8 to 1.1 m (Fig. 11B). These secondary faults show narrow shear zones in which the terrace gravels display vertically reoriented fabrics. Fault plane and striation measurements on these faults indicate consistent fault orientations N10-30E (Fig. 11A and B). Wedge-shaped post-terrace colluvial deposits made up of orange silty sands (5YR 7/6) with scattered gravels occur in the downthrown blocks of these faults. The *downdropped* deposits abutting the main antithetic fault display a bending-related drag-fold (b in Fig. 11B). In contrast, the other wedge-shaped alluvial bodies display scattered gravels with chaotic fabrics (c and d in Fig. 11B). The lower fine-grained part of these alluvial wedges with paler reddish-yellow colour (7.5YR 8/6) are intensely cemented by secondary carbonate and display tilting towards the fault plus drag folding, suggesting the rotation of blocks along shallow listric faults (Fig. 11B). These alluvial deposits and the intervening faults are unconformably overlain and truncated by a thin non-deformed colluvial veneer 20–30 cm thick of silty clays supporting a reddish-brown soil (5YR 6/4). Two samples collected from the westernmost wedge-shaped body have yielded OSL ages of 67.7 ± 4.2 ka and 54.7 ± 3.2 ka in correct stratigraphic order (Fig. 11B; Table 1). Considering the ages obtained from the deformed wedge-shaped deposits (MIS 4), this isotopic stage can be considered as the maximum age for the youngest surface-rupturing faulting event in this terrace. Geophysical and trenching data from this fault zone preliminary reported by Silva et al. (2023b) indicate that this localized Quaternary deformation is related to the highly soluble and mobile nature of the

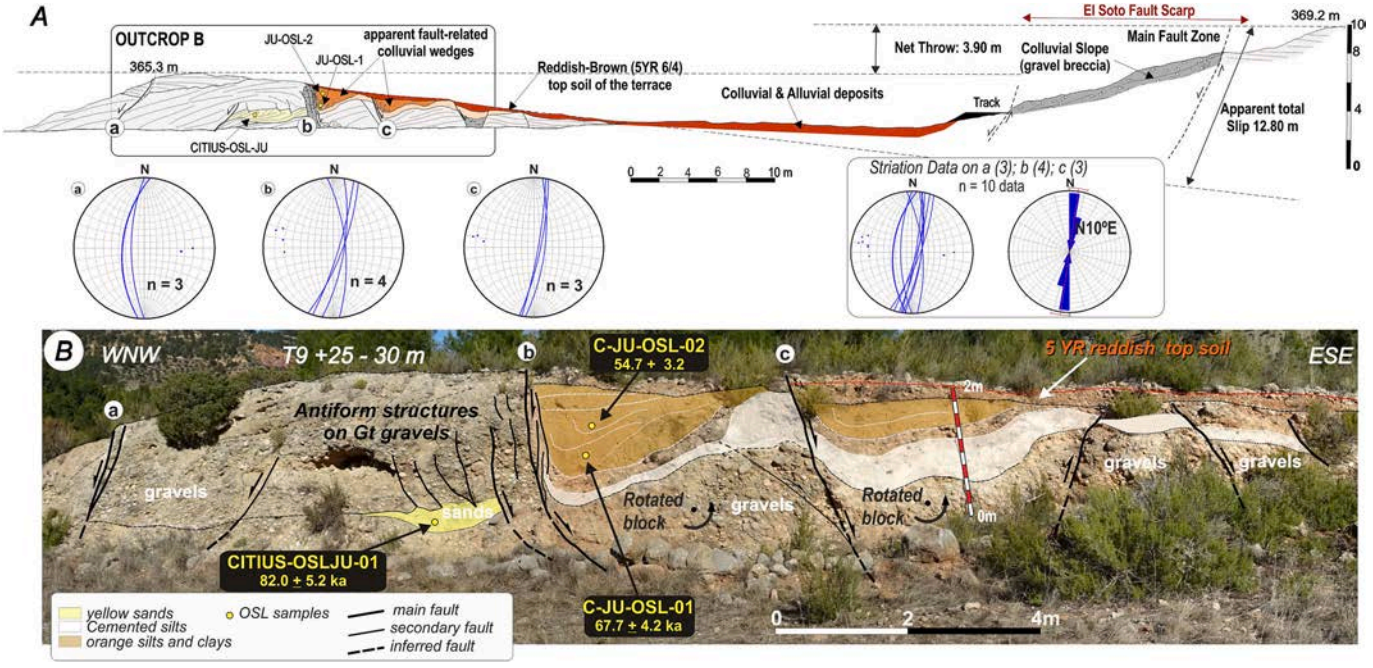

Fig. 11. Surface-rupturing and synsedimentary deformations at El Soto terrace (T9: +25–30 m) in the Júcar Valley. **A)** Topographic profile showing the main N10E-oriented fault scarp, the associated geomorphologic features, stereographs of striation measurements on faults a, b and c, as well as values of the far-field net throw (3.90 m) and rough apparent fault slip (12.80 m). **B)** Panoramic view showing the antithetic listric faults in an artificial excavation perpendicular to the main fault scarp of El Soto Terrace. The location of OSL samples collected from wedge-shaped colluvial deposits located in the downthrown blocks is indicated.

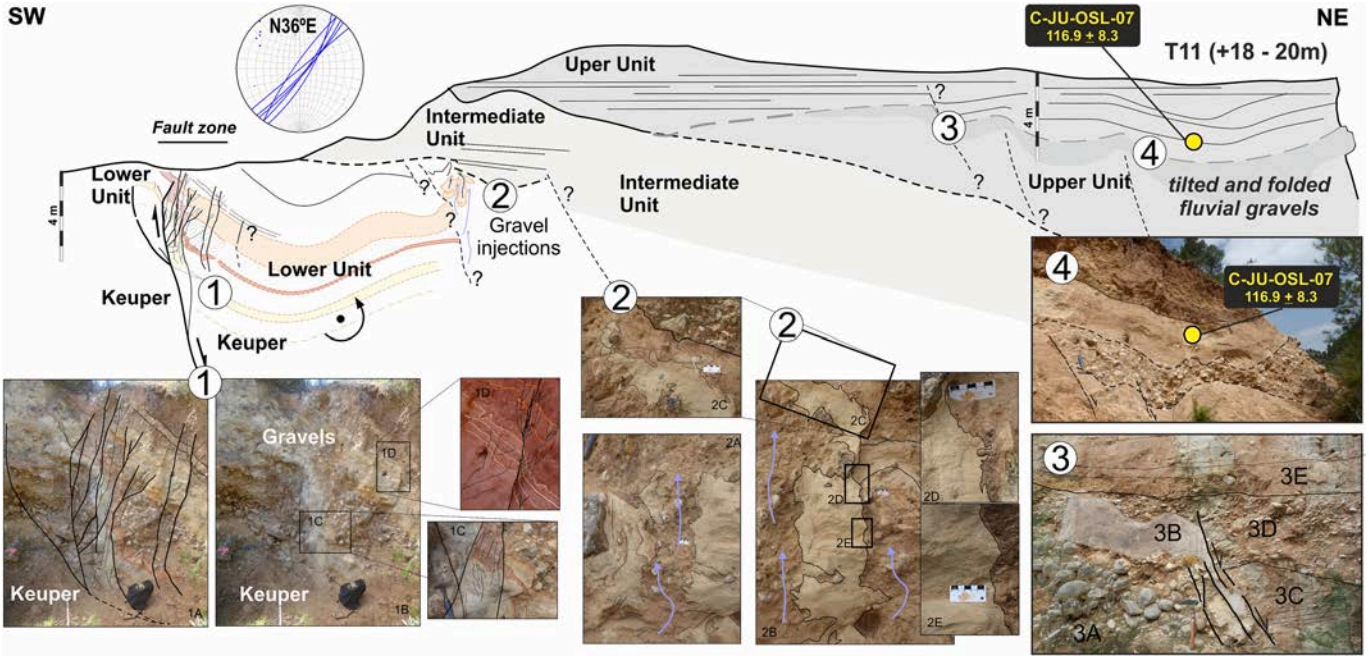

Fig. 12. Quaternary deformations in the terrace T11; (+18–20 M) at Las Parras Creek in the Júcar Valley: a) Sketch of the outcrop illustrating the three main sedimentary units (lower, intermediate and upper). The location of samples for geochronological analyses is indicated; b) Lower panel displaying the interpretation of the different deformations observed at the outcrop: (1) Main normal fault zone with listric geometry and a splay of secondary oversteepened faults in the hanging-wall producing complex deformation in the lower sedimentary unit. Note offsets of several tens of centimetres (1.A and 1.B) and a total vertical displacement of at least 3 m; (2) Gravel injections along subvertical discontinuities in the lower sedimentary unit (2.A); Large blocks of disrupted laminated sands displaying fluidization structures (2.B and 2.C); Details of sharp sand-gravel injection contacts (2.D and 2.E); (3) Discrete normal fault affecting the upper sedimentary unit; (4) Tilted and bent gravel beds in the upper sedimentary unit.

halite-bearing Keuper substratum (i.e., salt wall). Other sites with remnants of this terrace level include Casas de Alcance (Cabriel Valley) and the abandoned quarries in the El Burruchuelo, Alcarroya and La Isla meanders, the last adjacent to the Cofrentes Nuclear Power Plant (Fig. 4). In all these sites the terrace deposits were extensively quarried. Nonetheless, aerial photographs from the 1950s (American Flight, 1956–59) identify local terrace tilting away from the diapir axis (>15°E), as is the case of the Alcarroya meander (Fig. 4).

The thickened deposits of T11 terrace (+18–20 m), up to 8 m thick, also record significant synsedimentary deformations. One of the best examples is that of Las Parras Creek a few kilometers upstream of El Soto meander (Fig. 4). This terrace is also affected by the Rambla Start fault swarm. The studied outcrop shows three sedimentary units (Fig. 12). All units are thickened and display significant deformation, which intensity decreases upwards. The lower unit is locally in contact with the Keuper evaporitic materials by a fault plane. The contact is expressed as a subvertical normal fault, which is progressively steepened upwards and eventually reversed (i.e., oversteepened normal fault). The intense deformation includes complex drag-folds and faults observable in the interbedded sand and gravel layers of the basal terrace deposits. These beds display vertically re-oriented fabrics, antithetic reverse faults (Fig. 12.1) and injections of gravels along subvertical discontinuities indicating fluidification processes (Fig. 12.2). Fault strike measurements indicate NNE-SSW orientations roughly similar to those of the El Soto terrace (N30-36E). The intermediate unit displays some local NNE-SSW-oriented normal faults with 10–20 cm of vertical displacement (Fig. 12.3), but in general it does not show significant deformation. All the deformations are truncated by the upper nearly horizontal flood-plain sediments of the upper unit (Fig. 12.4). OSL dating from the basal zone of this upper unit provides an upper Pleistocene age of 116.9 ± 8.3 ka (Fig. 12; Table 1), indicating a Late Pleistocene age (MIS 5) for both the upper fluvial deposits and faulting at this site. However, terrace thickening (growth strata) and the internal angular unconformity suggest that the lower sedimentary unit of this terrace could correspond to overlapped deposits of the previous +25—30 m fluvial terrace, forming a complex thickened terrace (+18–20 m and +25–30 m terraces) recording the middle-late Pleistocene transition (i.e., synsedimentary thickening greater than subsequent entrenchment). The assemblage of sedimentary units and deformations illustrated in Fig. 12 suggests the interplay of collapse and sagging subsidence during the deposition of the lower sedimentary unit. Sudden synsedimentary collapses may facilitate the fluidization and vertical injection of gravels in failure zones (e.g., Gökkaya and Gutiérrez, 2022). As in El Soto terrace, measured fault strikes within the lower, intermediate and upper sedimentary units displays consistent NE-SW to NNE-SSW orientations suggesting collapse structures controlled by the distribution of the halite-rich units within the Ayora-Cofrentes Salt Wall. Similar examples of fluidization processes and complex salt-related deformations also occur in this same terrace (T11) at El Burruchuelo site (Fig. 4).

Terraces T10 (+25–20 m) and T12 (+12–15 m) mainly occur assembled with the above described T11 terrace (+18–20 m) displaying complex morpho-sedimentary arrangements with inset surfaces and stacked deposits up to 8–10 m thick. These sequences typically contain laterally-derived alluvial and colluvial deposits and are commonly topped by riverine calcareous tufas. This is the case of all the Quaternary fluvial deposits on the east slope of the Júcar Valley between Rambla Star and the Jalance Gorge, where these three terrace levels form a narrow staircased morphologic shoulder (Figs. 4, 6 and 13). The stratigraphy of the thickened sequence is complex including stacked bodies of gravels and large boulders topped by low-energy tufa deposits. The boulder units include large subrounded blocks (>1 m) of Cretaceous limestone, Triassic dolostone, but mainly Pliocene continental limestone (Fig. 13B). The latter were supplied by small flashy creeks with the headwaters in the Neogene depositional surface S1, as is the case of the Espadilla Creek coming from the incipient incision of the Carcelén Graben a few kilometers upstream (Figs. 3 and 5). These high-energy deposits are topped by riverine tufas dominated by phytoclast and bryophyte facies (Figs. 13 E and F). OSL dating of sandy beds located in

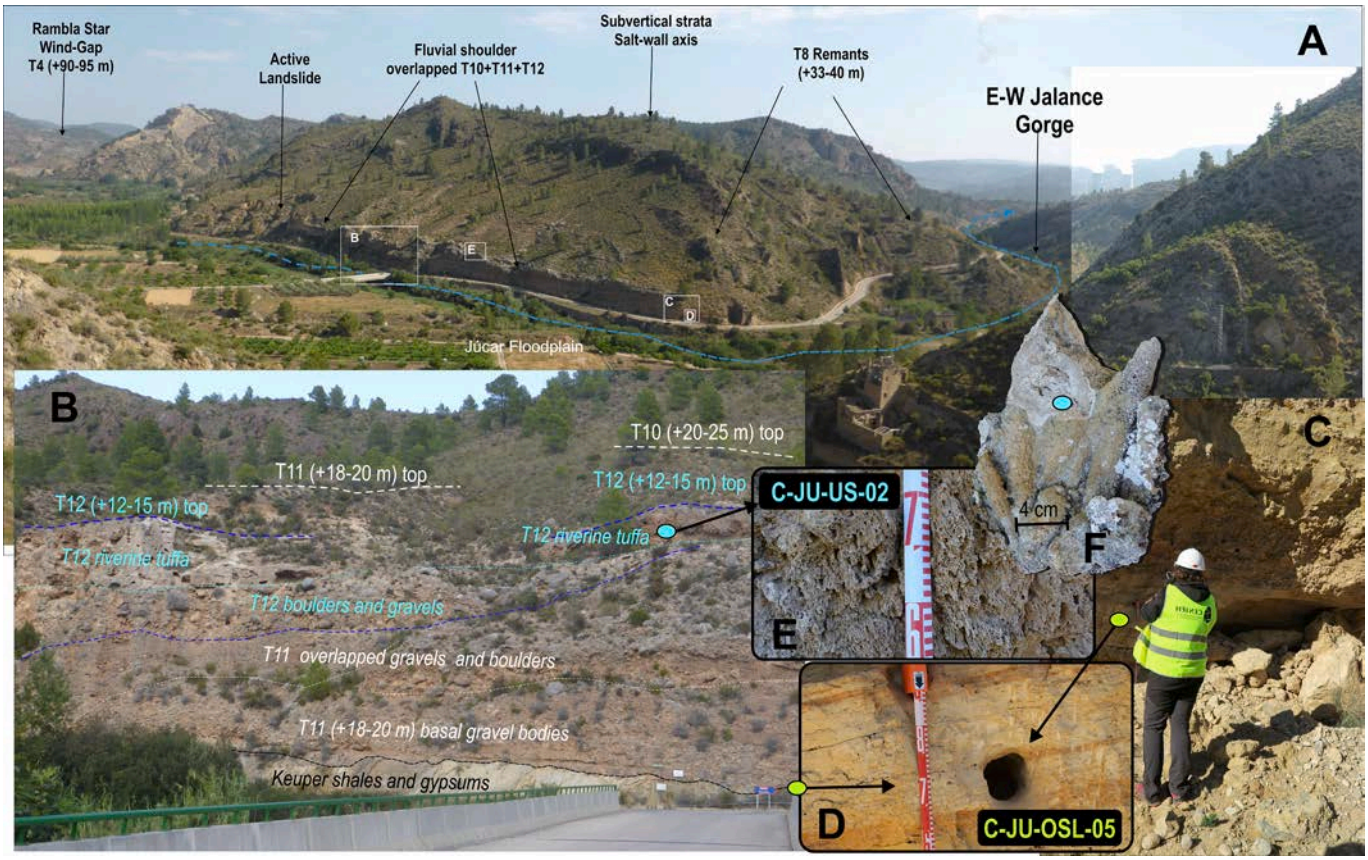

Fig. 13. Outcrops of the terraces T10, T11 and T12 on the left margin of the Jucar Valley between Rambla Star (North) and the Jalance Gorge (South). **A)** Panoramic view of the Jucar Valley showing the main geomorphological elements. **B)** View of the three terrace levels at the Júcar bridge site (El Puntal) with stacked deposits, showing the high-energy boulder gravel overlying unconformably the subvertical Triassic strata as well as the upper tufa deposits sampled for Th/U geochronological analysis. **C)** View of the sandy beds in the basal part of T11 sampled for OSL analysis (C-JU-OSL-05). **D)** Detailed view of the sediments sampled for OSL dating in T11. **E)** Detailed view of the tufa facies sampled for Th/U dating in T12. **F)** Dated tufa sample (C-JU-US-02) in phythoerm facies.

the base of the high-energy deposits of T11 overlying unconformably the Keuper bedrock yielded an age of 117.5 ± 6.7 ka (Fig. 13C and D). Th/U dating of the upper briophyte boundstones in T12 provide similar ages of 107.5 ± 0.4 ka (Fig. 13 E and F). These age estimates indicate that the stacked deposits of these two terraces were deposited during the MIS 5. In this zone T11 and T12 are inset in T10 which outcrops as a secondary narrow bench at +20–25 m (Figs. 3 and 13A). In these outcrops this upper terrace is also capped by tufa sediments, but mainly composed by massive phytoclast facies inadequate for U/Th dating. OSL dating of the basal sandy deposits underlying terrace T10 in the Rambla Star outlet (Figs. 4 and 6) indicate a Middle Pleistocene age of 193.4 ± 12.0 ka (MIS 6) as occur in the basal deposits of the thickened sequences of T9 and T11 (Table 1). Therefore, there is the possibility that terrace T12 can only be differentiated in this sector of the valley, whilst upstream can be included in the thickened and stacked sequences of T9 and T11. Similar thickened assemblages are also found in the complex terrace sequences recording the Middle-Upper Pleistocene transition in valleys of the Tagus and Ebro basins carved in Miocene evaporites (Silva et al., 2017; Benito et al., 2010). Consequently, some climatic signal linked to the late stages and termination of the cold stage MIS 6 and the onset of the last interglacial (MIS 5), may have contributed to the development of this set of young terraces.

The youngest terrace T13 (+8–10 m) is entirely developed during the Upper Pleistocene and the dated section in the Jucar Valley (Fuente Grande; Figs. 4 and 6) provided an age of 72.2 ± 4.89 ka (Table 1), which place its formation around the MIS 5/4 transition. However, MIS 4 alluvial and colluvial lateral deposits are common topping most of the thickened terrace sequences from T6 to T12 (Fig. 6). This fact suggests a water and sediment deficit in the axial fluvial systems during the early stages of the Last Glacial Cycle, compensated by lateral sedimentation from sourced from valley slopes and mantling the terrace surfaces. In many terrace sequences colluvial sedimentation is assisted, triggered or linked to important slope failure events (i.e., landsliding and mass-wasting processes). This younger terrace is completely submerged in the junction zone of the Cabriel and Júcar rivers by the tail of the Cortes de Pallás Reservoir (Fig. 4), where the water level is between +10–13 m above the original river thalwegs, so complementary dating was not possible. The deposits underlying the current floodplain (+3–5 m) have not been dated but have been generically assigned to the Holocene as occur in most of the valleys in the Iberian Peninsula (Silva et al., 2017).

6. Discussion

Here, we address different aspects regarding the long-term fluvial evolution of the zone: **(1)** analysis and chronology of geomorphic surfaces (planation and depositional) and their relationships with the graben systems and the longitudinal profile of the Júcar River; **(2)** chronology, processes and styles of valley development based on the geomorphological and geochronological analysis of the mapped terrace sequence; **(3)** similarities and differences between the studied terrace sequence with those of the Atlantic catchment of the Iberian Peninsula, suggesting possible regional factors influencing long-term fluvial evolution in the Mediterranean watershed.

Table 4
Chronosequence of main landforms in the Júcar-Cabriel fluvial system within the Ayora-Cofrentes Graben. Dating methods, laboratories and type of dated deposits/materials are indicated. Fig. 6 graphically illustrates this chronosequence.

Landform or process	Elevation +m	Age ka	Dating method and Lab	Type of deposit/material		
T1	130–135	>1800–2000[b]	K/Ar (Average Age)	Terrace deposits (cemented gravels)	Staircased terraces	Lower Pleistocene
Agrás Volcano	130–135	2400 ± 400[a]	K/Ar Coimbra (POR)	Basalt dykes and lava flows		
		1200 ± 200[a]	K/Ar Krueger (US)			
T2	110–112	No dated		Terrace deposits		
T3	105	No dated		Terrace deposits		
T4	90–95	No dated		Terrace deposits		
T5	70–75	No dated		Terrace deposits + Karstic depression		
T6	60	75.8 ± 5.6	OSL CNIEH (SP)	Colluvial deposits burying terrace	Local terrace thickening	Mid Pleistocene
		577.0 ± 43	ESR CNIEH (SP)	Terrace deposits		
T7	50	133.9 ± 8.2	OSL CNIEH (SP)	Colluvial deposits burying terrace		
		388.5 ± 32	ESR CNIEH (SP)	Terrace deposits		
Pico del Fraile Phreato-Vent	40–50	No dated		Piroclastic breccias, peperites pillow-breccias and pseudo-pillows		
T8	35–40	177.9 ± 9.7	OSL CNIEH (SP)	Terrace deposits		
T9	25–30	57.4 ± 0	OSL CNIEH (SP)	Colluvial deposits burying terrace	Widespread terrace thickening & superposition	Upper Pleistocene
		67.7 ± 4	OSL CNIEH (SP)	Colluvial deposits burying terrace		
		81.0 ± 5.3	OSL CITIUS (SP)	Terrace deposits		
		91.7 ± 4.8	Th/U CNIEH (SP)	Tufa deposits		
		105.9 ± 7.1	OSL CNIEH (SP)	Terrace deposits		
		180.1 ± 21	ESR CNIEH (SP)	Terrace deposits		
T10	20–25	193.4 ± 12	OSL CNIEH (SP)	Terrace deposits		
T11	18–20	116.9 ± 8.3	OSL CNIEH (SP)	Terrace deposits		
		117.6 ± 6.7	OSL CNIEH (SP)	Terrace deposits		
		137.0 ± 10.9	OSL CNIEH (SP)	Terrace deposits		
		167.9 ± 11.6	OSL CNIEH (SP)	Terrace deposits		
T12	12–15	80.2 ± 5.2	OSL CNIEH (SP)	Terrace deposits		
		107.5 ± 0.64	Th/U CNIEH (SP)	Tufa deposits		
T13	8–10	72.2 ± 4.89	OSL CNIEH (SP)	Terrace deposits		
T14	3–5	No dated		Floodplain		HOL

6.1. *Long-term fluvial evolution inferred from longitudinal profiles of geomorphic surfaces and rivers*

The described terrace sequence in the Júcar and Cabriel valleys is composed of 14 terrace levels at relative heights between +135 m +3–5 m, developed since at least 2.0–1.8 Ma as indicates the K/Ar dating of volcanic materials disrupting the uppermost terrace (T1). This terrace sequence is inset into previous pre-incision surfaces in the zone (S_0 and S_1; Figs. 5 and 14) and follows the path outlined by the E-W and N-S Neogene grabens of the area (Fig. 2). Longitudinal profiles of the main geomorphic surfaces mapped in the zone have been constructed by the calculation of successive pre-incision surfaces (S_0 to S_4). The mapped geomorphic and geologic features can be used to construct in a GIS environment theoretical DEMs of the successive surfaces (i.e., evolutionary stages) within the grabens. The paleotopography of the successive pre-incision surfaces have been calculated by means of ArcGis-based geostatistical tools developed to obtain theoretical pre-incision "ridgeline surfaces" following the method proposed for Menéndez et al. (2008) and Elez et al. (2020) to assess fluvial erosion of volcanic islands (Canary Islands).

S_0 is a planation surface mainly cut across folded Cretaceous carbonate rocks forming the tablelands at the margins of the grabens (e.g., Caroch Massif). S_0 is probably correlative to the so-called Main Planation Surface of the Iberian Chain, which truncates the folded Mesozoic and Paleogene formations and affected the development of Neogene grabens (Gutierrez-Elorza and Gracia, 1997). An Oligocene to Lower Mioccene age has been ascribed to this regional planation surface (Benito-Calvo and Perez-Gonzalez, 2007), which is consistent with the age of the oldest deposits of the graben system around the area (Santisteban et al., 1990; Roca et al., 2013; Gutiérrez et al., 2019).

The surface S_0 shows an upwarped profile coinciding with and interrupted by the Ayora-Cofrentes Graben (Fig. 14), suggesting that this deformation occurred during the development of the Neogene graben and the associated salt wall, and has been probably active also during the subsequent Quaternary graben dissection (e.g., Gutiérrez et al., 2019). This planation surface records a differential elevation of around 180–200 m with respect to the depositional surface S_1, as observed in the central zone of the graben (Fig. 14). This difference progressively decreases to the east and west, and about 50 km away in both directions the planation surface S_0 is overlapped and buried by the sediments underlaying the depositional surface S_1 (i.e., Llanura Manchega Plain to the west). Probably, most of the uplift occurred over the last 15 Ma (Langhian, middle Miocene), from the onset of the development of the Ayora-Cofrentes graben-salt wall system (Santisteban et al., 1990; Ruiz-Sanchez et al., 2011; Gutiérrez et al., 2019).

The late Neogene depositional surface S_1 records a more modest upwarping of around 40–50 m that occurred after the end of the sedimentary infill of the graben, dated at 2.5–2.0 Ma by the faunal content of the lacustrine limestones around the zone (Villafranchian; Alcalá et al., 1985). This late Neogene surface is mostly confined to the grabens in the studied area, where the Neogene sedimentary fill reaches a thickness of up to 500 m and is capped by the aforementioned Villafranchian limestones (Figs. 5 and 14). These sediments were also deposited beyond the graben system and merge towards the north, west and south with the Llanura Manchega plain, where the headward propagating fluvial incision wave has not reached and the Late Neogene plains remain undissected (Figs. 2 and 14). These aggradational plains constitute the most important ancient landforms in central Spain, recording extensive late

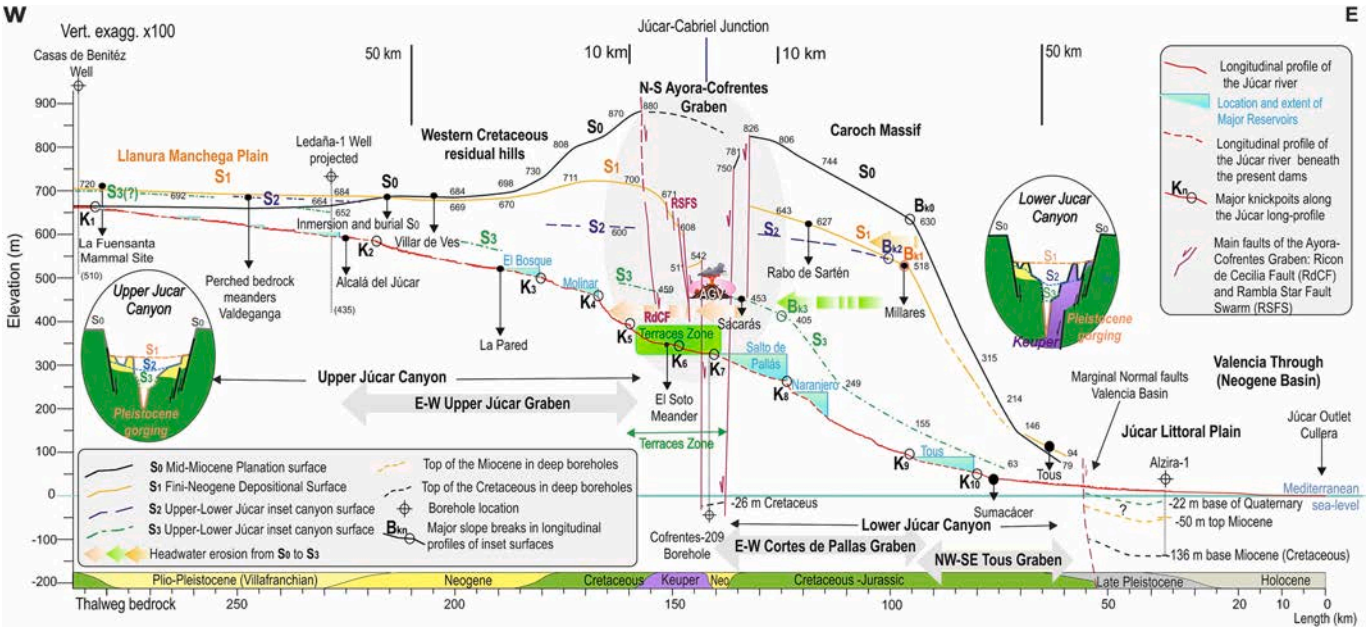

Fig. 14. Longitudinal profile of the Júcar River and profile of the regional surfaces (S_0 and S_1) projected on the Júcar Valley, illustrating the pre-fluvial incision stages and the significant upwarping of the planation surface S_0 and the collapse of the Pliocene limestones within the salt wall (depositional surface S_1). The graph also includes the projection of two inset erosional surfaces (S_2 and S_3) within the Upper and Lower Júcar canyons. Schematic cross-sections of the upper (left) and lower (right) Júcar canyons illustrate the geometric relationships of erosional landforms upstream and downstream of the Ayora-Cofrentes Graben. The location of the main faults and the most important slope breaks (Bk_0 to Bk_3) observed in the projected profiles of the surfaces and longitudinal profile of the Júcar River (K_1 to K_{10}) are indicated. The extrapolated profile of the Júcar River (from old topographic maps) beneath the present reservoirs (inundated zones of the valleys) is shown as dashed lines. Boreholes have been used to locate the elevation of relevant stratigraphic markers/discontinuities related to the plotted surface profiles. The green ellipse indicates the location of the terrace sequence analyzed in this study within the Ayora-Cofrentes Graben and its salt wall. Note vertical exaggeration is x100. (For interpretation of the references to colour in this figure legend, the reader is referred to the web version of this article.)

Neogene flat landscapes (i.e., Páramo Surface) that predate Quaternary fluvial incision (Pérez-González, 1994; Silva et al., 2017), as also occurs in the studied zone.

However, the most important deformation affecting S_1 and the underlying limestones is their subsidence along the salt wall below their regional elevation (Fig. 14). This lacustrine formation lies at an elevation of around 640 m west of the salt wall, whilst in the salt wall it is situated at about 510 m in Muela Star, indicating a minimum vertical displacement of 130 m (Fig. 4). The collapse of the Pliocene limestone within the diapir has also produced the conspicuous westward tilting of the Muela Star, as well as the Rambla Star normal fault system, dipping towards the salt wall axis and with a minimum cumulative throw of around 65 m. These subsidence structures confined to the deeply entrenched salt wall can be attributed to the collapse of the diapir by salt dissolution (e.g., Gutiérrez, 2004; Guerrero et al., 2015). Following these authors, the long-term solutional removal of salt form the subsurface is favored by the entrenchment of the fluvial system, that allows the interaction of unsaturated groundwater with progressively deeper evaporites (i.e., karst rejuvenation). Locally, this process may have been intensified by groundwater rising from below the Triassic evaporites, as indicates the presence of deeply-sourced springs (i.e., hypogene karst) such as Los Hervideros warm spring (Gutiérrez et al., 2019). Salt dissolution is most probably an active process at the present time as supports the observed geomorphic (e.g., karst depressions of Hoya de Agrás and Jalance) and structural evidence (e.g., local subsidence structures in recent terraces at El Soto, Burruchuelo and Las Parras terraces intersected by the Rambla Star Fault Swarm) (Fig. 5). Similar subsidence structures related to dissolution collapse of salt walls have been documented in the so-called salt valleys of the Canyonlands section of the Colorado Plateau (Doelling, 2000; Gutiérrez, 2004; Guerrero et al., 2015).

The progressive attenuation of the upwarping of surface S_1 towards the southern undissected sector of the Ayora-Confrentes Graben supports the important role played by the subsequent erosional unloading induced by fluvial incision in the Quaternary activity of the salt wall. In the northern zone of the graben, S_1 is offset by an important set of normal faults (Rambla Star; Figs. 5 and 14) along the western edge of the graben. Deformation of S_1 and several terraces along the axis of the diapir by dissolution-induced faults indicates that solutional has been the dominant deformation process during the Quaternary incision period. Nonetheless, local uplift is evident around the transverse Jalance Gorge (Fig. 5). Quaternary diapiric uplift has been documented in the nearby and barely dissected Navarrés salt wall, where fluvial terraces have been uplifted, tilted (away from diapir axis) and faulted (reverse faults) by salt rise (Fig. 2; Gutiérrez et al., 2019). Fluvial incision, salt rise and dissolution collapse are fully compatible processes with a positive feedback relationship. Fluvial entrenchment fosters salt rise towards the erosionally unloaded areas, as well as karst rejuvenation by both base-level drop and upward salt flow towards shallower zones with circulation of unsaturated groundwater.

The geomorphic analysis performed in the area allowed us to identify two additional lower erosional surfaces (S_2 and S_3) confined to the Upper and Lower Jucar canyons (Fig. 14), and hence related to fluvial erosion and valley formation. Various fluvial erosional landforms in the two Júcar canyons, such as hanging tributary valleys, perched bedrock meanders and rock-cut benches, record base-level stabilization stages older that the formation of the studied terrace sequence. As illustrated in Fig. 14, the projected longitudinal profiles of S_2 and S_3 are discontinuous restricting their analysis. They are absent within the Ayora-Cofrentes graben, being impossible to relate them with subsidence or uplift processes. However, they projection towards the east and west along the Júcar canyons allow to infer important slope breaks (Bk_0 to Bk_3; Fig. 14) related to regional evolution. Bk_0 defined by the planation surface S_0 indicates differential vertical tectonic displacement between El Caroch Massif and the littoral Valencia Basin reflecting the distribution, pattern and amount of uplift in the zone for at least the last 15 Ma. The projected

profile of S_1 is nearly subparallel to S_0 and displays a second prominent slope break (Bk_1) practically in the same zone around the locality of Los Millares, but inset 122 m below (Fig. 14). The subparallel pattern of S_0 and S_1 profiles indicate continuous and spatially similar uplift over the last 2.0–2.5 Ma. Downstream of Los Millares S_1 and S_0 converge progressively along the Lower Júcar Canyon to finally overlap S_0 around the locality of Tous 96 km away, where the Miocene sediments overlay the Cretaceous materials of El Caroch Massif.

A third important slope break (Bk_2) is associated with the eastern termination of the inset surface S_2 and nearly coincides in elevation with those of S_1 also around Los Millares (Fig. 14). Downstream this slope break is difficult to unravel relationships between these two surfaces (S_2 and S_1). However, upstream this slope break S_2 records the onset of fluvial incision within the grabens, as well as an apparent attenuation of regional uplift (minor gradient of the profile). Between Los Millares and Rabo de Sartén S_2 is represented by flat-floored valleys poorly incised into S_1, rock benches in the canyon slopes and cut-off incised meanders perched about +250–220 m above the Júcar River (Fig. 14), all of them relict landforms. In more distant upstream areas, a dense network of meandering valleys (bedrock-incised meanders; sense Harvey, 2007) is inset about 40 m into the Villafranchian surface S_1. In these zones S_1 forms the flat interfluve of the Júcar and Cabriel Valleys (Pérez-González, 1994) and merges with La Llanura Manchega plains (Fig. 14). This initial stage of base-level stabilization (S_2) produced small flat-floored gorges in the Lower Júcar Canyon and a dense network of incised bedrock meanders upstream of the Ayora-Cofrentes Graben (Fig. 14). These erosional landforms inset into S_1 record a low-gradient drainage network (S_2) formed before the onset of the aggressive fluvial entrenchment of the area.

Remnants of a lower erosional surface (S_3) recording a younger stage of base-level stabilization of the Júcar River have been also identified. They occur as discontinuous rock benches (strath terraces) within the Upper and Lower Júcar canyons delineating flat-floored canyons (presently perched valleys) developed before the deep gorging of the drainage. They are located at ~450–460 m a.s.l. in the Lower and Upper Júcar canyons between the reservoirs of El Molinar and Salto de Pallás (Fig. 14). Perched tributary valleys and erosional benches are located at relative heights of 150–140 m above the thalwegs and mark the initiation of fluvial terrace development in the Júcar and Cabriel valleys (T1 +130–135 m), dated in ca. 1.8 Ma in the Agrás Volcano (Sáenz-Ridruejo and López-Mariñas, 1975; Ancochea and Huertas, 2002). Therefore, it can be stated that the erosion period between the depositional surface (S_1) and this last erosional inset surface (S_3) can be ascribed to the early Pleistocene Gelasian stage or even to a wider Plio-Pleistocene "*Villafranchian period*". Transverse profiles of the upper and lower Júcar canyons sketched in Fig. 14 illustrate these different stages of erosion before valley gorging and terrace development within the Ayora-Cofrentes Graben. In fact, the longitudinal profile of S_3 delineates a convex longitudinal profile typical of river basins subject to active uplift (e.g., Hovius, 2000; Menéndez et al., 2008). Its profile displays the third major slope break (Bk_3) in the analyzed area (Fig. 14), a relict knickpoint related to the initiation of the aggressive entrenchment of the fluvial systems into the Neogene fill of the Ayora-Confrentes Graben. Bk_3 is located 34 km upstream and 85 m lower than Bk_2, suggesting a period of accelerated incision and important headward erosion for this pre-gorging stage during the Gelasian. Towards the west, the longitudinal profile of S_3 clearly converges with those of the previous geomorphic surfaces, merging in the zone of La Fuensanta (Fig. 14), where Lower Pleistocene faunal assemblages have been found in the upper Júcar terraces of the zone between +60 and +80 m (Mazo et al., 1990). These terraces located upstream the Júcar Canyon are poorly incised (<20 m) into the large Plio-Pleistocene alluvial platform of the Júcar (Fig. 2), but relationships among the studied surfaces, terraces and these upstream fluvial levels are difficult to unravel. The obtained data and convergent longitudinal profiles suggest that in these upstream zones headward erosion is moderate and Quaternary deposits are assembled in stacked sequences up to 8–10 m thick (Mazo et al., 1990) (Fig. 14). This makes difficult to correlate terrace sequences upstream and downstream the canyons, since terrace development is nearly null within the canyons.

The most important feature of the longitudinal profiles in Fig. 14 is that all of them are convergent upstream and downstream the canyons showing convex geometries in some cases domed (S_1 and S_0) because of tectonic and halokinetic processes. Maximum differences in elevation among the different geomorphic surfaces always occur around of the Ayora-Cofrentes Graben (Fig. 14), where all longitudinal surface profiles display convex geometries. This suggests that the erosional waves for the different surfaces, although of different amplitude, are kept nearly stationary around the Ayora-Cofrentes Graben, suggesting that fluvial incision has been sustained by localized regional uplift and salt tectonics within the graben. As indicated before the profile of S_3 is closely related to the construction of the first terrace (T1) and it displays a net convex geometry indicating active uplift (e.g., Hovius, 2000).

The present longitudinal profile of the Júcar River also displays an overall convex geometry connecting the LLanura Manchega flats (west) with the sedimentary fill of the littoral plain (east) throughout the upper and lower Júcar (Fig. 14). However, this overall convex geometry is stepped by numerous kinckpoints (K_1 to K_{10}) separating minor concave reaches and functioning as local base-levels. Some of the kinckpoints are clearly related to lithological changes (i.e., differential erosion) such as K_4 and K_7, at the contact between softer Neogene and Keuper materials and stronger Cretaceous limestones (Fig. 14). The erosional surface S_3 outlines the former convex longitudinal profile of the Júcar River, which is split into two profiles of different gradient upstream and downstream of knickpoint K_4, located at El Molinar Reservoir, upstream of the Ayora-Cofrentes Graben (Fig. 14). The section upstream K_4 displays a gently stepped profile where the present thalweg tends to converge with those of the ancient geomorphic surfaces (S_1 to S_3) inset within the graben system. On the other hand, the section between K_4 and K_{10} shows a stepped profile and a relatively high gradient, recording the aggressive entrenchment of the fluvial network in the Ayora-Cofrentes Graben and downstream, roughly up to the littoral plain dominated by an aggradational landscape. The lower knickpoint at Sumacárcer (Tous Reservoir; K_{10}) connects the Pleistocene fluvial valley with the ancient Holocene coastal plain (Carmona and Pérez Ballester, 2011). Geoarchaeological studies carried out by these authors around the Alzira area indicate the occurrence of a ~10 m thick fluvio-littoral Holocene succession from the last ca. 6000 yr overlying a significant accumulation of Pleistocene sediments (~50 m) (Fig. 14).

The studied terrace sequence exclusively occurs within the Ayora-Cofrentes Graben between knickpoints K_4 and K_7 but is mainly concentrated between K_5 and K_7 (Fig. 14). Internal kinckpoints within the graben zone cannot be solely attributed to lithological changes but mainly to the course of the Júcar channel across fault zones and/or the boundaries of the active salt wall. In other words, the analyzed area represents a very short reach within the Júcar Valley, but record the history of fluvial incision of the whole valley during the Quaternary, as well as its interference with vertical displacement related to upward salt flow and dissolution collapse within the salt wall. The relationships between these shallow deformation processes with deeper basement faults and volcanic processes in the zone remain obscure, but geophysical surveys (Roca et al., 2021) and inferences derived from the Pleistocene volcanic activity in the zone points to the occurrence of these crustal faults in the zone (Silva et al., 2015, 2023a).

6.2. Chronology, processes and styles of valley development

The present study identifies fourteen terraces in the Júcar and Cabriel valleys (Fig. 6). The obtained geochronological data (OSL, ESR, Th/U) allow grouping the identified terraces in three different sequences, which can be ascribed to the main stages of the Quaternary period. The upper terrace sequence between +135 and 70–75 m (T1 to T5) can be mainly attributed to the Calabrian stage (1.80–0.78 Ma) of the Early

Pleistocene as indicated by the K/Ar ages (2.0–1.2 Ma) of the volcanic materials (Agrás Volcano) disrupting terrace T1 in the Cabriel Valley. Previous fluvial evolution can be referred to the Gelasian stage (2.58–1.80 Ma), as can be deduced from the analysis of the geomorphic surfaces (S_2 and S_3) inset into the Villafranchian depositional surface S_1. These two surfaces merge with the alluvial platform at the headwaters of the Júcar, upstream La Fuensanta site (Figs. 2 and 14), and their Lower Pleistocene faunal assemblages support its relationship with the upper terrace sequence. That is, this set of old staircased terraces in the studied zone converges upstream, and seems to be correlative in the deposits underlying the alluvial platform. At La Fuensanta fossil site fluvial deposits display a condensed sequence 8 to 10 m thick (Mazo et al., 1990).

During this first stage of fluvial evolution (T1 to T5), the entrenchment of the valley network follows the path delineated by the Neogene graben system in a case of structural control of the drainage, that can be labelled as *"tectonically-controlled drainage"* (Fig. 15). The Cabriel Valley, roughly during the development of terrace T1, was locally disrupted (affected) by the phreatomagmatic activity of the Agrás Volcano, which seems to be a small monogenetic basaltic edifice growing in an ancient floodplain (Sáenz-Riduejo and López Marinas, 1977; Silva et al., 2015), but with minor impact in fluvial evolution. Within the present Júcar Valley this set of upper staircased terraces are only well represented in the N-S Burruchelo ridge, delineating the north-directed path of the Júcar River during the Early Pleistocene (Fig. 5). A similar strip of old strath terraces is also found in the headwaters of the N-S La Espadilla Creek but absent within the Júcar Valley downstream the Jalance Gorge. This set of upper terraces is also found in the Cabriel Valley upstream of the present Cabriel-Júcar junction (Fig. 5). The distribution of the upper terrace sequence strongly suggests that the drainage adapted to the western flank of the salt wall, forcing a N-S direction within the graben directed to the north, towards Rambla Star (Fig. 15). In this scenario the outlet of the Júcar River from the upper canyon would connect with a N-S drainage that flowed into the Cabriel River through the Rambla Star, which headwaters preserve perched fluvial deposits at +90–95 m (T4; Figs. 4 and 5)). In this sense, the present headwaters of Rambla Star connecting the Cabriel and Júcar valleys can be considered as a wind gap marking the ancient confluence zone of the Júcar and Cabriel valleys west of the incipient salt ridge (Fig. 15B). This ancient water gap was probably facilitated by the collapse of the western flank of the uprising salt ridge along the Rambla Star Fault swarm. The concurrence in N-S oriented normal faults, and the N-S elongated salt ridge was an obstacle for E-W valley incision, deflecting the drainage to the north throughout the Rambla Star wind gap (T4). During this initial stage of valley entrenchment (Lower Pleistocene) the Júcar-Cabriel system transversally incised the N-S growing salt ridge north of Muela Star (Fig. 15C) leading to a case of antecedence drainage across the salt wall. The karstic depression (Hoya de Agrás) correlative to T5 (+70–75 m) on the eastern flank of the salt ridge testifies the occurrence and persistence of this kind of dissolution-induced subsidence processes around the uprising salt ridge during the end of the Lower Pleistocene (Fig. 4).

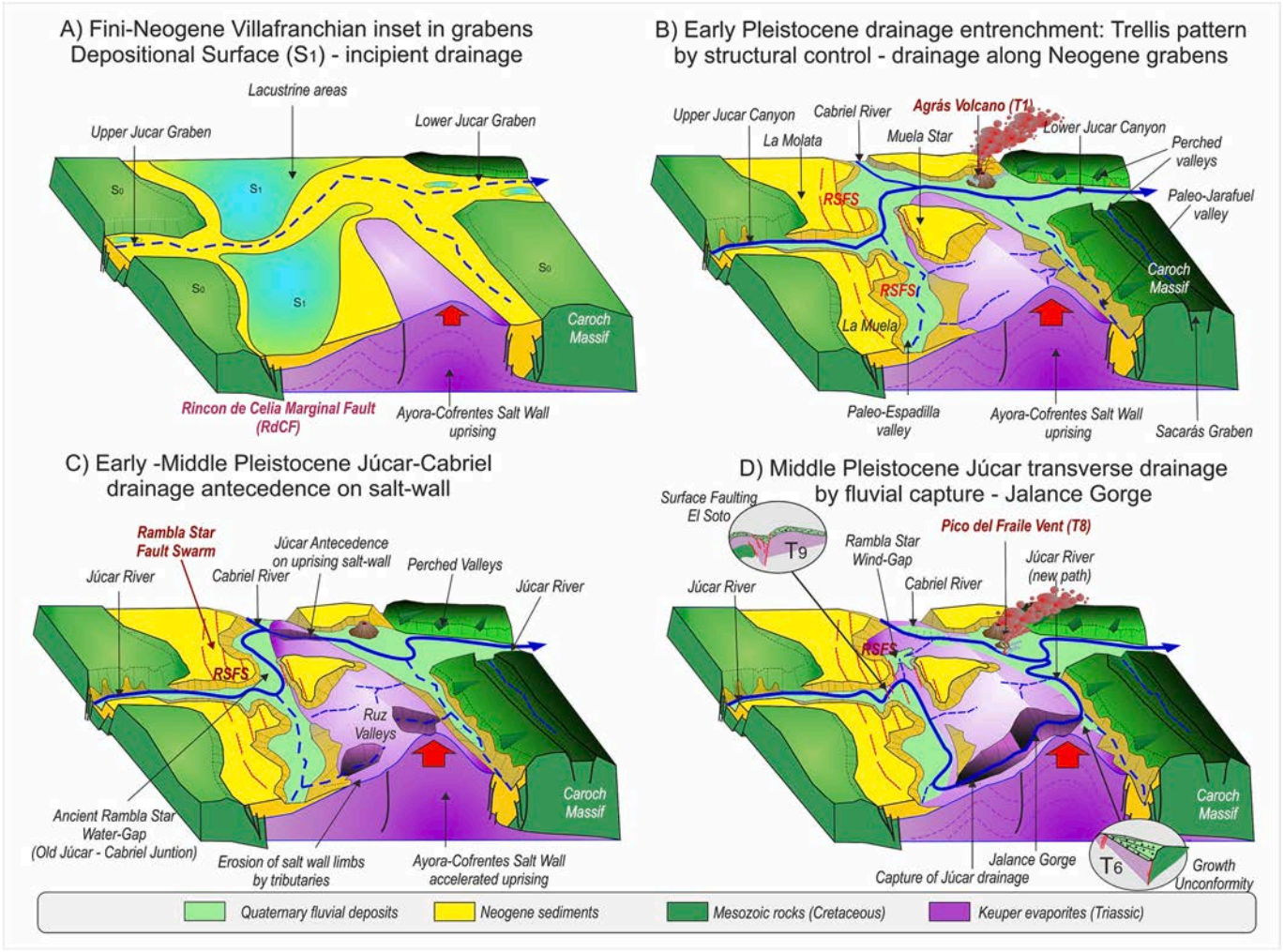

Fig. 15. Evolutionary stages of the Cabriel and Júcar fluvial system during A: Plio-Pleistocene (Villafranchian); B: Early Pleistocene; B: Early-Middle Pleistocene transit; C: Middle Pleistocene to Present.

During the end of the Lower Pleistocene the western flank of the salt ridge was drained by another N-S-oriented stream corresponding to an ancient Jarafuel Valley. Orthogonal tributaries to the primitive Jarafuel (east) and Espadilla creeks (west) started to generate *ruz-type* creeks (i.e., down-dip cataclinal valleys) at both limbs of the salt ridge (Fig. 15C).

The middle terrace sequence between +60–65 m and +25–30 m (T6 to T9) shows thickened deposits and deformations recording the synsedimentary continuation of the subsidence processes and differential uplift of the axial salt ridge within the Ayora-Cofrentes Valley. The geochronological data indicate that the first terrace of the sequence (T6) has an ESR age of 577 ± 43 ka and the upper sediments of T9 belong to the last interglacial with OSL ages of around 100 ka (Fig. 4; Tables 1 and 2). Consequently, this terrace sequence developed during the whole Middle Pleistocene from MIS 15–14 to the end of the last interglacial MIS 5. These thickened terraces show an important component of lateral supply of alluvial deposits, formed by sub-angular clasts of mainly Triassic dolostones and angular boulders of well-cemented Neogene conglomerates and limestones. Most of the colluvial facies in the thickened terrace deposits were sourced from the growing salt ridge and overlying Neogene sediments. On the contrary, well-rounded fluvial gravels come mainly from Cretaceous and Jurassic limestones. This process is documented in T6 (+60–65 m) immediately downstream of the Jalance Gorge, where fluvial deposits record an important thickening and a striking progressive unconformity on the eastern flank of the salt ridge (Fig. 8). The OSL age of the upper alluvial deposits above the unconformity (75.8 ± 5.6 ka) indicates that a nearly continuous deformation occurred throughout the Middle Pleistocene. However, the most significant amount of alluvial and colluvial deposits occur in the thickened sequences of T6 and T7 terraces (Fig. 4), suggesting that major activity extended until ca. 380 ka (MIS 11). On the contrary, the thickened sequences of terraces T8 and T9 display a small proportion of colluvial-alluvial deposits, with dominant fluvial facies of sand and gravel bodies with crossbedding topped by floodplain laminated silts, clays and reddish soils (e.g., Figs. 10 and 11). The clear dominance of fluvial facies (s.s.) in these lower terraces of the sequence suggest that a stable (steady) fluvial connectivity is achieved all along the Júcar River channel over the last ca. 200 ka (Fig. 4). The obtained age estimations allow us to relate the two upper terraces with the Middle Pleistocene (Chibanian Stage) warm marine isotopic stages MIS 15 (T6) and MIS 11 (T7). Considering the older ESR age estimates for these terraces they can be related with two of the three first prominent glacial terminations VII, VI and V shown in the isotopic marine records (e.g., Lisiecki and Raymo, 2005; Bardají and Lario, 2022). In this case, the formation of the two oldest Middle Pleistocene terraces seems to be related to important climatic forcing. On the other hand, estimated ages for T8 and T9 place their development between MIS 7/6 and 5. In fact, the thickened sequences of T9 (+25–30 m) record the transition between the Middle and Upper Pleistocene. Consistent ESR, OSL and Th/U ages (four dates) obtained in this key terrace support this chronological interpretation (Fig. 6; Tables 1, 2 and 3). Additional OSL data in the colluvial-alluvial deposits of this terrace indicate that these are only important at the top of the sequence once the terrace became dissected and perched during the MIS 4 (ca. 68–55 ka; Fig. 4).

The performed analysis indicates that during this Middle Pleistocene stage the N-S oriented paleo Espadilla and Jarafuel valleys connected through the Jalance Gorge cutting across the uprising salt ridge (Fig. 15D). The important amount of colluvial lateral deposits within the progressive unconformity (growth strata) of T6 reveals important erosion on the flanks of the salt ridge immediately downstream the Jalance Gorge. Therefore, lithology, sedimentology and synsedimentary deformations in T6 indicate that this first Middle Pleistocene terrace is linked to the initiation of the transverse E-W Jalance Gorge (Fig. 15D), documenting an interesting case of antecedent drainage and capture. The Jucar River abandoned its ancient path towards the north (Cabriel) across the present wind gap of Rambla Star, turning to the south surrounding eventually cutting the salt ridge. Then the present drainage pattern conforms across the Jalance Gorge (Figs. 4 and 5). The new drainage pattern is featured by two N-S reaches of the Júcar flanking the protruding salt ridge and connected by the Jalance transverse E-W gorges allowing the present connection between the Upper and Lower Júcar canyons (Fig. 15D). Nowadays, La Espadilla and Jarafuel rivers remain as N-S tributaries upstream and downstream of the E-W antecedent gorge, testifying the previous paleogeographic stage (Fig. 15C; D). On the other hand, during this Middle Pleistocene stage, volcanic activity is renewed at the toe of the Agrás Volcano (AGV) during the deposit of terraces T7 and T8 at the Pico del Fraile vent (PDF; Figs. 4 and 5). This volcanic episode is featured by products of explosive phreatomagmatic origin that interfered with terrace development. The preserved outcrops make possible to identify a subcircular rim of pyroclastic basaltic breccia injected in T7 and T8, as well as abundant materials derived from magma-water interactions at the surface. Peperite materials, pseudo-pillow lavas and pseudo pillow-breccias present in T8 (Fig. 9) indicate the interaction and mixture of volcanic flows with water-saturated sediments. In this case, the subaqueous environment will correspond with the fluvial channel related with the accumulation of terrace T8, dated at ca. 180 ka (Fig. 5). The preliminary data presented here need to be complemented with further petrologic and stratigraphic analyses (e.g., Silva et al., 2023b) to define the extent of the impact of the PDF volcanic event in fluvial evolution, as well as their relationships with the pyroclastic-gravel materials of the Castillo de Cofrentes outcrop (CDC) in the opposite margin of the Cabriel Valley (Fig. 4).

The lower terrace sequence, between +20–25 m and +3–5 m (T10 -T14), developed during the Upper Pleistocene as indicated by the obtained OSL and Th/U ages (Tables 1 and 3). However, as observed in T9 (El Soto Terrace), the basal deposits of T10 and T11 overlie late Middle Pleistocene (MIS 6) stacked sequences because of continuous synsedimentary subsidence and aggradation (Fig. 6). The deformations displayed by these thickened terraces (e.g., Fig. 12) document the persistence of dissolution-induced subsidence and collapse processes around the salt ridge. These are especially important along the western margin of the Ayora-Cofrentes Graben, where the normal faults of the Rambla Star Fault Swarm affect to the deposits of T10, T11 at Las Parras and Burruchuelo sites, but also to T9 at El Soto Meander (Fig. 6). This fault system extends about 15 km to the south affecting to older terraces and the Villafranchian depositional surface S_1, as also occurs in the wind gap of Rambla Star (Fig. 4). OSL and Th/U ages (Tables 1 and 3) indicate that this set of young terraces mainly developed during the Upper Pleistocene (<126 ka), with the youngest age of ca. 72 ka obtained from T13 (ca. 72 ka). These terraces consist of fluvial sand and gravel facies with tufa deposits locally replacing the clayey floodplain facies and soils at the top of the sedimentary sequences (e.g., Fig. 13). Alluvial and colluvial deposits have a minor representation in these terraces, and only show some importance at the top of the sequences, as occur in El Soto Terrace (T9), where these deposits have a MIS 4 age (Fig. 6). In addition to the synsedimentary deformations, this set of terraces is significantly affected by landslides across the perimeter of the present salt ridge. This is especially important along the western flank of the salt wall in the Júcar Valley upstream and within the Jalance Gorge (Figs. 4 and 13). Mass wasting processes indicate the instability of the slopes in the salt ridge because of the combination of fluvial incision and salt rise. The analyzed data suggest that from the deposit of T6, terrace thickening became important and synsedimentary deformations increase in the different terraces of the sequence, indicating a clear relationship between increasing fluvial erosion and halokinetic and karstic processes. Within the Ayora-Cofrentes Graben, the relief created by diapiric activity increases in the areas with deeper fluvial entrenchment and higher erosional unloading. These data suggest that differential loading induced by fluvial entrenchment contributes to enhance diapiric activity and increase the amount of topographic relief in the region as occurs in other graben basin with salt walls around the Caroch Massif region and around the world (see review in Gutiérrez et al., 2019). These

mechanisms were probably also important for the deformation and doming of geomorphic surfaces S_0 and S_1 across the Graben.

6.3. Comparison of terrace development in the Atlantic and Mediterranean catchments of the Iberian Peninsula

As indicated in the introductory section, age-elevation data for the Mediterranean catchment of the Iberian Peninsula are only mainly available for the Ebro drainage basin (e.g., Lewis et al., 2009; Lewis, 2017; Soria-Jáuregui et al., 2016; Benito-Calvo et al., 2022). The existing data indicate that the Atlantic catchments consistently display younger ages for terraces at similar relative heights above the thalwegs. (e.g., Silva et al., 2017), which suggest slower uplift in the Ebro catchment. However, terrace ages obtained in this study indicate that the Júcar-Cabriel catchment behaves in a similar way than the Atlantic catchments, displaying even somehow higher uplift rates. In that way, the Ebro River basin, is the most ancient one of the Iberian Peninsula opened before the MSC (García-Castellanos and Larrasoaña, 2015). They overall longitudinal profile display a smooth concave profile typical of evolved fluvial systems, which contrast with the convex profiles of the Atlantic rivers subject to ongoing headward erosion predicting long-term eastwards migration of the Iberian divide (Struth et al., 2019). However, this situation seems to be not the same for the Mediterranean fluvial systems south of the Ebro catchment and the Iberian Range. Numerical data for the Betic Cordillera indicate that erosional unloading triggered by the MSC promoted peak uplift values of 407 ± 20 m for early Messinian littoral landforms and sediments, whilst in the Atlantic watershed uplift values did not surpass 150 ± 20 m (Elez et al., 2020). These spatial differences in bulk uplift between the Atlantic and Mediterranean catchments (~250 m maximum) dimmish along the Pliocene and Pleistocene (Elez et al., 2016, 2020), but would be beyond the important gorging of relatively small river basins in the Mediterranean slope (Fig. 1). Regardless the probable role played by the MSC on drainage initiation around the Mediterranean, renewed sedimentation in most of other tectonic Neogene basins along the Betic Cordillera after the MSC (i.e., Pliocene) is featured by endorheic terrestrial deposits disconnected from the sea (Sanz de Galdeano and Alfaro, 2004; Guerra-Merchán et al., 2019). This also occurred in the studied graben system, where Plio-Pleistocene terrestrial sedimentation partially replenishes the Neogene graben system and the onset of valley development occurred during the early Quaternary (Fig. 2). Fossil mammal-sites along the upper Jucar Graben (Pérez-González, 1994) support a Lower Pleistocene (i.e., Late Gelasian) for the initiation of fluvial incision within the grabens. As indicated in the introductory section, age-height data of terraces for the Mediterranean catchment of the Iberian Peninsula are only mainly available for the Ebro drainage basin (e.g., Lewis et al., 2009; Lewis, 2017; Soria-Jáuregui et al., 2016; Benito-Calvo et al., 2022). The existing data indicate that the Atlantic and Mediterranean catchments display contrasting ages for terraces at similar relative heights above the thalwegs and that they record variable uplift-rate trends (e.g., Silva et al., 2017; Benito-Calvo et al., 2022). For a similar relative height, the terraces of the Atlantic margin are older than those of the Ebro during the Lower Pleistocene, indicating higher relative uplift of the Mediterranean margin for this period. However, this situation is reversed from terraces below +70–75 m (MPT), which show higher relative heights in the Atlantic margin. Both situations are numerically described by the empirical age-height chronofunctions developed for the Atlantic valleys by Silva et al. (2017) and for the Ebro Basin by Benito-Calvo et al. (2022). The ages obtained in the present work indicate that the Júcar-Cabriel catchment behaves in a similar way than the Atlantic basins. Even from the MPT the ages of the terraces are slightly younger than in the Atlantic margins, suggesting that from the Middle Pleistocene onwards the uplift is renewed throughout the Mediterranean margin south of the Ebro Basin. As previously mentioned, the Ebro River basin is the most ancient of the Iberian Peninsula, opened before the MSC (García-Castellanos and Larrasoaña, 2015). The overall longitudinal profile of the Ebro River displays a smooth concave profile typical of mature fluvial systems, which contrast with the concave-convex profiles of the Atlantic rivers subject to ongoing headward erosion envisaging long-term eastwards migration of the Iberian divide (Struth et al., 2019). However, this situation does not seem to be the same for the Mediterranean fluvial systems south of the Ebro catchment and the Iberian Range (Fig. 1). In fact, the studied catchment shows a concave-convex longitudinal profile (Fig. 14) similar to those of the Atlantic rivers, suggesting less matures stage of development than the Ebro Basin. Numerical data for the Betic Cordillera indicate that erosional unloading triggered by the MSC promoted peak uplift values of 407 ± 20 m for early Messinian littoral landforms and sediments, being about an 70 % higher than in the Mediterranean (Elez et al., 2016, 2020). Following these authors, the spatial differences in bulk uplift between the Atlantic and Mediterranean catchments (~250 m maximum) diminished over the Pliocene and Pleistocene but could be behind the important gorging of relatively small river basins in the Mediterranean slope of the Betic Cordillera (Fig. 1).

Renewed sedimentation in most tectonic Neogene basins along the Betic Cordillera after the MSC (i.e., Pliocene) is featured by endorheic terrestrial deposits disconnected from the sea (Sanz de Galdeano and Alfaro, 2004; Guerra-Merchán et al., 2019). This also occurred in the studied area, located in the junction zone between the Iberian and the Betic cordilleras (Fig. 2), where Plio-Pleistocene terrestrial sedimentation partially replenishes the Neogene graben systems (Santisteban et al., 1990; Gutiérrez et al., 2019). Fossil mammal-sites in the upper Jucar Graben (Alcalá et al., 1985; Alberdi et al., 1997) support a Lower Pleistocene age (i.e., Late Gelasian) for the initiation of fluvial incision within the grabens (Fig. 2). This chronology also coincides with both; (a) the recorded MPT reversion in uplift trends and; (b) the diversion towards the Mediterranean of the early Quaternary Júcar-Cabriel drainage system (old fluvial platform; Fig. 1) proposed by Pérez-González (1994). Middle to Late Pleistocene terraces in the Júcar Valley display similar relative elevations than in the Atlantic catchments. In this case, fluvial downcutting enhanced erosional unloading and probably promote local diapiric uplift within the grabens. These interlinked processes may alter the terrace relative heights (Gutiérrez et al., 2019), sustaining convex river profiles within the grabens despite the occurrence of local subsidence processes and terrace thickening. Recent studies of long-term fluvial incision based in comprehensive terrace chronologies, including the oldest alluvial levels and/or pre-incision surfaces indicate that valley entrenchment may occur at decelerating rates trending to steady state base-levels (i.e., Sartégou et al., 2018; Benito-Calvo et al., 2022). This is of special importance in subsiding areas where vertical displacements are counterbalanced by aggradation and the generation of thickened terraces with stacked alluvial sequences. In the Júcar Valley these processes are clear from the T6 terrace (ca. 600 ka), but specially from the more modern set of terraces (T9 to T13) recording the last ca. 200 ka. These terraces (10–12 m thick) present basal sequences of the Middle Pleistocene (MIS 6), overlain by alluvial sediments of the last Interglacial (MIS 5) and capped by locally-derived alluvial- colluvial deposits corresponding to the MIS 4 (Fig. 6). In detail, terraces T9 to T12 (between +25 and +15 m) display complex geomorphic assemblages with cut and fill juxtaposed sequences with comparable base-levels illustrating the aforementioned near steady-state trend. These inset terrace sequences are recorded in the evaporitic materials of the graben surrounding the axial salt ridge and are located between two prominent knickpoints of the river longitudinal profile (K_5 and K_7). These are located between the Upper and Lower Júcar Canyon, which seems to be worked as effective internal thresholds for the upstream propagation of incision waves derived from sea-level changes favoring alluvial aggradation vs fluvial dissection in this stretch of the valley (Fig. 14).

Climatic and sea-level changes induced by glacial-interglacial cycles may control the alternation of aggradation and incision phases responsible for the construction of individual terraces (Stokes et al., 2012). On the other hand, the long-term entrenchment of the valley in the bedrock

(and the formation of canyons) will require of the cumulative potential energy resulting from repeated base-level falls, subsequent erosional unloading and isostatic uplift sustaining the headward propagation of fluvial incision waves (Bridgland, 2000; García et al., 2004; Elez et al., 2016; Benito-Calvo et al., 2022). The convex geometry of the longitudinal profiles of the Pliocene to Quaternary inset surfaces (S_1 to S_3) seems to reflect the westward propagation of incision waves throughout the graben system after their capture by the external drainage network, showing a less mature landscape (Fig. 14). Some authors indicate that these kind of morphologies in river longitudinal profiles reflect the onset and headward propagation of incision waves (e.g., Sartégou et al., 2018; Benito-Calvo et al., 2022). Similar convex geometries of age-incision curves derived from the geochronological analysis of fluvial terraces have a similar meaning (Silva and Roquero, 2022). In our case the important altitudinal step between K_4 and K_7 (~130 m) achieve the bulk relative elevation of the studied terrace sequence (+130–135 m). This step seems to represent the entrenchment related to the propagation of the Quaternary incision wave throughout the Ayora-Cofrentes Graben from the Lower Pleistocene, which is roughly delineated by the sigmoidal profile of S_3, otherwise nearly coincident in elevation with that of terrace T1. The elevation difference with the present stepped concave profile of the Júcar River within the graben (Fig. 14) represents the overall magnitude of the incision.

7. Concluding remarks

Geomorphological analysis of the Júcar and Cabriel river valleys in their confluence zone within the Ayora-Cofrentes Graben reveals a fluvial terrace sequence composed of at least 14 terraces lying up to +135–130 m above the present river thalwegs. This sequence shows a lower number of terrace levels than that of the Ebro River (22 terraces; Benito-Calvo et al., 2022), but similar to those of the Iberian Atlantic catchment (i.e., Tagus, Duero) for terraces below +70 m (Middle Pleistocene). Younger Late Pleistocene terraces below +30 m (T9 to T13; Fig. 6) show slightly younger ages than those of equivalent relative heights in the Atlantic margin. Therefore, the studied catchment displays a similar behaviour to those of the Atlantic catchment from the Lower-Middle Pleistocene transition (i.e., MPT), displaying similar long-term uplift trends and convex long-profile geometries, different from the graded concave profiles showed by the more mature Ebro catchment, which has a more protracted evolution started in Late Neogene times (e.g., Struth et al., 2019). In absence of field data indicating a poor preservation of fluvial landforms between the Ebro and Júcar catchments, their differences might indicate (a): a more recent Quaternary development of the drainage in the Mediterranean catchment south to the Ebro Basin and the Iberian Range (Fig. 1); and (b): sustained uplift within the graben system related to the interplay of erosional unloading and diapiric processes in the evaporitic substratum, which is supported by the consistent convex morphology of the computed longitudinal profiles (Fig. 14) and the relative younger ages of the mid to late Pleistocene terrace levels (Fig. 6; Table 4). As occur in the Atlantic valleys, the change in the long-term uplift trends also can be situated around the MPT. However, additional geochronological data from younger terraces in the Ebro Valley and older terraces in the Júcar-Cabriel catchment will be necessary to unambiguously validate this hypothesis. Further age data for the more recent Mediterranean basins of the Betic Cordillera will be necessary to obtain a comprehensive view of the fluvial evolution of the Mediterranean catchments during the Quaternary.

The timing of terrace development presented in this paper is supported by the set of 20 new numerical ages obtained by means of OSL, ESR and Th/U methods. These age data allow differentiating three sets of terrace sequences belonging to the Calabrian stage of the Lower Pleistocene (T1-T5), Middle Pleistocene (T6-T9) and Upper Pleistocene (T8-T13). T14 corresponds to the present floodplain attributed to the Holocene (Fig. 6). Geochronological data are available for the complete terrace sequence below +70–75 m (T5). The oldest age corresponds to the K/Ar dating of volcanic materials intruding and disrupting terrace T1 (+135–130 m), bracketed between 2.2 and 1.2 Ma by Sanchéz Ridruejo and Lopez Mariñas (1977). However, considering the more similar behaviour to the Atlantic rivers, published chronofunctions for this catchment will support the younger age of ca. 1.2 Ma provided by the volcanic materials by the Coimbra dating Laboratories (Table 4).

The oldest age obtained in this study corresponds to the ESR-dated terrace T6 (+60–65 m; 577 ± 43 ka), corresponding to the MIS 15 or MIS16/15 transition within the Middle Pleistocene. The youngest terrace sequence down to +25–30 m (T9–T13) belong to the last 200 ka, but essentially to the Last Interglacial (MIS 5). Most of the OSL and Th/U ages obtained in the top sequences of this younger terrace set cluster between 120 and 72 ka, suggesting an apparent base-level stabilization sustained by subsidence related to the dissolution of the evaporite bedrock, leading to important terrace thickenings (10–12 m). In fact, these terraces display stacked alluvial sequences with basal deposits belonging to the final stages of the Middle Pleistocene (190–170 ka). Differential ground deformation occurred along the perimeter of the N-S salt ridge (salt wall) protruding along the axial zone of the Ayora-Cofrentes Graben. Gradual subsidence and sudden collapse events produced by the dissolution of the underlying evaporites are recorded as progressive unconformities (growth strata), subvertical gravel and sand injections, soft-sediment deformation structures and steep normal and pseudo-reverse faults. Gravitational faulting is particularly important along the western margin of the graben where N-S surface faulting along the Rambla Star Fault Swarm affects to T9 (El Soto Terrace). Growth unconformities, terrace thickening and the incorporation of a substantial amount of laterally-derived alluvial and colluvial materials are important since the development of T6 (+65–60 m), related to the onset of the rise of the salt ridge in the axial zone of the graben. The activity of this N-S elongated salt diapir interfered with fluvial evolution, forcing different processes in the drainage network such as superposition, capture, and antecedence accompanied by significant palaeogeographical changes (Fig. 15).

Terrace sequences, dates and their geographical distribution allow distinguishing different evolutionary stages in the Cabriel-Júcar Valley junction. In an initial stage the drainage was conditioned by the basin and range topography inherited from the Late Neogene graben system, allowing the installation of a main west-to-east drainage connecting the Late Neogene E-W Upper and Lower Júcar grabens (Fig. 15B). In this stage, the Júcar-Cabriel junction was located to the north of the present Rambla Star wind gap (the ancient water-gap of the Júcar towards the Cabiel). This scheme also included NNE-SSW to N-S tributaries (Espadilla, Jarafuel, Cabriel) flanking the axial salt ridge within the Ayora-Cofrentes Graben. In a following stage the salt ridge propagated to the north protruding within the graben and allowing a process of drainage antecedence across the rising diapir (Fig. 15 C). Erosion on the flanks the uprising salt ridge diapir allow the generation of down-dip valleys. This palaeogeographical scenario remained at least until the development of T5 (>600 ka). T6 records the connection of the N-S tributaries bordering the salt ridge through the transverse Jalance Gorge (Fig. 15 D). This represents another transverse drainage generated by the capture of the ancient Espadilla Creek by the old Jarafuel Stream, redirecting the Júcar River to the south. This episode led to the abandonment of the ancient Cabriel-Júcar junction across the Rambla Star, presently a wind gap between both valleys (Fig. 4), and the establishment of the present zig-zag pattern of the drainage within the Ayora-Cofrentes Graben. In this changing palaeogeographical scenario volcanic eruptions of the Agrás Volcano (AGV; T1) and El Pico de El Fraile vent (PDF; T7-T8) occurred around the Cabriel-Júcar junction. These were endogenous phreato-magmatic explosive eruptions that produced a variety of magma-water interaction features recorded in the terraces (peperites, cauliflower bombs, pseudo pillow-breccias, pyroclastic flows and rims, etc.). The OSL dating of T8 (ca. 180 ka) reported in this paper allows us to date the youngest volcanic activity in the zone (PDF) during the end of the

Middle Pleistocene revising previous estimates indicating a Lower Pleistocene age for all the volcanic materials around the locality of Cofrentes.

CRediT authorship contribution statement

Pablo G. Silva: Writing – review & editing, Writing – original draft, Validation, Supervision, Project administration, Methodology, Investigation, Funding acquisition, Conceptualization. **Fernando Tapias:** Investigation, Formal analysis, Data curation. **Javier Élez:** Visualization, Software, Investigation, Formal analysis, Data curation. **Elvira Roquero:** Writing – original draft, Methodology, Investigation, Formal analysis, Data curation. **Francisco Gutiérrez:** Writing – review & editing, Writing – original draft, Resources, Methodology, Investigation, Funding acquisition, Formal analysis, Conceptualization. **Miren del Val:** Investigation, Formal analysis, Data curation. **Francisco José Pérez-Torrado:** Investigation, Formal analysis, Data curation. **Jorge Luis Giner-Robles:** Visualization, Investigation, Formal analysis, Data curation. **Davinia Moreno:** Methodology, Investigation, Formal analysis, Data curation.

Declaration of competing interest

The authors declare that they have no known competing financial interests or personal relationships that could have appeared to influence the work reported in this paper.

Data availability

Detailed OSL age data in Supplementary information S1.

Acknowledgements

This research is part of the Spanish Research Project I + D + i PID2021-123510OB-I00 (QTECIBERIA-USAL) funded by the MICIN/AEI/10.13039/501100011033/. The work by FG has been supported by DIAPERNO-UNIZAR Project (PID2021-123189NB-I00) funded by the Spanish Government (Ministerio de Ciencia e Innovación). Authors are grateful to Alfonso Benito-Calvo and one anonymous reviewer by the valuable comments improving the original manuscript.

Appendix A. Supplementary data

Supplementary data to this article can be found online at https://doi.org/10.1016/j.geomorph.2024.109066.

References

Aitken, M.J., Xie, J., 1990. Moisture correction for annual gamma dose. Ancient TL 8, 6–9.

Alberdi, M.T., Cerdeño, E., López-Martínez, N., Morales, J., Soria, D., 1997. La Fauna Villafranquiense de El Rincón-1 (Albacete). Estud. Geol. 53, 69–93. https://doi.org/10.3989/egeol.97531-2248.

Alcalá, L., Mazo, A.V., Morales, J., 1985. Mamíferos de las cuencas del Júcar y Cabriel. In: Informe IGME. Proyecto MAGNA Instituto Geológico y Minero de España, IGME. Madrid, Spain, 37 p. http://info.igme.es/.

Ancochea, E., Huertas, M.J., 2002. Nuevos datos geocronológicos y geoquímicos de las manifestaciones volcánicas de Picasent y Cofrentes (Valencia). Geogaceta 32, 31–34.

Baena, J., Moreno, F., Nozal, F., Alfaro, J.A., Barranco, L.M., 1991. Mapa Neotectónico de España 1:1.000.000.. In: PDF Publication 2009 ITGE-ENRESA, Madrid. Spain, 237 pp. http://info.igme.es/.

Baena, R., Fernández-Caro, J.J., Guerrero, I., 2014. La Terraza Compleja del río Guadalquivir en "Las Jarillas" (La Rinconada, Sevilla. SW de España): cronoestratigrafía, industria lítica y macrofauna asociada. Cuaternario Geomorfol 28 (3–4), 107–125.

Bardají, T., Lario, J., 2022. Estadios Isotópicos Marinos. Estratigrafía de los isótopos del oxígeno (marine isotope stages: oxygen isotope stratigraphy). Cuaternario Geomorfol 36 (3–4), 143–154. https://doi.org/10.17735/cyg.v36i3-4.94172.

Benito, G., Sancho, C., Peña, J.L., Machado, M.J., Rhodes, E.J., 2010. Large-scale karst subsidence and accelerated fluvial aggradation during MIS6 in NE Spain: climatic and paleohydrological implications. Quat. Sci. Rev. 29, 2694–2704. https://doi.org/10.1016/j.quascirev.2010.06.020.

Benito-Calvo, A., Perez-Gonzalez, A., 2007. Erosion surfaces and Neogene landscape evolution in the NE Duero basin (North-central Spain). Geomorphology 88, 226–241. https://doi.org/10.1016/j.geomorph.2006.11.005.

Benito-Calvo, A., Pérez-González, A., Pares, J.M., 2008. Quantitative reconstruction of Late Cenozoic landscapes: a case study in the Sierra de Atapuerca (Burgos, Spain). Earth Surf. Process. Landf. 33, 196–208. https://doi.org/10.1002/esp.1534.

Benito-Calvo, A., Ortega, A.I., Pérez-González, A., Campaña, I., Bermúdez de Castro, J. M., Carbonell, E., 2017. Palaeogeographical reconstruction of the Sierra de Atapuerca Pleistocene sites (Burgos, Spain). Quat. Int. 433, 379–392. https://doi.org/10.1016/j.quaint.2015.10.034.

Benito-Calvo, A., Moreno, D., Fujioka, T., López, G.I., Martín-González, F., Martínez-Fernández, A., Hernando-Alonso, I., Karampaglidis, T., Bermúdez de Castro, J.M., Gutiérrez, F., 2022. Towards the steady state? A long-term river incision deceleration pattern during Pleistocene entrenchment (Upper Ebro River, Northern Spain). Glob. Planet. Chang., 103813 https://doi.org/10.1016/j.gloplacha.2022.103813.

Brennan, B., 2003. Beta doses to spherical grains. Radiat. Meas. 37, 299–303. https://doi.org/10.1016/S1350-4487(03)00011-8.

Brennan, B.J., Lyons, R.G., Phillips, S.W., 1991. Attenuation of alpha particle track dose for spherical grains. Int. J. Radiat. Appl. Instrum. Nucl. Tracks Radiat. Meas. 18, 249–253.

Bridgland, D., Westaway, R., 2008. Climatically controlled river terrace staircases: a worldwide Quaternary phenomenon. Geomorphology 98, 285–315. https://doi.org/10.1016/j.geomorph.2006.12.032.

Bridgland, D.R., 2000. River terrace systems in north-West Europe: an archive of environmental change, uplift and early human occupation. Quat. Sci. Rev. 19, 1293–1303. https://doi.org/10.1016/S0277-3791(99)00095-5.

Burbank, D.W., Anderson, R.S., 2001. Tectonic Geomorphology. Blackwell Science.

Carbonel, D., Gutiérrez, F., Linares, R., Roqué, C., Zarroca, M., McCalpin, J., Guerrero, J., Rodríguez, V., 2013. Differentiating between gravitational and tectonic faults by means of geomorphological mapping, trenching and geophysical surveys. The case of Zenzano Fault (Iberian Chain, N Spain). Geomorphology 189, 93–108. https://doi.org/10.1016/j.geomorph.2013.01.020.

Carmona, P., Pérez Ballester, J., 2011. Geomorphology, geoarchaeology and ancient settlement in the Valencian Gulf (Spain). Méditerranée 117, 61–72. http://mediterranee.revues.org/5920.

Carner, J., 2001. Neotectònica de la Vall de Cofrents. Msc. Thesis. Universitat de Barcelona (Spain), 49 pp.

Cheng, H., Edwards, R.L., Shen, C.C., Polyak, V.J., Asmeron, Y., Woodhead, J., Hellstrom, J., Wang, Y., Kong, X., Spotl, C., Wang, X., Alexander, E.C., 2013. Improvements in 230 Th and 234U half-life values, and U-Th isotopic measurements by multi-collector inductively coupled plasma mass spectrometry. Earth Planet. Sci. Lett. 371-372, 82–91. https://doi.org/10.1016/j.epsl.2013.04.006.

Cunha, P.P., Martins, A.A., Daveau, S., Friend, P.F., 2005. Tectonic control of the Tejo River fluvial incision during the late Cenozoic, in Ródão – Central Portugal (Atlantic Iberian border). Geomorphology 64, 271–298. https://doi.org/10.1016/j.geomorph.2004.07.004. Elsevier Science Publishers.

Cunha, P.P., Martins, A.A., Gomes, A., Stokes, M., Cabral, J., Lopes, F.C., Pereira, D., de Vicente, G., Buylaert, J.P., Murray, A.S., Antón, L., 2019. Mechanisms and age estimates of continental-scale endorheic to exorheic drainage transition: Douro River, Western Iberia. Glob. Planet. Chang. 181, 102–985. https://doi.org/10.1016/j.gloplacha.2019.10298.

De Vicente, G., Vegas, R., Muñoz Martín, A., Silva, P.G., Andriessen, P., Cloetingh, A., González-Casado, J.M., Alvarez, J., Olaiz, A., 2007. Cenozoic thick-skinned deformation and topographic evolution of the Spanish Central System. Glob. Planet. Chang. 58 (1–4), 335–381. https://doi.org/10.1016/j.gloplacha.2006.11.042.

Doelling, H.H., 2000. Geology of Arches National Park, Grand County, Utah. In: Sprinkel, D.A., Chidsey, T.C., Anderson, P.B. (Eds.), Geology of Utah's Parks and Monuments, 28. Utah Geological Association Publication, pp. 11–36.

Duller, G.A.T., 2008. Luminescence Dating: Guidelines on Using Luminescence Dating in Archaeology. English Heritage, Swindon.

Duller, G.A.T., 2015. The Analyst Software Package for Luminescence Data: Overview and Recent Improvements, 33, p. 8.

Durcan, J.A., King, G.E., Duller, G.A.T., 2015. DRAC: dose rate and age calculator for trapped charge dating. Quat. Geochronol. 28, 54–61. https://doi.org/10.1016/j.quageo.2015.03.012.

Duval, M., Grün, R., Falguères, C., Bahain, J.-J., Dolo, J.-M., 2009. ESR dating of Lower Pleistocene fossil teeth: Limits of the single saturating exponential (SSE) function for the equivalent dose determination. Radiat. Meas. 44, 477–482. https://doi.org/10.1016/j.radmeas.2009.03.017.

Duval, M., Sancho, C., Calle, M., Guilarte, V., Pena-Monné, J.L., 2015. On the interest of using the multiple center approach in ESR dating of optically bleached quartz grains: some examples from the Early Pleistocene terraces of the Alcanadre River (Ebro basin, Spain). Quat. Geochronol. 29, 58–69. https://doi.org/10.1016/j.quageo.2015.06.006.

Duval, M., Bahain, J.J., Bartz, M., Falgères, C., Guilarte, V., Moreno, D., Tissoux, H., del Val., M., Voincet, P., Arnold, L.J., 2017. Defining minimum reporting requirements for ESR dating of optically bleached quartz grains. Ancient TL 35, 11–19.

Elez, J., Silva, P.G., Huerta, D., Perucha, M.A., Civis, J., Roquero, E., Rodríguez-Pascua, M.A., Bardají, T., Giner-Robles, J.L., Martínez-Graña, A.M., 2016. Quantitative paleotopography and paleogeography around the GibraltarArc (South Spain) during the Messinian Salinity Crisis. Geomorphology 275, 26–45. https://doi.org/10.1016/j.geomorph.2016.09.023.

Elez, J., Silva, P.G., Martínez-Graña, A.M., 2020. Quantification of erosion and uplift in a rising orogen—a large-scale perspective (Late Tortonian to present): the case of the Gibraltar Arc, Betic Cordillera, Southern Spain. Remote Sens. 12, 3492. https://doi.org/10.3390/rs12213492.

Galbraith, R.F., Roberts, R.G., 2012. Statistical aspects of equivalent dose and error calculation and display in OSL dating: an overview and some recommendations. Quat. Geochronol. 11, 1–27. https://doi.org/10.1016/j.quageo.2012.04.020.

García, A.F., Zhu, Z., Ku, T.L., Chadwick, O.A., Montero, J.C., 2004. An incision wave in the geologic record, Alpujarran Corridor, southern Spain (Almería). Geomorphology 60, 37–72. https://doi.org/10.1016/j.geomorph.2003.07.012.

García-Castellanos, D., Larrasoaña, J.C., 2015. Quantifying the post-tectonic topographic evolution of closed basins: the Ebro basin (Northeast Iberia). Geology 43, 663–666. https://doi.org/10.1130/G36673.1.

García-Castellanos, D., Estrada, F., Jiménez-Munt, I., Gorini, C., Fernández, M., Vergés, J., De Vicente, R., 2009. Catastrophic flood of the Mediterranean after the Messinian salinity crisis. Nature 462, 778–781. https://doi.org/10.1038/nature08555.

Gökkaya, E., Gutiérrez, F., 2022. Poljes in the Sivas gypsum karst, Turkey. Geomorphology 417, 108451. https://doi.org/10.1016/j.geomorph.2022.108451.

Goy, J.L., Cruz, R., Martínez-Graña, A.M., Valdés, V., Yenes, M., 2020. Geomorphological map and quaternary landscape evolution of the Monfragüe Park (Cáceres, Spain). Sustainability 12, 10099. https://doi.org/10.3390/su122310099.

Grün, R., 1994. A cautionary note: use of the water content and depth for cosmic ray dose rate in AGE and DATA programs. Ancient TL 12, 50–51. http://ancienttl.org/ATL_12-2_1994/ATL_12-2_Grun_p50-51.pdf.

Guérin, G., Mercier, N., Adamiec, G., 2011. Dose-rate conversion factors: update. Ancient TL 29, 5–8.

Guérin, G., Mercier, N., Nathan, R., Adamiec, G., Lefrais, Y., 2012. On the use of the infinite matrix assumption and associated concepts: a critical review. Radiat. Meas. 47, 778–785.

Guerra-Merchán, A., Francisco Serrano, J., García-Aguilar, M., Sanz de Galdeano, C., Ortiz, J.E., Torres, T., Sánchez-Palencia, Y., 2019. The Late Cenozoic landscape development in the westernmost Mediterranean (southern Spain). Geomorphology 327, 456–471. https://doi.org/10.1016/j.geomorph.2018.11.008.

Guerrero, J., Bruhn, R.L., McCalpin, J.P., Gutiérrez, F., Willis, G., Mozafari, M., 2015. Salt-dissolution faults versus tectonic faults from the case study of salt collapse in Spanish Valley, SE Utah (USA). Lithosphere 7, 46–58. https://doi.org/10.1130/L385.1.

Gutiérrez, F., 2004. Origin of the salt valleys in the Canyonlands section of the Colorado Plateau. Evaporite-dissolution collapse versus tectonic subsidence. Geomorphology 57, 423–435. https://doi.org/10.1016/S0169-555X(03)00186-7.

Gutiérrez, F., Gutiérrez, M., Gracia, F.J., McCalpin, J.P., Lucha, P., Guerrero, J., 2008. Plio-Quaternary extensional seismotectonics and drainage network development in the central sector of the Iberian Range (NE Spain). Geomorphology 102 (1), 21–42. https://doi.org/10.1016/j.geomorph.2007.07.020.

Gutiérrez, F., Linares, R., Roqué, C., Zarroca, M., Rosell, J., Galve, J.P., Carbonell, D., 2012. Investigating gravitational grabens related to lateral spreading and evaporite dissolution subsidence by means of detailed zapping, trenching, and electrical resistivity tomography (Spanish Pyrenees). Lithosphere 4, 331–353. https://doi.org/10.1130/L202.1.

Gutiérrez, F., Sevil, J., Silva, P.G., Roca, E., Escosa, F., 2019. Geomorphic and stratigraphic evidence of Quaternary diapiric activity enhanced by fluvial incision. Navarrés salt wall and graben system, SE Spain. Geomorphology 342, 176–195. https://doi.org/10.1016/j.geomorph.2019.06.002.

Gutiérrez, F., Moreno, D., López, G.I., Jiménez, F., del Val, M., Alonso, M.J., Martínez-Pillado, V., Guzmán, O., Martínez, D., Carbonel, D., 2020. Revisiting the slip rate of Quaternary faults in the Iberian Chain, NE Spain. Geomorphic and seismic-hazard implications. Geomorphology 363, 107233. https://doi.org/10.1016/j.geomorph.2020.107233.

Gutierrez-Elorza, M., Gracia, F.J., 1997. Environmental interpretation and evolution of the Tertiary erosion surfaces in the Iberian range (Spain). In: Widdowson, M. (Ed.), Palaeosurfaces: Recognition, Reconstruction and Palaeoenvironmental Interpretation, vol. 120. Geological Society Publication, pp. 147–158.

Harvey, A., 2007. High-sinuosity bedrock channels: response to rapid incision. Examples in SE Spain. Cuaternario Geomorfol 21, 21–47.

Hovius, N., 2000. Macroscale process systems of mountain belt erosion. In: Summerfield, M.A. (Ed.), Geomorphology and Global Tectonics. Wiley, Chichester, England, pp. 77–105.

Ivanovich, M., Harmon, R.S., 1992. Uranium-series Disequilibrium: Applications to Earth, Marine, and Environmental Sciences, , 2nd edition99. Clarendon Press, Oxford, U.K., p. 910. https://www.osti.gov/etdeweb/biblio/6970644

Karampaglidis, T., Benito-Calvo, A., Rodés, A., Braucherd, R., Pérez-González, A., Pares, J., Di Stuart, F., Nicola, L., Bourles, D., 2020. Pliocene endorheic-exhoreic drainage transition of the Cenozoic Madrid Basin (Central Spain). Glob. Planet. Chang. 194, 103295 https://doi.org/10.1016/j.gloplacha.2020.103295.

Lendínez, A., Tena, M., 1980. *Mapa Geológico de España a escala 1:50,000*, hoja n° 745 (Jalance) y memoria. Serie MAGNA 2° Ed. IGME, Servicio Publicaciones Ministerio de Industria, Madrid (España), 32 pp.

Lewis, C.J., McDonald, E.V., Sancho, C., Peña, J.L., Rhodes, E.J., 2009. Climatic implications of correlated Upper Pleistocene glacial and fluvial deposits on the Cinca and Gállego Rivers (NE Spain) based on OSL dating and soil stratigraphy. Glob. Planet. Chang. 67, 141–152. https://doi.org/10.1016/j.gloplacha.2009.01.001.

Lewis, C.J., Sancho, C., McDonald, E.V., Peña-Monn'e, J.L., Pueyo, E.L., Rhodes, E., Calle, M., Soto, R., 2017. Post-tectonic landscape evolution in NE Iberia using staircase terraces: combined effects of uplift and climate. Geomorphology 292, 85–103. https://doi.org/10.1016/j.geomorph.2017.04.037.

Lisiecki, L., Raymo, M., 2005. A Pliocene – Pleistocene stack of 57 globally distributed benthic δ18O records. Paleoceanography 20, PA1003, 17pp. https://doi.org/10.1029/2004PA001071.

Martí, J., Mitjavila, J., Aparicio, A., 1992. Cenozoic magmatism of the Valencia trough (western Mediterranean): relationship between structural evolution and volcanism. Tectonophysics 203, 145–165. https://doi.org/10.1016/0040-1951(92)90221-Q.

Martínez del Olmo, W., Motis, K., Martín, D., 2015. El papel del diapirismo de la sal triásica en la estructuración del Prebético (SE de España). Rev. Soc. Geol. Esp. 28, 3–24.

Mazo, A.V., Pérez-González, A., Aguirre, E., 1990. Las faunas pleistocenas de Fuensanta del Júcar y El Provencio y su significado en la evolución del Cuaternario de la Llanura manchega. Bol. Geol. Min. 101 (3), 404–418.

Méndez-Quintas, E., Sanatonja, M., Pérez-González, A., Arnoldd, L.J., Demurod, M., Duval, M., 2020. Multidisciplinary overview of the lower Miño River terrace system (NW Iberian Peninsula). Quat. Int. 566–567, 57–77. https://doi.org/10.1016/j.quaint.2020.04.022.

Menéndez, I., Silva, P.G., Martín-Betancor, M., Pérez-Torrado, F.J., Guillou, H., Scaillet, S., 2008. Fluvial dissection, isostatic uplift, and geomorphological evolution of volcanic islands (Gran Canaria, Canary Islands, Spain). Geomorphology 102, 189–203. https://doi.org/10.1016/j.geomorph.2007.06.022.

Moreno, D., Falguères, C., Pérez-González, A., Duval, M., Voinchet, Pl, Benito-Calvo, A., Ortega, A.I., Bahain, J.J., Sala, R., Carbonell, E., Bermúdez de Castro, J.M., Arsuaga, J.L., 2012. ESR chronology of alluvial deposits in the Arlanzon valley (Atapuerca,Spain): contemporaneity with Atapuerca Gran Dolina site. Quat. Geochronol. 10, 418–423. https://doi.org/10.1016/j.quageo.2012.04.018.

Moreno, D., Duval, M., Rubio-Jara, S., Panera, J., Bahain, J.J., Shao, Q., Pérez-González, A., Falguères, C., 2019. ESR dating of Middle Pleistocene archaeo-paleontological sites from the Manzanares and Jarama river valleys (Madrid basin, Spain). Quat. Int. 2019 (520), 23–38. https://doi.org/10.1016/j.quaint.2017.09.003.

Moreno, D., Gutiérrez, F., del Val, M., Carbonel, D., Jiménez, F., Alonso, M.J., Martínez-Pillado, V., Guzmán, O., López, G.I., Martínez, D., 2021. A multi-method dating approach to reassess the geochronology of faulted Quaternary deposits in the central sector of the Iberian Chain (NE Spain). Quat. Geochronol. 65, 101185 https://doi.org/10.1016/j.quageo.2021.101185.

Murray, A.S., Wintle, A.G., 2000. Luminescence dating of quartz using an improved single-aliquot regenerative-dose protocol. Radiat. Meas. 32, 57–73. https://doi.org/10.1016/S1350-4487(99)00253-X.

Németh, K., Kósik, S., 2020. Review of explosive hydrovolcanism. Geosciences 10, 44. https://doi.org/10.3390/geosciences10020044.

Ortega-Becerril, J.A., Garzón, G., Tejero, R., Meriaux, A.S., Delunel, R., Merchel, S., Rugel, G., 2018. Controls on strath terrace formation and evolution: the lower Guadiana River, Pulo do Lobo, Portugal. Geomorphology 319, 62–77. https://doi.org/10.1016/j.geomorph.2018.07.015.

Ortí, F., 2004. Últimas etapas de actividad del rifting. Sedimentos asociados. In: Vera, J. A. (Ed.), Geología de España. IGME-SGE, Madrid (Spain), pp. 492–495.

A fundamental archive for the European Pleistocene: the Manzanares and Jarama valleys (Madrid, Spain). In: Panera, J., Rubio-Jara, S., Pérez-González, A. (Eds.), 2019. Spec. Issue *Quatern. Int*, 520, pp. 86–95. https://doi.org/10.1016/j.quaint.2019.07.030.

Parés, J.M., Duval, M., Soria-Jáuregui, A., González-Amuchástegui, J.M., 2021. First chronological constraints for the high terraces of the Upper Ebro Catchment. Quaternary 4, 25. https://doi.org/10.3390/quat4030025.

Pedley, H.M., 1990. Classification and environmental models of cool freshwater tufas. Sediment. Geol. 68, 143–154. https://doi.org/10.1016/0037-0738(90)90124-C.

Pérez, N.M., Nakai, S., Wakita, H., Albert-Bertrán, J.F., Redondo, R., 1996. Preliminary results on $^{3}He/^{4}He$ isotopic ratios in terrestrial fluids from the Iberian península: seismotectonic and neotectonic implications. Geogaceta 20, 830–833.

Pérez-González, A., 1994. Depresión del Tajo. In: Gutiérrez Elorza, M. (Ed.), Geomorfología de España. Ed. Rueda, Madrid (Spain), pp. 389–436.

Pérez-González, A., Gallardo-Millán, J.L., Uribelarrea del Val, D., Panera, J., Rubio-Jara, S., 2013. La inversión Matuyama-Brunhes en la secuencia de terrazas del río Jarama entre Velilla de San Antonio y Altos de la Mejorada, al SE de Madrid (España). Estud. Geol. 69 (1), 35–46. https://doi.org/10.3989/egeol.40862.173.

Prescott, J.R., Hutton, J.T., 1994. Cosmic ray contributions to dose rates for luminescence and ESR dating: large depths and long term time variations. Radiat. Meas. 23, 497–500. https://doi.org/10.1016/1350-4487(94)90086-8.

Regard, V., Vacherat, A., Bonnet, S., Mouthereau, F., Nørgaard, J., Knudsen, M.F., 2021. Late Pliocene-Pleistocene incision in the Ebro Basin (North Spain). BSGF - Earth Sci. Bull. 192 (1), 30.

Roca, E., Beamud, E., Rubinat, M., Soto, R., Ferrer, O., 2013. Paleomagnetic and inner diapiric structural constraints on the kinematic evolution of a salt-wall: the Bicorb-Quesa and northen Navarrés salt-wall segments case (Prebetic Zone, SE Iberia). J. Struct. Geol. 52, 80–95. https://doi.org/10.1016/j.jsg.2013.04.003.

Roca, E., Escosa, F., Ferrer, O., Gutiérrez, F., Silva, P.G., Elez, J., Granado, P., Gratacós, O., 2021. Structure and kinematics of the Ayora-Cofrentes Diapir (eastern Betics): role of basement faulting in the salt and suprasalt deformation of the Mesozoic cover. Geotemas 18, 112–115.

Rodríguez-Rodríguez, L., Antón, L., Rodés, A., Pallàse, R., García-Castellanos, D., Jiménez-Munt, I., Struth, L., Leannig, L., the ASTER Team, 2022. Dates and rates of endo-exorheic drainage development: insights fluvial terraces (Duero River, Iberian Peninsula). Glob. Planet. Chang. 193, 103271 https://doi.org/10.1016/j.gloplacha.2020.103271.

Rubinat, M., Ledo, J., Roca, E., Rosell, O., Queralt, P., 2010. Magnetotelluric characterization of a salt diapir: a case study on Bicrob-Quesa Diapir (Prebatic Zone, SE Spain). J. Geol. Soc. Lond. 167, 145–153.

Ruiz-Sanchez, F.J., Santisteban, C., Crespo-Roures, V.D., Freudenthal, M., 2011. New rodent faunas from Middle Miocene and Mio-Pliocene in the Cabriel Basin (Valencia, Spain). J. Iber. Geol. 37 (2), 161–172. https://doi.org/10.5209/rev_JIGE.2011.v37.n2.5.

Sáenz-Ridruejo, C., López-Mariñas, J.M., 1975. La edad del vulcanismo de Cofrentes, provincia de Valencia. Tecniterrae 6, 8–14.

Sancho, C., Arenas, C., Vázquez-Urbez, M., Pardo, G., Lozano, M.V., Peña-Monné, J.L., Hellstrom, J., Ortiz, J.E., Osácar, M.C., Auqué, L., Torres, T., 2015. Climatic implications of the quaternary fluvial tufa record in the NE Iberian Peninsula over the last 500 ka. Quat. Res. 84 (3), 398–414. https://doi.org/10.1016/j.yqres.2015.08.003.

Sancho, C., Calle, M., Peña-Monné, J.L., Duval, M., Oliva-Urcia, B., Pueyo, E.L., Benito, G., Moreno, A., 2020. Dating the Earliest Pleistocene alluvial terrace of the Alcanadre River (Ebro Basin, NE Spain): insights into the landscape evolution and involved processes. Quat. Int. 407, 86–95. https://doi.org/10.1016/j.quaint.2015.10.050.

Santisteban, C., Saiz, J., Bello, D., Ruiz-Sánchez, F.J., 1990. Tectónica y sedimentación en el margen oeste del rift terciario del valle de Ayora-Cofrentes (Valencia). Geogaceta 8, 44–47.

Santisteban, J.I., Schulte, L., 007. Fluvial networks of the Iberian Peninsula: a chronological framework. Quat. Sci. Rev. 26, 2738–2757. https://doi.org/10.1016/j.quascirev.2006.12.019.

Santonja, M., Pérez-González, A., Panera, J., Rubio-Jara, S., Méndez-Quintas, E., 2016. The coexistence of acheulean and ancient middle palaeolithic techno-complexes in the middle Pleistocene of the Iberian Peninsula. Quat. Int. 411, 367–377. https://doi.org/10.1016/j.quaint.2015.04.056.

Sanz de Galdeano, C., Alfaro, P., 2004. Tectonic significance of the present relief of the Betic Cordillera. Geomorphology 2004 (63), 175–190. https://doi.org/10.1016/j.geomorph.2004.04.002.

Sartégou, A., Bourlès, D.L., Blard, P.-H., Braucher, R., Tibari, B., Zimmermann, L., Leanni, L., Aumaître, G., Keddadouche, K., 2018. Deciphering landscape evolution with karstic networks: a Pyrenean case study. Quat. Geochronol. 43, 12–29. https://doi.org/10.1016/j.quageo.2017.09.005.

Schulte, L., Julià, R., Burjachs, F., Hilgers, A., 2008a. Middle Pleistocene to Holocene geochronology of the River Aguas terrace sequence (Iberian Peninsula). Geomorphology 98, 13–33. https://doi.org/10.1016/j.geomorph.2007.03.018.

Schulte, L., Julià, R., Burjachs, F., Hilgers, A., 2008b. Middle Pleistocene to Holocene geochronology of the River Aguas terrace sequence (Iberian Peninsula). Geomorphology 98, 13–33. https://doi.org/10.1016/j.geomorph.2007.03.018.

Silva, P.G., 2003. El Cuaternario del Valle Inferior del Manzanares (Cuenca de Madrid, España). Estud. Geol. 59, 107–131. https://doi.org/10.3989/egeol.03591-488.

Silva, P.G., Roquero, E., 2022. Cronofunciones: modelización estadística de conjuntos de dataciones numéricas para el estudio del Cuaternario: Ejemplos para la Península Ibérica. Cuaternario Geomorfol. 36 (3–4), 123–142. https://doi.org/10.17735/cyg.v36i3-4.93733.

Silva, P.G., Giner-Robles, J.L., Elez, J., Rodríguez-Pascua, M.A., Perucha, M.A., Roquero, E., Martínez-Graña, A., 2015. Tectonic Geomorphology and Volcanism in the Ayora-Cofrentes Tectonic Corridor, Valencia (Prebetic, SE Spain). XIV Reunión Nacional de Cuaternario, Granada, pp. 162–166.

Silva, P.G., Roquero, E., López-Recio, M., Huerta, P., Martínez-Graña, A.M., 2017. Chronology of fluvial terrace sequences for large Atlantic rivers in the Iberian Peninsula (Upper Tagus and Duero drainage basins, Central Spain). Quat. Sci. Rev. 166, 188–203. https://doi.org/10.1016/j.quascirev.2016.05.027.

Silva, P.G., Roquero, E., Bardají, T., Medialdea, A., 2021. Pleistocene to Holocene phases of sedimentation and soil formation in the semiarid SE Spain (Eastern Betic Cordillera). Cuaternario Geomorfol. 34 (1–2), 9–39. https://doi.org/10.17735/cyg.v34i1-2.78815.

Silva, P.G., Pérez-Torrado, J.F., Elez, J., Pérez-López, R., Roquero, E., Sánchez-Sánchez, Y., Bardají, T., 2023a. Interference Among Volcanism, Faulting and Quaternary Fluvial Terraces in the Cabriel Valley (Valencia, East Spain). Abstracts XXI INQUA Congress, Rome (Italy).

Silva, P.G., Gutiérrez, Elez, J., Giner-Robles, J.L., Roquero, E., Del Val., Miren, Santos, G., Tapias, F., 2023b. Trenching and Geophysical Investigation of Recent Faulting in Late Pleistocene to Holocene Fluvial Deposits Within the Júcar Valley (Valencia, Eastern Spain). Abstracts XXI INQUA Congress, Rome (Italy).

Silva, P.-G., López Recio, M., Tapias, F., Roquero, E., Morín, J., Rus, I., Carrasco-García, P., Rodríguez-Pascua, M.A., Pérez-López, R., Giner-Robles, J.L., 2013. Stratigraphy of the Arriaga Palaeolithic sites. Implications for the geomorphological evolution recorded by thickened fluvial sequences within the Manzanares River valley (Madrid Neogene Basin, Central Spain). Geomorphology 196, 138–161. https://doi.org/10.1016/j.geomorph.2012.10.019.

Soria-Jáuregui, A., González-Amuchástegui, M.J., Mauz, B., Lang, A., 2016. Dynamics of Mediterranean late Quaternary fluvial activity: an example from the river Ebro (north Iberian Peninsula). Geomorphology 268, 110–122. https://doi.org/10.1016/j.geomorph.2016.06.006.

Stokes, M., Mather, A.E., 2003. Tectonic origin and evolution of a transverse drainage: the Río Almanzora, Betic Cordillera, Southeast Spain. Geomorphology 50 (1–3), 59–81. https://doi.org/10.1016/S0169-555X(02)00208-8.

Struth, L., Garcia-Castellanos, D., Viaplana-Muzas, M., Vergés, J., 2019. Drainage network dynamics and knickpoint evolution in the Ebro and Duero basins: from endorheism to exorheism. Geomorphology 327, 554–571. https://doi.org/10.1016/j.geomorph.2018.11.033.

Suárez Alba, J., 2007. La Mancha Triassic and Lower Lias Stratigraphy, a well log interpretation. J. Iber. Geol. 33 (1), 55–78.

Tissoux, H., Falguères, C., Voinchet, P., Toyoda, S., Bahain, J.J., Despriée, J., 2007. Potential use of Ti-center in ESR dating of fluvial sediment. Quat. Geochronol. 2 (1–4), 367–372. https://doi.org/10.1016/j.quageo.2006.04.006.

Torres, T., Ortiz, J.E., García de la Morena, M.A., Llamas, J.F., Goodfriend, G., 2005. Ostracode based aminostratigraphy and aminochronology of a tufa system in central Spain. Quat. Int. 135, 21–33. https://doi.org/10.1016/j.quaint.2004.10.021.

Toyoda, S., Voinchet, P., Falguères, C., Dolo, J.M., Laurent, M., 2000. Bleaching of ESR signals by the sunlight: a laboratory experiment for establishing the ESR dating of sediments. Appl. Radiat. Isot. 52, 1357–1362. https://doi.org/10.1016/S0969-8043(00)00095-6.

Vera, J.A., 1983. Las zonas externas de las cordilleras Béticas. In: Comba, J.A. (Ed.), Geología de España 2, Libro Jubilar J. M. Rios. IGME, Madrid, pp. 218–225.

Vera, J.A., Martín-Algarra, A., 004. Cordillera Bétrica y Baleares. Divisiones mayores ynomenclatura. In: Vera, J.A. (Ed.), Geología de España. IGME-SGE, Madrid, Spain, pp. 348–350.

Viveen, W., Braucher, R., Bourlès, D., Schoorl, J.M., Veldkamp, A., Van Balen, R.T., Wallinga, J., Fernandez-Mosquera, D., Vidal-Romani, J.R., Sanjurjo-Sanchez, J., A., 2012. 0.65 Ma chronology and incision rate assessment of the NW Iberian Miño River terraces based on ^{10}Be and luminescence dating. Glob. Planet. Chang. 94 (95), 82–100. https://doi.org/10.1016/j.gloplacha.2012.07.001.

Voinchet, P., Falguères, C., Laurent, M., Toyoda, S., Bahain, J.J., Dolo, J.M., 2003. Artificial optical bleaching of the aluminium center in quartz implications to ESR dating of sediments. Quat. Sci. Rev. 22, 1335–1338. https://doi.org/10.1016/S0277-3791(03)00062-3.

Westaway, R., Bridgland, D.R., Sinha, R., Demir, T., 2009. Fluvial sequences as evidence for landscape and climatic evolution in the Late Cenozoic: a synthesis of data from IGCP 518. Glob. Planet. Chang. 68 (4), 237–253. https://doi.org/10.1016/j.gloplacha.2009.02.009.

Whitfield, R.G., Macklin, M.G., Brewer, P.A., Lang, A., Mauz, B., Whitfield, E., 2013. The nature, timing and controls of the Quaternary development of the Rio Bergantes, Ebro basin, northeast Spain. Geomorphology 196, 106–121. https://doi.org/10.1016/j.geomorph.2012.04.014.

Woda, C., Wagner, G.A., 2007. Non-monotonic dose dependence of the Ge- and Ticentres in quartz. Radiat. Meas. 42, 1441–1452. https://doi.org/10.1016/j.radmeas.2007.03.003.

Zazo, C., Mercier, N., Lario, J., Roquero, E., Goy, J.L., Silva, P.G., Cabero, A., Borja, F., Dabrio, C.J., Bardají, T., Soler, V., García-Blázquez, A., de Luque, L., 2008. Palaeoenvironmental evolution of the Barbate–Trafalgar coast (Cadiz) during the last ~140 ka: climate, sea-level interactions and tectonics. Geomorphology 100, 212–222. https://doi.org/10.1016/j.geomorph.2007.10.031.